

**AN EXPERIMENTAL INVESTIGATION ON THE
PROPERTIES OF Cu-Al-Be-X SHAPE MEMORY
ALLOYS FOR VIBRATION DAMPING APPLICATIONS**

Thesis

Submitted in partial fulfillment of the requirements for the degree of

DOCTOR OF PHILOSOPHY

by

KALINGA T.



DEPARTMENT OF MECHANICAL ENGINEERING
NATIONAL INSTITUTE OF TECHNOLOGY KARNATAKA,
SURATHKAL, MANGALORE - 575025

JUNE - 2022

**AN EXPERIMENTAL INVESTIGATION ON THE
PROPERTIES OF Cu-Al-Be-X SHAPE MEMORY
ALLOYS FOR VIBRATION DAMPING APPLICATIONS**

Thesis

Submitted in partial fulfillment of the requirements for the Degree of

DOCTOR OF PHILOSOPHY

by

KALINGA T.

(165043 ME16F06)

Under the Guidance of

Prof. S.M. Murigendrappa

Professor

Department Of Mechanical Engg.

NITK, Surathkal

Dr. S. Kattimani

Associate Professor

Department Of Mechanical Engg.

NITK, Surathkal



DEPARTMENT MECHANICAL ENGINEERING

NATIONAL INSTITUTE OF TECHNOLOGY KARNATAKA,

SURATHKAL, MANGALORE -575025

JUNE - 2022

DECLARATION

I hereby declare that the Research Thesis entitled “**AN EXPERIMENTAL INVESTIGATION ON THE PROPERTIES OF Cu-Al-Be-X SHAPE MEMORY ALLOYS FOR VIBRATION DAMPING APPLICATIONS**” which is being submitted to the **National Institute of Technology Karnataka, Surathkal** in partial fulfilment of the requirements for the award of the Degree of **Doctor of Philosophy in Mechanical Engineering** is a *bonafide report of the research work carried out by me*. The material contained in this Research Thesis has not been submitted to any other Universities or Institutes for the award of any degree.

Register Number: **165043 ME16F06**

Name of the Research Scholar: **KALINGA T.**

Signature of the Research Scholar: 

Department of Mechanical Engineering

Place: NITK, Surathkal

Date: *20/06/2022*

CERTIFICATE

This is to certify that the Research Thesis entitled “AN EXPERIMENTAL INVESTIGATION ON THE PROPERTIES OF Cu-Al-Be-X SHAPE MEMORY ALLOYS FOR VIBRATION DAMPING APPLICATIONS” submitted by Mr. KALINGA T. (Register Number: 165043 ME16F06) as the record of the research work carried out by him, *is accepted as the Research Thesis submission* in partial fulfilment of the requirements for the award of the degree of **Doctor of Philosophy**.

Research Guides



Prof. S.M. Murigendrappa

Professor

Department of Mechanical Engineering

NITK, Surathkal



Dr. S. Kattimani

Associate Professor

Department of Mechanical Engineering

NITK, Surathkal



Chairman-DRPC

Department of Mechanical Engineering

National Institute of Technology Karnataka, Surathkal

Dr. Ravikiran Kadoli
Professor & Head
Dept. of Mechanical Engineering
National Institute of Technology Karnataka, Surathkal
Srinivasnagar - 575 025, Mangalore (INDIA)

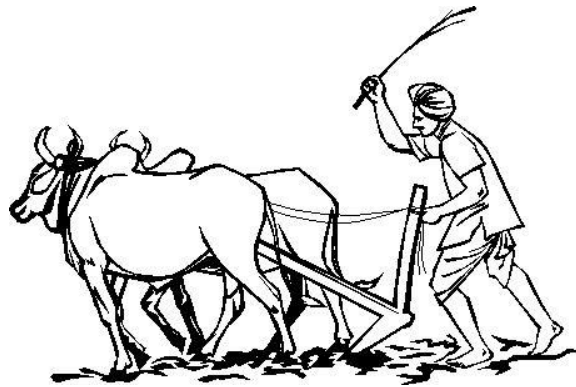
Dedicated to...

My Parents

Smt. Saroja Bai and Late Thippeshi Naik

BELOVED FAMILY MEMBERS

and



FARMERS

ACKNOWLEDGMENT

I cannot believe this long journey called Ph.D. has come to an end. It has been a very intensive but yet invaluable experience in my life, and its successful completion would not have been possible without the precious help of my supervisors, faculty members, colleagues, friends and family. It is a pleasure to have an opportunity to convey my thanks to them all.

Firstly, I would like to express my deepest sense of gratitude and heartfelt thanks to my supervisors **Prof. S.M. Murigendrappa**, Professor, and **Dr. S. Kattimani**, Associate Professor, Department of Mechanical Engineering, National Institute of Technology Karnataka Surathkal, for the invaluable constructive guidance, support and encouragement throughout my research study.

I would like to thank the **Department of Science and Technology, Science and Engineering Research Board (SERB)**, India, for financially supporting this research under the grant No. **EMR/2016/001247**.

I would like to thank my Research Progress Assessment Committee members **Dr. Ramesh M. R.**, Associate Professor, Department of Mechanical Engineering, and **Prof. Anandhan Srinivasan**, Professor, Department of Metallurgical and Materials Engineering, National Institute of Technology Karnataka Surathkal, for their critical evaluation and valuable inputs, useful discussions, and suggestions during the progress of this research.

I would like to thank **Prof. Ravikiran Kadoli**, Head, Department of Mechanical Engineering, and **Prof. S. M. Kulkarni**, **Prof. Shrikantha S. Rao**, **Prof. Narendranath S.**, and **Prof. Gangadharan K. V.**, the former Heads, Department of Mechanical Engineering, for their direct and indirect support throughout this research and providing all kinds of the necessary facilities in the department to carry out the experimental work.

I gratefully acknowledge my heartfelt gratitude to **Prof. Narendranath S**, **Dr. Ramesh M. R.**, and **Dr. Mrityunjay Doddamani**, Department of Mechanical Engineering, NITK Surathkal, for extending support to use the lab facility to conduct the experimental work.

I am greatly indebted to **Prof. Udaya Bhat K.**, **Dr. Mohammad Rizwanur Rahman**, and **Dr. Ravishankar K. S.**, Department of Metallurgical and Materials Engineering, NITK Surathkal, for extending support to use the lab facility to conduct the experiments.

I would like to thank all the teaching and non-teaching staff of the Department of Mechanical Engineering and Department of Metallurgical and Materials Engineering, NITK Surathkal, for their timely help in completing my experimental work.

I heartfully acknowledge and convey special thanks to my research team members, **Dr. Bala Narasimha G.**, **Dr. Susheelkumar N.**, **Mr. Suman M.L.J.**, **Mr. Ratnesh Kumar Singh**, **Mr. P. V. S. Phanikumar**, **Mr. Vinayak Kallannavar**, **Mr. Chetan H.C.**, **Mr. Mohammed Sohail Bakshi**, **Naveen Kumar H. S.**, and **Mr. Atul S.G.**, with whom I enjoyed working with them and sharing the ideas in developing knowledge.

It is also a pleasure to acknowledge and convey thanks to **Mr. Manoj I.V.**, **Dr. Mahendra K.**, **Dr. Brijesh K.**, and **Mr. Darshan M. L.**, for their help in conducting the experimental tests and characterizations.

I would like to pay a special thanks to **Mr. Basavaraj Chavan**, **Dr. Santosh Chavan**, **Dr. Santosh Kumar B. Y.**, **Mr. Vashista G.A.**, **Mr. Mohanraj G.T.**, **Mr. Pavankumar**

R. Sondar, and **Dr. Aruna M. N.**, for their constant help, encouragement, and with whom I shared many laughs and tears. They have been supportive at all my ups and downs and their timely help and moral support.

Finally, I would like to pay my sincere and deepest sense of gratitude to **my parents** and **entire family members** who taught me values and brought up me to achieve this higher degree, and constant encouragement, love and affection throughout life have made it possible for me to reach this one of the dream stages. They have been patient in positioning themselves with me when I was stressed, and they have been unselfishly pleased with my accomplishments. Without their unending support, I would never have been able to do what I managed to reach this stage.

The list keeps going on, and there are many others I mention. There are people who have helped me in all the way and provided their support directly or indirectly and encouraged me throughout all these years. I merely will have to limit myself to a few words: **I THANK YOU ALL..!** The successful completion of this thesis would not have been possible without them.


KALINGA T.

ABSTRACT

Smart materials are a new class of materials that possess adaptive capabilities which include sensing, responding and regulatory in a precise manner to the change of its environment stimuli, and are of great interest in structural, robotics, biomedical, marine, aerospace, and spacecraft technologies. Fiber Optics, Piezoelectric (PE), Magnetorheological (MR), Magnetostrictive (MS), Chromogenic, Electrorheological (ER), Electrostrictive (ES), Shape Memory Polymers (SMPs), and Shape memory alloys (SMAs) are the most common smart materials. Among these, SMAs exhibit a peculiar property in that deformed material can restore its original/predefined shape either by increasing the temperature or removing the load, which is known as the shape memory effect (SME) and “pseudoelasticity (PE) or superelasticity (SE)”, respectively. In addition, certain SMAs can exhibit the magnetic shape memory effect (MSME) by undergoing magnetic-field-induced reverse martensitic transformations. The merits of these unique properties attract the use of SMAs as dampers and actuators in smart/adaptive structures to suppress unwanted vibrations and provide seismic protection with the adoption of passive, active, semi-active, or hybrid control strategies.

The functional and mechanical properties of various groups of SMAs are still being progressive in the development and implementation of a novel, cost-effective, and long functional SMA for the vibration damping and isolation of mechanical and civil structures. Ni-Ti-based shape memory alloys (popularly known as Nitinol-based SMAs) are the most commonly used in many applications and already had a commercial presence due to their superior advantages, such as high strain recovery and long functional life, however, these are restricted its vast usage due to shortcomings like processing difficulties and high cost. Cu-Al-based SMAs are selected as a prime alternative to Ni-Ti-based SMAs owing to their ease of manufacture and economical, and this has motivated to develop the suitable Cu-Al-based shape memory alloys.

The aim of this thesis is to design and develop Cu-Al-Be-based polycrystalline shape memory alloys with improved microstructure, enhanced mechanical properties, better pseudoelastic shape/strain recovery, and suitability for use as seismic protection material to isolate vibrations through a passive control strategy. The present investigation has been carried out on the influence of variations in the weight percentage of Copper (Cu), Aluminium (Al), Beryllium (Be) and the grain refiners, namely Boron (B), zirconium (Zr), on the alloy phases, microstructure, mechanical, and pseudoelastic hysteresis properties. Outcomes of the present investigation reveals that Al followed by Be plays a vital role in the alloy phase modifications i.e., parent austenite, martensite or mixed phase at room temperature. The minimal addition of quaternary boron and zirconium grain refiners leads to substantial grain refinement, enhanced mechanical properties, and better pseudoelastic shape recovery. Because of these improvements in properties, they are identified as suitable for the passive damper in mechanical and civil structure applications at ambient temperature.

Keywords: *Cu-Al-Be shape memory alloys, Grain refinement, Heterogeneous nucleation, Serrated grains, Phase transformation temperatures, Mechanical properties, Pseudoelasticity.*

CONTENTS

CONTENTS	i
LIST OF FIGURES.....	iv
LIST OF TABLES.....	vii
ABBREVIATIONS.....	viii
ROMAN SYMBOLS	ix
GREEK LETTERS	xi
1 INTRODUCTION.....	1
1.1 BACKGROUND OF STUDY	1
1.2 SMART MATERIALS	3
1.2.1 Types of Smart Materials.....	3
1.3 SHAPE MEMORY ALLOYS	7
1.3.1 Crystallography of Phase Transformations in SMAs	7
1.3.2 Phenomenology of Phase Transformation in SMAs.....	8
1.4 CURRENT DEVELOPMENT AND APPLICATIONS OF SMART MATERIALS	11
1.5 LIMITATIONS OF STUDY	13
1.6 MOTIVATION OF THE PRESENT WORK	14
1.7 ORGANIZATION OF THESIS	14
2 LITERATURE SURVEY.....	16
2.1 INTRODUCTION	16
2.2 SHAPE MEMORY ALLOYS	16
2.3 TYPES OF SHAPE MEMORY ALLOYS.....	17
2.3.1 Ni-Ti SMAs	18
2.4 TYPES OF COPPER-BASED SHAPE MEMORY ALLOYS ..	19
2.4.1 Cu-Zn SMAs.....	20
2.4.2 Cu-Zn-Al SMAs.....	21

2.4.3	Cu-Al SMAs	22
2.4.4	Cu-Al-Ni SMAs	24
2.4.5	Cu-Al-Mn SMAs	27
2.4.6	Cu-Al-Be SMAs.....	29
2.5	GRAIN REFINEMENT	31
2.5.1	Heat Treatments	32
2.5.2	Grain Refiners	34
2.5.3	Severe Plastic Deformation.....	39
2.5.4	Melt Spinning.....	40
2.6	PHASE TRANSFORMATION TEMPERATURES	40
2.6.1	Quaternary Alloying Elements	41
2.6.2	Effect of Thermal Treatments.....	42
2.7	PSEUDOELASTIC BEHAVIOR	43
2.8	IDENTIFICATION OF THE PROBLEM	46
2.9	RESEARCH GAPS	47
2.10	OBJECTIVES	48
2.11	CLOSURE.....	48
3	MATERIALS AND METHODS.....	49
3.1	INTRODUCTION.....	49
3.2	ELEMENTAL COMPOSITIONS	49
3.3	METALS AND PURITY	50
3.4	METHODOLOGY.....	51
3.4.1	Alloy Preparation	53
3.4.2	Characterization	56
3.5	CLOSURE.....	62
4	RESULTS & DISCUSSION	63
4.1	INTRODUCTION.....	63
4.2	TERNARY Cu-Al-Be SMAs	63
4.2.1	X-ray Diffraction (XRD) – Phases Identification.....	64
4.2.2	Microstructure – Grain Size.....	65

4.2.3	Phase Transformation Temperatures	66
4.2.4	Mechanical Properties and Fracture Morphology.....	67
4.2.5	Pseudoelasticity and Microstructural Modifications	69
4.3	QUATERNARY Cu-Al-Be-B SMAs.....	70
4.3.1	Phases and Morphology.....	70
4.3.2	Microstructure – Grain Size.....	72
4.3.3	Phase Transformation Temperatures	74
4.3.4	Mechanical Properties and Fracture Morphology.....	77
4.3.5	Pseudoelasticity and Microstructural Modifications	79
4.4	QUATERNARY Cu-Al-Be-Zr SMAs.....	87
4.4.1	Phases and Morphology.....	87
4.4.2	Microstructure – Grain Size.....	90
4.4.3	Phase Transformation Temperatures	92
4.4.4	Mechanical Properties and Fracture Morphology.....	94
4.4.5	Pseudoelasticity and Microstructural Modifications	97
4.5	CLOSURE	106
5	CONCLUSIONS & FUTURE SCOPE	107
5.1	CONCLUSIONS.....	107
5.2	SCOPE FOR FURTHER RESEARCH	109
	REFERENCES	110
	LIST OF PUBLICATIONS BASED ON Ph.D. RESEARCH WORK	144
	BIODATA.....	145

LIST OF FIGURES

Figure 1.1 Tree of smart materials based on types of coupling.	4
Figure 1.2 Types of smart materials based on energy transformation.	6
Figure 1.3 Phases and their crystal structures	8
Figure 1.4 Shape Memory Effect behavior of SMAs	9
Figure 1.5 Pseudoelastic behavior of SMAs.....	10
Figure 1.6 Product forms of shape memory alloy.....	13
Figure 2.1 Types of binary SMAs.....	18
Figure 2.2 Types of Cu-based SMAs.....	20
Figure 2.3 Pseudo-binary Cu-Zn-Al ₆ phase diagram.....	21
Figure 2.4 Binary Cu-Al phase diagram	23
Figure 2.5 Pseudo-binary Cu-Al-Ni ₄ phase diagram	25
Figure 2.6 Pseudo-binary Cu-Al-Mn ₁₀ phase diagram	27
Figure 2.7 Quasi-binary Cu-Al-Be _{0.47} phase diagram.....	30
Figure 3.1 Copper.	50
Figure 3.2 Aluminium buttons.....	50
Figure 3.3 CuBe ₄ master alloy.....	51
Figure 3.4 (a) Photograph of CuB ₂ inoculant and (b) EDS of CuB ₂ inoculant.	51
Figure 3.5 (a) Photograph of Cu ₅₁ Zr ₁₄ inoculant and (b) EDS of Cu ₅₁ Zr ₁₄ inoculant..	51
Figure 3.6 Flow chart of methodology.	52
Figure 3.7 Photographs of (a) Induction melting furnace with argon gas setup and (b) Muffle furnace with argon gas setup.	54
Figure 3.8 Photographs of (a) Alloy plate and (b) Tensile specimen.	54
Figure 3.9 Stages of the preparation and processing of Cu-Al-Be-based SMAs.....	55
Figure 3.10 Schematic of the measurement for phase transformation temperatures from DSC curves.	58
Figure 3.11 Schematic of the pseudoelasticity (PE) test.....	61
Figure 4.1 Normalized X-ray diffractograms of Cu-Al-Be SMAs.....	64
Figure 4.2 Microstructures of Cu-Al-Be SMAs: (a) A ₁ , (b) A ₂ , (c) A ₃ and (d) A ₄	65
Figure 4.3 DSC curves of Cu-Al-Be SMAs.....	66

Figure 4.4 Tensile properties of Cu-Al-Be SMAs: (a) engineering stress-strain plots and (b) ultimate tensile stress (σ_{max}) and ultimate tensile strain (ϵ_{max}).....	68
Figure 4.5 FESEM images of the fracture surface of Cu-Al-Be SMAs: (a) A_2 , (b) A_3 and (c) A_4	69
Figure 4.6 Normalized XRD profiles of the betatized and quenched Cu-Al-Be-B SMAs.	71
Figure 4.7 (a) FESEM image of alloy B_4 and (b)-(d) EDS spectrums of alloy B_4	72
Figure 4.8 Microstructures of Cu-Al-Be-B SMAs: (a) B_1 , (b) B_2 , (c) B_3 and (d) B_4 ..	74
Figure 4.9 DSC curves of Cu-Al-Be-B SMAs.....	76
Figure 4.10 Tensile properties of Cu-Al-Be-B SMAs: (a) engineering stress-strain plots and (b) ultimate tensile stress (σ_{max}) and ultimate tensile strain (ϵ_{max}).	78
Figure 4.11 FESEM images of the fracture surface of Cu-Al-Be-B SMAs: (a) B_1 , (b) B_2 , (c) B_3 and (d) B_4	79
Figure 4.12 (a) Stress-strain hysteresis responses of Cu-Al-Be-B SMAs for the deformation strain, $\epsilon_d = 3\%$ and (b) Optical micrograph of the pseudoelastically deformed alloy B_4	82
Figure 4.13 Stress-strain hysteresis responses of Cu-Al-Be-B SMAs for the deformation strain, $\epsilon_d = 4\%$	83
Figure 4.14 Stress-strain hysteresis responses of Cu-Al-Be-B SMAs for the deformation strain, $\epsilon_d = 5\%$	84
Figure 4.15 Retained martensite in SMAs: (a) A_3 , (b) B_1 , (c) B_2 , and (d) B_3	84
Figure 4.16 Variations in the residual strain (ϵ_r) for different deformation strains, ϵ_d	85
Figure 4.17 Normalized XRD profiles of the pseudoelastically deformed Cu-Al-Be-B SMAs.	86
Figure 4.18 Normalized X-ray diffractograms of Cu-Al-Be-Zr SMAs.....	88
Figure 4.19 FESEM images of Cu-Al-Be-Zr SMAs: (a) Zr_1 , (b) Zr_2 , (c) Zr_3 , (d) Zr_4 and (e) Zr_5 , and (f-h) EDS of Zr_5	89
Figure 4.20 Microstructures of Cu-Al-Be-Zr SMAs: (a) Zr_1 , (b) Zr_2 , (c) Zr_3 , (d) Zr_4 and (e) Zr_5	91
Figure 4.21 DSC thermograms of Cu-Al-Be-Zr SMAs.....	93

Figure 4.22 Tensile properties of Cu-Al-Be-Zr SMAs: (a) engineering stress-strain plots and (b) ultimate tensile stress (σ_{max}) and ultimate tensile strain (ϵ_{max}).....	95
Figure 4.23 FESEM images of the fracture surface of Cu-Al-Be-Zr SMAs: (a) Zr_1 , (b) Zr_2 , (c) Zr_3 and (d) Zr_4 and (e) Zr_5	97
Figure 4.24 (a) Stress-strain hysteresis of the alloy Zr_1 and (b) optical micrograph of the pseudoelastically deformed alloy Zr_1	101
Figure 4.25 (a) Stress-strain hysteresis of the alloy Zr_2 and (b) optical micrograph of the pseudoelastically deformed alloy Zr_2	102
Figure 4.26 (a) Stress-strain hysteresis of the alloy Zr_3 and (b) optical micrograph of the pseudoelastically deformed alloy Zr_3	103
Figure 4.27 (a) Stress-strain hysteresis of the alloy Zr_4 and (b) optical micrograph of the pseudoelastically deformed alloy Zr_4	104
Figure 4.28 Residual strain of Cu-Al-Be-Zr SMAs: Zr_1 (◆), Zr_2 (●), Zr_3 (▲) and Zr_4 (▼) for different deformation strains.....	105
Figure 4.29 Stress hysteresis of Cu-Al-Be-Zr SMAs: Zr_1 (◆), Zr_2 (●), Zr_3 (▲) and Zr_4 (▼) for different deformation strains.....	105
Figure 4.30 Normalized X-ray diffractograms of the pseudoelastically deformed Cu-Al-Be-Zr SMAs.....	106

LIST OF TABLES

Table 3.1 Elements and their weight percentages.....	49
Table 3.2 Type of metals and their purity.....	50
Table 4.1 Elemental compositions of Cu-Al-Be SMAs.....	64
Table 4.2 Phase transformation temperatures ($^{\circ}\text{C}$), enthalpies (J/g), and thermal hysteresis ($^{\circ}\text{C}$) of Cu-Al-Be SMAs.	67
Table 4.3 Elemental compositions of Cu-Al-Be-B SMAs.....	70
Table 4.4 Transformation temperatures ($^{\circ}\text{C}$), enthalpies (J/g) and thermal hysteresis ($^{\circ}\text{C}$) of Cu-Al-Be-B SMAs.	76
Table 4.5 Elemental compositions of Cu-Al-Be-Zr SMAs.	87
Table 4.6 Transformation temperatures ($^{\circ}\text{C}$), enthalpies (J/g), e/a ratio and thermal hysteresis ($^{\circ}\text{C}$) of Cu-Al-Be-Zr SMAs.	94

ABBREVIATIONS

ARB	-	Accumulative roll bonding
ASTM	-	American society for testing material
BCC	-	Body-centered cubic
DSC	-	Differential scanning calorimeter
ECAP	-	Equal channel angular pressing
ECAR	-	Equal channel angular rolling
EDS	-	Energy dispersive spectrum
FCC	-	Face centered cubic
FESEM	-	Field emission scanning electron microscope
ICP-OES	-	Inductively coupled plasma optical emission spectrometer
OM	-	Optical microscope
PE	-	Pseudoelasticity
REE	-	Rare-earth element
SMA	-	Shape memory alloy
SME	-	Shape memory effect
UTM	-	Universal testing machine
XRD	-	X-ray diffraction

ROMAN SYMBOLS

Al	-	Aluminium
A_f	-	Austenite finish temperature
A_s	-	Austenite start temperature
Au	-	Aurum (Gold)
B	-	Boron
Be	-	Beryllium
Cd	-	Cadmium
Ce	-	Cerium
Co	-	Cobalt
Cr	-	Chromium
Cu	-	Copper
Fe	-	Iron
FeCl₃	-	Ferric chloride
Ga	-	Gallium
Gd	-	Gadolinium
HCl	-	Hydrochloric acid
Hf	-	Hafnium
HNO₃	-	Nitric acid
In	-	Indium
M_f	-	Martensite finish temperature
Mg	-	Magnesium
Mn	-	Manganese
Mo	-	Molybdenum
MPa	-	Mega Pascal
M_s	-	Martensite start temperature
Nb	-	Niobium
Ni	-	Nickel
Pd	-	Palladium
Pt	-	Platinum
Si	-	Silicon

Sn - Tin
Ti - Titanium
Tl - Thallium
V - Vanadium
wt.% - Weight Percentage
Y - Yttrium
Zn - Zinc
Zr - Zirconium

GREEK LETTERS

μm	-	Micron or Micrometer
σ_{cs}	-	Critical stress to start stress-induced martensite
$d\sigma_{PE}/d\varepsilon$	-	Pseudoelastic transition slope
$\Delta\sigma$	-	Stress hysteresis
ε_d	-	Deformation strain
ε_r	-	Residual strain
β	-	Disordered austenite
β_1	-	DO_3 -type ordered austenite
β'_1	-	Orthorhombic $18R$ -type martensite
γ'_1	-	Monoclinic $2H$ -type martensite
γ_2	-	Cu_9Al_4
ΔH	-	Enthalpy difference

CHAPTER 1

INTRODUCTION

1.1 BACKGROUND OF STUDY

Over the past three decades, significant research efforts have been made in the domain of structural vibration control devices to study and mitigate critical vibration problems (Shiba et al. 1998). Vibration is one of the most relevant problems regularly encountered in machine components, automobiles, aerospace vehicles, and civil structures. The effect of severe vibration induced by the seismic and/or wind energies generates extreme deformations and leads to instability and catastrophic failures of the structures. Due to this, vibrational analysis has become an important aspect for the safe designing of mechanical, acoustic, and structural systems. A conventional structural system is typically designed to achieve a specific set of intended functions under pre-determined loads. Such a conventional system cannot succeed in developing its ability against unexpected severe vibrations, loads, and forces unless a protective safety factor is sufficiently large. However, this conventional approach incurs increased construction costs. Besides, the randomness and severity of vibration/force excitations exceeds the design criterion and leads the structures to catastrophic failures (Mo et al. 2019; Zhang et al. 2009b), emphasizing the importance of the mitigation of vibration on the critical civil structures which includes bridges and buildings.

The current goals of the mechanical and civil engineering industries required light weight and the least number of advanced composite materials with simple design, and to improve the efficiency as well as the performance level of structures by isolating the unwanted vibrations caused by wind and/or seismic loading. To meet these requirements, many new smart materials have been developed and embedded in the composites, which yields higher stiffness, greater flexibility (automatically adapt/adjust to the service conditions toward structural safety), economic considerations, and good serviceability of the structures. Moreover, this type of embedded structure offers significant vibration absorption and seismic isolation with the conjunction of various

active, semi-active, passive or hybrid control strategies (Alvandi and Ghassemieh 2014; Symans and Constantinou 1999). Therefore, these structures are popularly termed “smart structures” or “adaptive structures”.

The most commonly adopted smart materials in vibration dampers and seismic isolators for the mitigation of unwanted vibrations of structural systems are piezoelectric materials, magnetostrictive (MS) materials, magnetorheological (MR) materials, and shape memory alloys (SMAs). The smart materials are highly responsive to changes in electric, magnetic field, thermal or mechanical load, leading to significant changes in shape, stiffness, natural frequency, damping, and other mechanical parameters. Piezoelectric materials have a unique reversible electro-mechanical coupling effect. Due to this effect, an electric charge (voltage) is generated when a mechanical load is applied, and conversely, an applied voltage (electric field) will be produced mechanical deformations *viz.* stress and/or strains. The piezoelectric materials are employed as actuators for active control (Chen et al. 2019; Fallah and Ebrahimnejad 2013) and semi-active control (Lu et al. 2010; Ozbulut and Hurlebaus 2010) of the seismic responses of building structures. The magnetostrictive effect/response of materials is similar to piezoelectric materials. The MS effect is based on the coupling of magnetic field and dipoles, which makes them useful in the actuators and sensors for vibration damping and health monitoring of the bridge structures (Braghin et al. 2012; Clemente et al. 2016; Moon et al. 2007). MR fluids and MR elastomers are a class of MR materials, which exhibit field-dependent properties that are changed as a function of the magnetic field, and are termed as MR effect. These two MR materials are also used to develop semi-active control systems for the seismic isolation of both bridge and building structures (Gu et al. 2020; Li et al. 2013; Spencer and Nagarajaiah 2003). SMAs hold peculiar thermomechanical behaviors/properties such as shape memory effect (SME) and pseudoelasticity (PE) associated with thermal- or stress-induced reversible hysteretic austenite and martensite phase transformations. These two special properties have made them the most popular substances for vibration controllers and seismic isolators (Saadat et al. 2002; Song et al. 2006). Shape memory alloy undergoes relatively large deformations that include bending, twisting, stretching or compressing, and the deformed SMA returns to its original shape by heating (SME) and mechanical

unloading (PE). The shape memory effect property of SMAs is used for designing an actuator, which acts as a vibration suppression element with the conjunction of active or semi-active control strategies (Suzuki and Kagawa 2010; Tai and Ahn 2011; Vishal et al. 2018). The pseudoelastic behavior of SMAs makes them well-suited passive dampers for vibration control and seismic response isolation of several civil structures (Ozbulut et al. 2011).

1.2 SMART MATERIALS

Smart composite/alloy materials are a new group of materials that possess adaptive capabilities in a specific manner for environmental/external stimuli. These smart materials change their properties based on the functions of external stimuli, such as thermal, electrical, magnetic, static/dynamic loads, pressure, nuclear radiation, chemicals, and environmental factors including humidity, moisture, heat and light. The changeable physical properties/parameters of these stimuli are associated with shape, stiffness, frequency, viscosity, buckling or damping. This kind of ‘smartness’ in the materials is achieved by altering its elemental composition, using special processing techniques, or microstructure modifications, which allows them to respond in a controlled manner to various levels of stimuli. Smart materials when interacting with structural systems should have the capability to sense, respond, measure, adapt, and detect the change of its selected variables. For that reason, the smart materials are also referred to as intelligent, adaptive or responsive materials, and these materials have great interest to use in aerospace, marine, space-craft automotive, robotics, biomedical, and structural industries (Bahl et al. 2020; Chopra and Sirohi 2013; Saadat et al. 2002; Yun et al. 2011) for reliable and improved performance of the systems.

1.2.1 Types of Smart Materials

Smart materials are categorized on the basis of their types of coupling capabilities as well as their kind of energy transformation between the systems. Classification with a brief explanation of the different smart material families, as shown in Figures 1.1 and 1.2.

1. Types of coupling

- a. *Direct coupling*: occurs when one of the mechanical or non-mechanical field acts as the input and the other as the output.
- b. *Indirect coupling*: The mechanical behavior of the smart system is indirectly coupled with the electric/magnetic field. A change in electric or magnetic field causes a change in the viscosity of the fluid, which alters the mechanical behavior of the smart system.

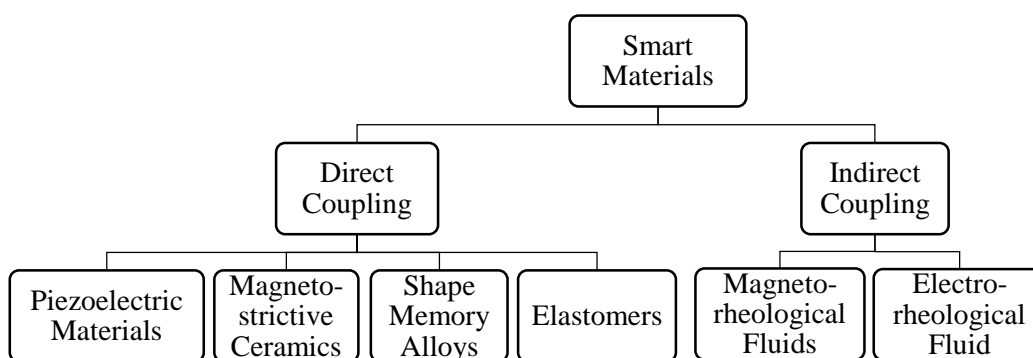


Figure 1.1 Tree of smart materials based on types of coupling.

2. Type of energy transformation

- a. *Photo-Mechanical*: Fibre optics.
 - **Photomechanical materials**: undergo a shape change when exposed to light
- b. *Magneto-Mechanical*: Magnetorheological fluids and elastomers, Magnetostrictive materials.
 - **Magnetorheological fluids (MRFs)**: are fluids whose physical state can be modified by altering the magnetic field. MRFs are composed of magnetizable particles (micro-size iron powder), carrier fluid (water, ethanol, silicone oil), and additives (silica, grease).
 - **Magnetorheological elastomers (MREs)**: are a type of soft magneto-active viscoelastic solid materials, whose mechanical properties are altered

by varying the magnetic field, e.g., polyurethane or silicone rubber containing carbonyl iron powder.

- **Magnetostrictive materials:** are ferromagnetic materials that exhibit a change in shape under the stimulus of a magnetic field, e.g., Co-Ni, Fe-Co, Fe-Al, Fe-Ni, and ferrites.

c. *Electro-Mechanical:* Piezoelectric materials, Electrorheological fluids and elastomers, and Electrostrictive materials.

- **Piezoelectric materials:** The term “piezo” means ‘pressure’, and “electricity”, denoting electrical charges. The piezoelectric effect generally takes place in all directions and is classified into two main groups: 1) direct and 2) inverse. Piezoelectrics are available in the form of ceramics and polymers that converts mechanical work (i.e., stress) into voltage/electric charge across the material and is called a direct piezoelectric effect, also known as generator/sensor effect. On the other hand, these materials exhibit a mechanical property change (i.e., strain) by varying the voltage/electric fields and are called the inverse piezoelectric effect (i.e., actuator effect). Piezoelectric materials, such as lead zirconate titanate, polyvinylidene fluoride, lithium niobate, quartz, etc., are also known as ferroelectric materials.
- **Electrorheological fluids (ERFs):** change their properties like stress and viscosity when they are subjected to a change in the electric fields. ERFs are composed of carrier fluids (silicone oil, kerosene, paraffin, vegetable oil) and additive particles (cellulose, alumina, silicates, charcoal, zeolites, titania, starch).
- **Electrorheological elastomers (EREs):** are electro-active polymers composed of dielectric materials that modifies the mechanical properties upon the application of the electric fields, e.g., styrene-acrylic-copolymer, styrene-butadiene, and silicone rubber containing barium titanate.

- **Electrostrictive materials:** are electroactive materials that undergo a shape change upon the stimulus of an electric field, e.g., lead magnesium niobate, lead magnesium niobate-lead titanate, lanthanum-doped lead magnesium niobate-lead titanate, and lead lanthanum zirconate titanate.

d. *Thermo-Mechanical:* Shape memory alloys.

- **Shape memory alloys (SMAs):** changes the shape under large deformation and recover to their original/predefined shape either by thermal load imposition (SME) or mechanical load-removal (PE). The popular types of SMAs are Ni-Ti, Ni-Ti-X (X = Cu, Cr, V, Zr, Co, Hf, Pd), Cu-Zn-Al, and Cu-Al-X (X = Ni, Mn, Be, Fe).

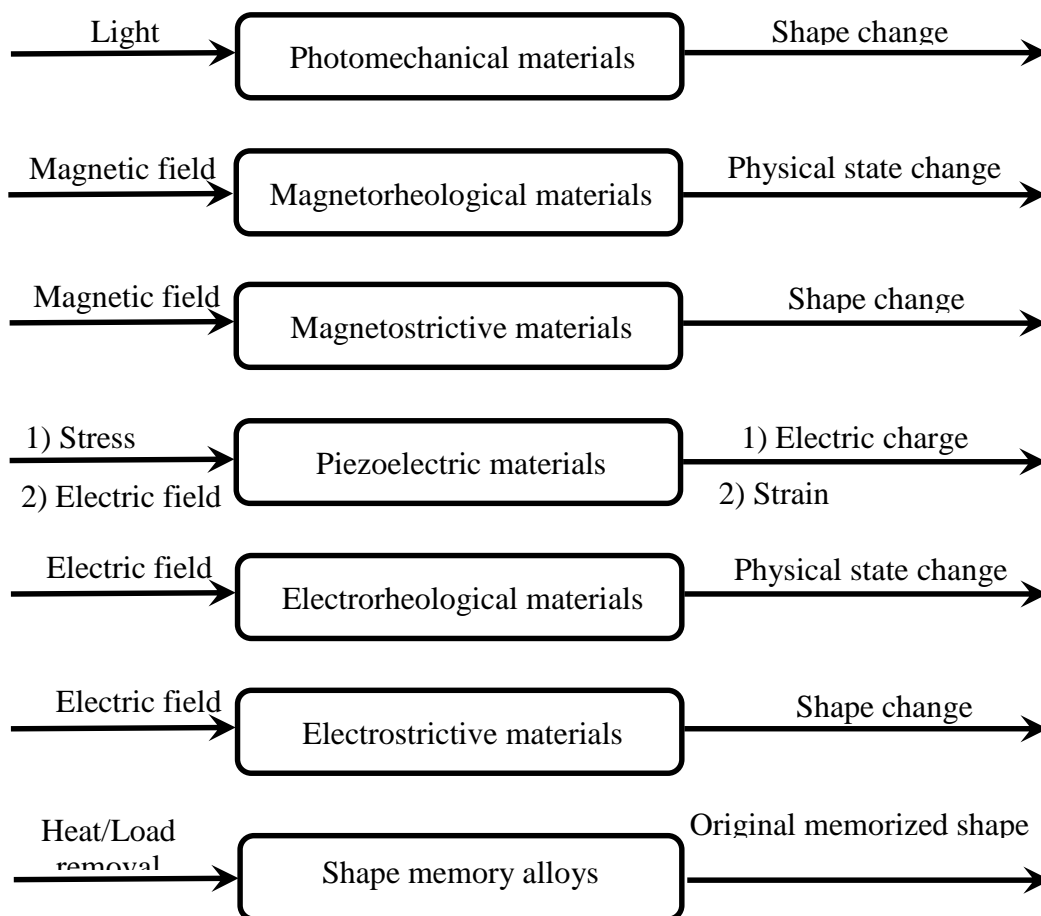


Figure 1.2 Types of smart materials based on energy transformation.

1.3 SHAPE MEMORY ALLOYS

Shape memory alloys (SMAs) are a family of metallic materials that possess unique thermo-mechanical properties. These distinct properties of SMAs unveil that mechanically deformed materials are possibly reverted back to their original/predefined shape either by thermal load imposition or simply removing the mechanical load (Perkins and Sponholz 1984; Tadaki 1998; Ziółkowski 2015). SMAs undergo a first-order, solid-solid diffusionless shear transformation known as martensitic transformation and this martensitic transformation is crystallographically reversible (Montecinos et al. 2006; San Juan et al. 2012; Torra and Tachoire 1992). In SMAs, the martensitic transformation is thermoelastic, in which the phase interfaces possess good migration capability.

1.3.1 Crystallography of Phase Transformations in SMAs

Shape memory alloys have shown two thermodynamically stable phases, namely, austenite and martensite. Austenite is a high-temperature phase, also called the parent phase that has a close-packed Face-Centred-Cubic (FCC) crystal structure. Martensite is a low-temperature phase with a crystal structure of Body-Centred Cubic (BCC) in Ni-Ti-based SMAs and “Orthorhombic or Monoclinic” in Cu-Al-based SMAs (Narasimha 2020). Figure 1.3 depicts a schematic of various crystal structures of shape memory alloys. Martensite consists of different orientation directions, called variants. These variants are usually arranged in two ways, i.e., twinned martensite (combination of self-accommodated variants with no observable macroscopic shape change) and detwinned martensite (single variant with large macroscopic shape change). The crystal structures of both martensitic and austenitic phases are temperature-dependent and therefore possess distinct properties for every phase. The martensitic phase is relatively soft and has a twinned molecular structure in the absence of applied load/deformation, which reorients into a detwinned structure when deformed or loaded. The austenitic phase is a stronger, harder and rigid phase of shape memory alloys. Transformation temperatures are those temperatures at which austenite and martensite of the alloy change from one state to another. The phase transformations start at one temperature and end at another because SMAs do not undergo their forward transformation (i.e.,

from austenite to martensite) and reverse transformation (i.e., from martensite to austenite) at the same temperature. Therefore, the start and finish temperatures of austenite and martensite are different depending on whether the alloy is heating (endothermic reaction) or cooling (exothermic reaction), as confirmed from (Moghaddam et al. 2017; de Oliveira Ramos et al. 2018; Suresh and Ramamurty 2008; Treadway et al. 2015). In order of lowermost to uppermost transformation temperatures, are defined as follows:

- **Martensite finish temperature (M_f):** is the temperature at which the SMA is completely twinned martensite.
- **Martensite start temperature (M_s):** is the temperature at which austenite of SMA begins to change into martensite.
- **Austenite start temperature (A_s):** is the temperature at which martensite of SMA begins to change into austenite.
- **Austenite finish temperature (A_f):** is the temperature at which the SMA is complete austenite.

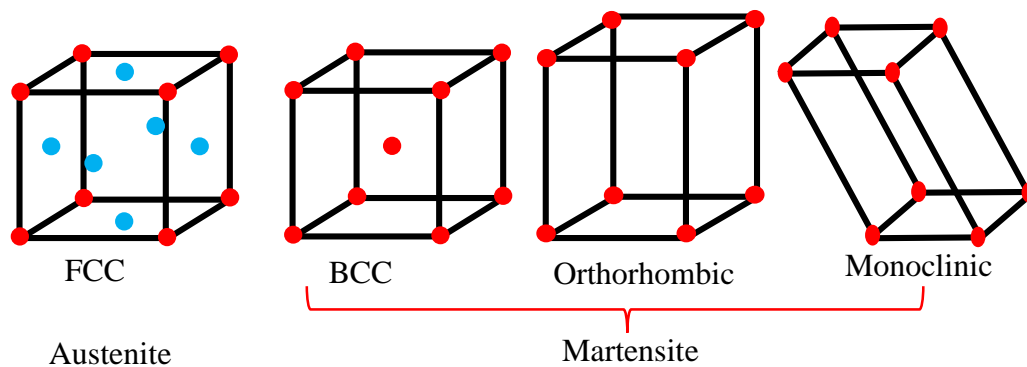


Figure 1.3 Phases and their crystal structures (Narasimha 2020).

1.3.2 Phenomenology of Phase Transformation in SMAs

Shape memory alloys are distinct from conventional metals and alloys because of their unique functional properties, namely the pseudoelasticity and shape memory effect, which are connected to reversible solid-state phase transformations.

1.3.2.1 Shape memory effect (SME)

“Shape memory effect” describes the ability to recover the original shape of deformed materials through a heating process (Duerig et al. 1990; Lagoudas 2008; Tadaki 1998). If the shape memory alloy quenched from the high-temperature disordered austenitic β -phase to ambient temperature (T), i.e., below the martensite finish temperature (M_f) forms the “martensite” phase in a self-accommodating twinned structure. In the low-temperature martensitic phase (i.e., $T < M_f$), SMA is easily deformed upon loading, causes a macroscopic shape change, and generates a large percent of inelastic strain due to the transformations from twinned martensite to detwinned martensite. In this phenomenon, the reoriented detwin configuration with a high residual strain is retained after unloading, and reverts back to its parent austenitic phase after being heated above the austenite finish temperature (A_f) and the deformation is completely recovered without residual strain, as shown in Figure 1.4. Further cooling to a temperature below its M_f , leads to the formation of twinned martensite again with no associated shape change is observed. Further, cooling to a temperature below its M_f results in the formation of twinned martensite again with no discernible shape change is observed (Hefzy et al. 2020; Lagoudas 2008). This feature provides good repeatability of SMAs to actuator applications.

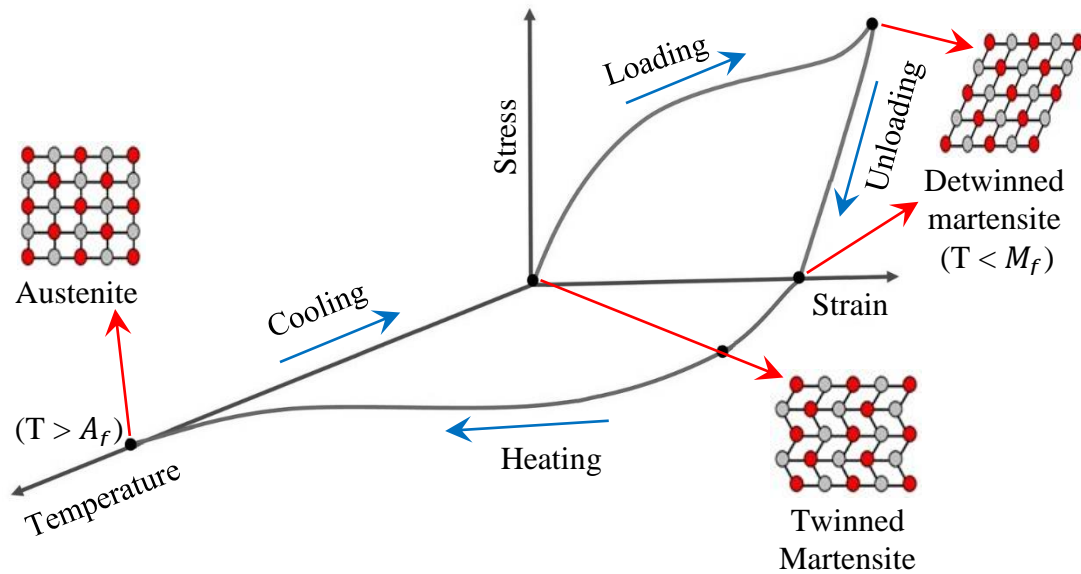


Figure 1.4 Shape Memory Effect behavior of SMAs (Behera et al. 2021, 2022).

1.3.2.2 Pseudoelasticity (PE)

“Pseudoelasticity” refers to the ability to recover the original shape of deformed materials by simple unloading (Duerig et al. 1990; Lagoudas 2008; Ziółkowski 2015), and this phenomenon is also known as “Superelasticity (SE)”. If the shape memory alloys are in their high-temperature parent phase (i.e., $T > A_f$), cubic austenite phase turns into stress-induced martensite (SIM) when it is subjected to deforming/loading. This occurrence is called “Forward Martensite Transformation” which produces a shear-like deformation strain. The stress-induced martensitic phase possesses a detwinned structure, which becomes unstable upon unloading. Hence, removal of the applied load causes the SMA to returns back to its parent austenitic phase, called “Reverse Martensite Transformation”, and the original/undeformed shape is restored without residual strain, as shown in Figure 1.5. The prefix “pseudo” in the phenomenon's name emphasizes that the loading-unloading cycle of SMA exhibits non-linear hysteresis loops, and this pseudoelastic hysteresis behavior differs from conventional non-linear elastic materials.

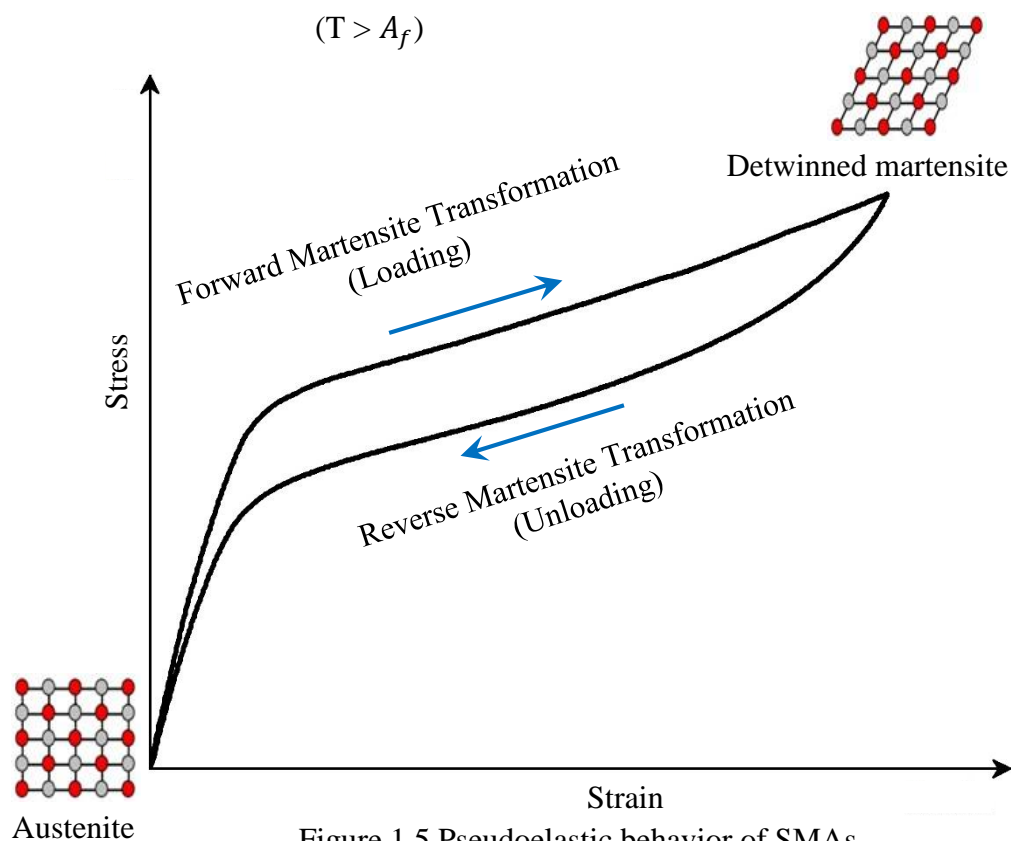


Figure 1.5 Pseudoelastic behavior of SMAs.

Pseudoelastic/Superelastic property of SMAs becomes a focus for energy absorption and dissipation due to their advantageous features that include high stiffness, passive vibration control strategy, and essential self-centering capability (Asgarian et al. 2016; Janke et al. 2005; Song et al. 2006; Zhu and Zhang 2007), makes them well suited as a damper in seismic applications.

1.4 CURRENT DEVELOPMENT AND APPLICATIONS OF SMART MATERIALS

Many researchers investigated the implementation of smart materials using various active, semi-active or passive control systems, as well as their limitations for vibration control and seismic isolation. In active control systems, piezoelectric actuators require a huge external power source to generate desired control forces for the attenuation of undesirable vibrations. The control forces are developed based on active feedback signals from sensors that measure the vibration excitations and/or response of the structures and are sent to the control actuators (Liao et al. 2011; Pastia et al. 2005). Semi-active control systems are a family of active systems, that requires a small external power source to change the parameters/properties of the control system (Li and Huo 2010; Liao et al. 2014). However, active control systems have several disadvantages including high energy consumption and large activation force. Semi-active control systems do not have the potential to destabilize the structures like active control systems (Spencer and Nagarajaiah 2003). In passive control systems, the use of smart materials attached or embedded in a structure improves the stiffness, structural damping, and controls the motion of the structure, thereby making it more stable to mitigate unwanted vibrations. These systems operate without external power sources, and they are economical and simple to use in vibration control applications to suppress seismic and wind-induced vibrations of the structures (Parulekar and Reddy 2009).

A seismic isolator, as a passive vibration control system, is one of the most widely accepted ways of preventing earthquake- and wind-induced damage to structures. Pseudoelastic/Superelastic behavior of SMAs in the seismic-resistant structures recovers relatively large inelastic deformation without any residual or negligible unrecoverable permanent deformation. Besides, the limitations in the passive hysteretic

damper application of SMAs are martensite stabilization and/or defects like dislocations/slip lines generated by cyclic deformation, which causes deterioration of pseudoelastic shape recovery and an increase in residual strains with respect to an increased number of loading-unloading cycles. Comparing the advantages and disadvantages, shape memory alloys have numerous advantages such as simple, easy installation, flexible configuration, large strain cycles, high energy density, great durability, high damping capacity, excellent re-centering capability, superior safety levels, good control of large forces, high resistance to fatigue and corrosion, no degradation with ageing, solid-state passive damper, and ease of serviceability (Alvandi and Ghassemieh 2014; Ozbulut et al. 2011; Parulekar and Reddy 2009). Therefore, pseudoelastic shape memory alloys are considered as the right candidate in civil structures for shape restoration, energy dissipation, seismic mitigation, and vibration damping applications, utilizing reversible stress-induced phase transformation of the alloy at temperatures higher than austenite finish temperature (A_f).

Past two decades, the pseudoelastic nitinol (Ni-Ti) SMAs in various geometrical shapes *viz.* plates/strips, bars/billets, wires, and tubes, as shown in Figure 1.6, have been considered as dampers in the adaptive structures for passive vibration control applications. This prime importance owing to their superior properties, i.e., high inelastic strain recovery, excellent corrosion resistance, better mechanical properties, good biocompatibility, and no external power supply required for deformation recovery. Besides, the pseudoelastic property of SMA is related to reversible stress-induced martensitic transformation, which occurs in the high-temperature phase (austenite). Both thermally- and stress-induced martensitic transformations in binary nitinol SMAs are influenced by the chemical composition of alloying elements. As the nickel content increases in binary Ni-Ti alloys, the transformation temperatures lowering and that requires higher critical stress to induce the martensitic transformation. The transformation temperatures of SMAs below ambient temperature resulted in stable pseudoelastic behavior. Ni-Ti SMAs possess transformation temperatures over the range of $15\text{ }^\circ\text{C} < A_f < 100\text{ }^\circ\text{C}$ by changing chemical composition of alloying elements. If the ambient/operating temperature is less than $15\text{ }^\circ\text{C}$ leads to degradation of pseudoelastic effect and is not feasible in real-time passive damping applications.

Further, ternary alloying elements, such as Cr, V and Cu have been investigated extensively to decrease the transformation temperatures though not feasible to use in practical applications owing to degradation of the pseudoelastic shape recovery with Cr and V (He et al. 2007). The addition of Cu to Ni-Ti alloy reduces the compositional sensitivity to the transformation temperatures (Gil et al. 2004).

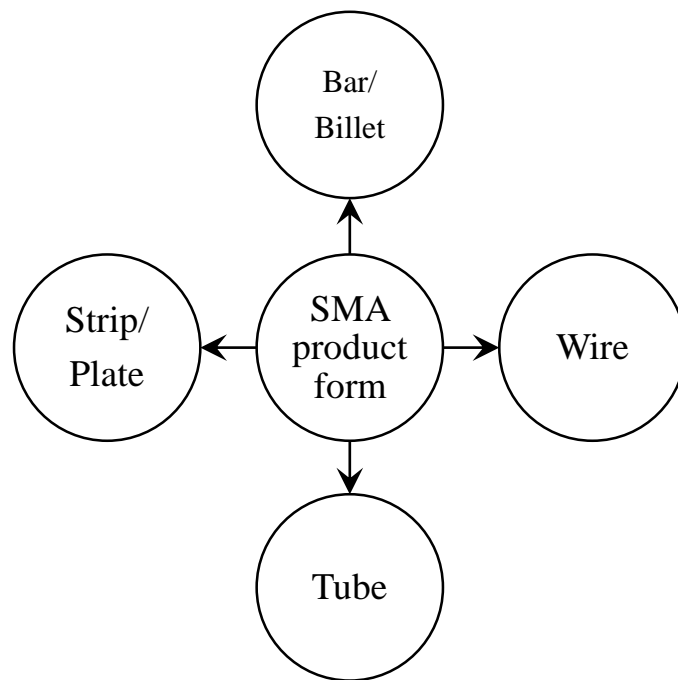


Figure 1.6 Product forms of shape memory alloy.

1.5 LIMITATIONS OF STUDY

Despite the advantages of Nitinol and Ni-Ti-based SMAs, still have some shortcomings, like their high cost and difficult manufacturability. The fabrication and processing of Nitinol implanted smart devices are complicated and thereby making them expensive. Due to the high reactivity of titanium element (Nakahata 2011; Ziółkowski 2015), melting and processing of SMAs must be carried out in vacuum controlled atmosphere to avoid contamination of the alloy (oxidation) that deteriorates the functional and mechanical characteristics as well as its performance.

1.6 MOTIVATION OF THE PRESENT WORK

The existing literature unveils that the copper-based alloys, such as Cu-Zn and Cu-Al binary alloys, also have pseudoelasticity and shape memory effect capabilities. As compared to the Ni-Ti-based SMAs, these SMAs are economical due to easy manufacturability and less expensive. Ternary element doped Cu-Al and Cu-Zn alloys i.e., Cu-Al-Be, Cu-Al-Mn, Cu-Al-Ni, and Cu-Zn-Al, SMAs have been developed (Higuchi et al. 1982; Lopez Del Castillo et al. 1986; Otsuka and Shimizu 1970; Pops and Ridley 1970), and their good strain recovery by PE and SME, superior damping and ease of modifying the phase transformation temperatures make them as a prime alternative to Ni-Ti-based SMAs. These advantageous features attracted and motivated to design an optimal elemental composition in order to develop a novel Cu-Al-based passive damper with the desired and improved properties for use as seismic protection material in smart structures.

1.7 ORGANIZATION OF THESIS

The thesis of the present study is composed of five chapters to address the purpose and nature of the research work. In summary, the chapters of this research work are organized as follows:

- **Chapter 1** introduces the background, types, working phenomenology, current development, and limitations of the smart materials for vibration damping applications. Further, this chapter discusses the motivation of the present research work.
- **Chapter 2** presents the types of shape memory alloys and a comprehensive literature survey on numerous techniques for modifications/enhancements in the properties of SMAs, viz. grain-size refinement, phase transformation temperatures, mechanical properties, and pseudoelastic responses. Finally, based on the existing literature, the research gaps and objectives of the present investigation are presented.

- **Chapter 3** discusses the details of materials, methods, apparatus, and methodology adopted in this investigation to fabricate and process the alloy plates/samples and their characterization.
- **Chapter 4** presents the investigation results, interpretation, and discussion of the evaluated SMAs.
- **Chapter 5** presents the key conclusions drawn from the investigation results and the recommendations for future research work.

CHAPTER 2

LITERATURE SURVEY

2.1 INTRODUCTION

This chapter provides a review of relevant literature that mainly focuses on the most significant and major contributions to the existing shape memory alloys (SMAs), such as thermal treatments, grain refiners-doping, and secondary processing methods. First, the literature on the historical developments in the research of SMAs is discussed. Further, the types of SMAs are reviewed. Second, the literature on numerous techniques for the enhancement in grain-size refinement, mechanical, and pseudoelastic response characteristics is presented. Third, dependent phase transformation temperatures and morphology on the alloying ternary- and quaternary-doped elements, their elemental compositions, and the different heat treatment processes are discussed. Finally, based on the existing literature, the identification of the problem, research gap, and objectives of the present investigation are presented.

2.2 SHAPE MEMORY ALLOYS

The history of research investigation on shape memory alloys (SMAs) and their inspirable unique properties, namely shape memory effect (SME) and pseudoelasticity (PE) are mainly linked to the solid-state thermoelastic martensitic transformations (which is a diffusion-less shear martensitic transformations) and a number of physical phenomena *viz.* Twinning and Detwinning are responsible for thermal shape memory (SME) and elastic shape memory (PE) effects in metallic alloys (Chowdhury and Sehitoglu 2017; Delaey et al. 1974; Duerig et al. 1990; Stoeckel 1995). In the 19th-century, the German physicist Adolf Martens recognized the first “low-temperature phase”, martensite microstructure using an optical microscope, and the first “high-temperature phase”, austenite, was named from the research work of the English physicist Charles Austen. In the 1930s, the first shape memory phenomenon was discovered. The origin of rubber-like elastic behavior at room temperature was found

from the research work of Olander in β -phase Au-Cd alloys (Ölander 1932), and this is the first evidence of pseudoelastic behavior in metallic alloys. Later, in 1938, Greninger and Mooradian observed thermoelastic effects, i.e., the appearance and disappearance of a martensite structure in the β -phase Cu-based alloys by cooling and heating, respectively (Greninger and Mooradian 1938).

The terminology of “Martensite transformation” was first proposed from the studies of Greninger in rapidly quenched β -phase Cu_{90.7}-Al_{9.3} (at.%) alloy (Greninger 1939a). A detailed study of thermoelastic martensitic transformations in Cu-based alloys was reported by Kurdyumov and Khandros (1949). The research work of Chang and Read have stated the SME behavior in Au-Cd alloys (Chang and Read 1951) by thermoelastic responses of the martensite phase, i.e., the transformations from austenite (β_1) to martensite (β'_1) on cooling below its martensite start temperature (M_s) and vice-versa on heating. The pseudoelastic behavior was originally reported from the studies of Reynolds and Bever in Cu-Zn alloys (Reynolds and Bever 1952) and subsequently, its appearance in In-Tl alloys (Burkart and Read 1953 and Basinski and Christian 1954) and Cu-Al-Ni alloys (Rachinger 1958). Buehler et al. (1961) discovered the first Nickel-Titanium (Ni-Ti) alloy at the Naval Ordnance Laboratory, United States Department of Defence. Since then, this alloy was commercialized under the standard trade name “Nitinol” simply derived from the combination of “chemical symbol of employed elements (NiTi) and in honor of Naval Ordnance Laboratory (NOL)”. The importance and the demand for shape memory alloys in most engineering and technological applications were not recognized, until the discovery of SME behavior in Nitinol SMA (Buehler et al. 1963; Buehler and Wang 1968). After this discovery, research interests became progressively more active in the development of a new family of shape memory alloys.

2.3 TYPES OF SHAPE MEMORY ALLOYS

The elements present in the middle part of the periodic table whose binary alloy systems exhibit shape memory properties. They are gold-cadmium (Au-Cd), silver-cadmium (Ag-Cd), indium-thallium (In-Tl), indium -cadmium (In-Cd), copper-zinc (Cu-Zn), copper-tin (Cu-Sn), copper-aluminium (Cu-Al), titanium-niobium (Ti-Nb),

titanium-gold (Ti-Au), titanium-palladium (Ti-Pd), titanium-platinum (Ti-Pt), nickel-aluminium (Ni-Al), iron-nickel (Fe-Ni), iron-palladium (Fe-Pd), iron-platinum (Fe-Pt), etc., including nickel-titanium (Ni-Ti). Amongst these SMAs, mainly three binary alloy systems, namely Ni-Ti, Cu- and Fe-based alloys are popularly known to exhibit the shape memory properties *viz.* SME and PE have been the focus of research in design, development and applications. Figure 2.1 presents the family tree of popular binary SMAs.

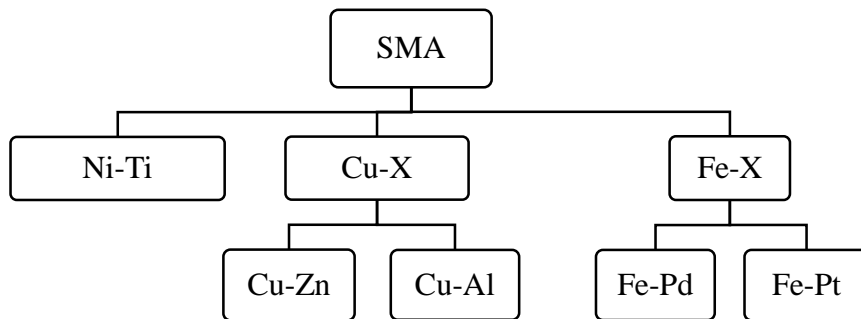


Figure 2.1 Types of binary SMAs.

2.3.1 Ni-Ti SMAs

Nitinol (Ni-Ti) SMAs exhibit excellent shape memory effect, thermal stability, good pseudoelastic strain recovery, and high corrosion resistance. These advantages of the nitinol shape memory alloys are used as actuators/sensors/dampers in numerous non-medical fields, such as aircraft (Hartl and Lagoudas 2007), robotics (Furuya and Shimada 1991; Wen et al. 1994), spacecraft (Garafolo and McHugh 2018; Wilke et al. 2000), Micro-Electro-Mechanical Systems (MEMS) and mini-actuators (Fujita and Toshiyoshi 1998; Mehrpouya and Bidsorkhi 2017; Nespoli et al. 2010), civil structures (Auricchio et al. 2006; Dieng et al. 2013; Torra et al. 2013), and automotive applications (Bellini et al. 2009; Stoeckel 1990). In addition, the researchers (Duerig et al. 1999; El Feninat et al. 2002; Sabahi et al. 2020) have presented a review on biomedical applications of nitinol SMAs due to their excellent biocompatibility. However, the martensitic transformation temperatures were modified at a limited level

by varying binary Ni-Ti SMAs chemical composition (Frenzel et al. 2010; Tang et al. 1999) and the different thermos-mechanical treatment processes and parameters (Kök et al. 2016; Razali and Mahmud 2015; Shahmir et al. 2011; Yeung et al. 2004; Yoon and Yeo 2004). Further, the addition of ternary alloying elements into Ni-Ti SMAs, such as Cr, V, Co, Al, Nb, Mo, Fe, and Cu have been investigated by the researchers (Frenzel et al. 2015; Fu et al. 2009; Liu et al. 2006; Tatar and Kurt 2020) to reduce the martensitic transformation temperatures. Such that good permanence of pseudoelastic and shape memory behaviors occurs at well below ambient temperature. Though the use of Ni-Ti-based SMAs is limited in applications because of their difficulties in manufacturing and expensive. An economical alternative to Ni-Ti-based SMAs, Cu-based SMAs were developed since the 1960s by the addition of binary and ternary alloying elements.

2.4 TYPES OF COPPER-BASED SHAPE MEMORY ALLOYS

Copper-based SMAs have shown potential to use in numerous applications due to their considerable good shape recovery behavior, small transformation hysteresis, high damping coefficient, ease of manufacturing, low cost, wide transformation temperatures range because of easy to reduce the martensitic transformation temperatures by selecting an appropriate alloy composition, which makes them an economical alternative to Ni-Ti-based SMAs (Aldas et al. 2014; Dasgupta et al. 2014; Niitsu et al. 2011; Nnamchi et al. 2019; Özkul et al. 2019). The most popular binary Cu-based shape memory alloys, namely Cu-Zn and Cu-Al SMAs are classified on the basis of alloying ternary-doped elements and are depicted in Figure 2.2. Additionally, they are briefly explored, including their advantages, limitations, and different strategies for overcoming the numerous challenges that come upon replacing the Ni-Ti-based SMAs, and these are discussed in the proceeding sections.

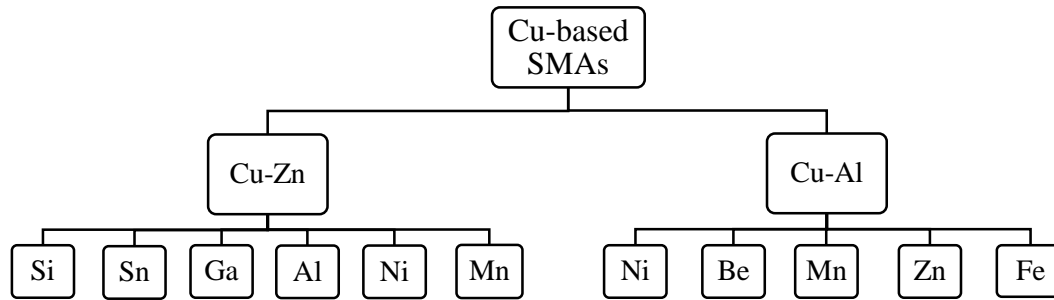


Figure 2.2 Types of Cu-based SMAs.

2.4.1 Cu-Zn SMAs

Binary Cu-Zn alloys containing 38.40 - 41.97 wt.% of Zn were investigated by the researchers for shape memory effect and pseudoelastic behavior (Cornelis and Wayman 1974; Schroeder et al. 1976; Wayman and Shimizu 1972), and the investigated results reveal that Cu-Zn SMAs exhibit good strain recovery. However, the main difficulty in the thermoelastic behavior of martensite in binary Cu-Zn alloys owes to the very high sub-zero martensitic transformation temperatures of these alloys (Cornelis and Wayman 1974). It is noted that the martensitic transformation temperatures of Cu-Zn alloys can be increased by the additions of ternary alloying elements such as Si, Sn, Ga, Al, or Ni (Dutkiewicz et al. 1993; Dutkiewicz and Morgiel 1989; Perkins 1974; Rapacioli and Ahlers 1979; Saburi and Nenno 1974; Sathish et al. 2014). Further, investigated for shape memory effect and/or pseudoelastic behavior on a number of ternary-doped Cu-Zn-X alloys, namely Cu-Zn-Al (Humbeeck et al. 1978; Perkins 1974; Rogueda et al. 1991), Cu-Zn-Si (Wield and Gillam 1972), Cu-Zn-Sn (Dvorak and Hawbolt 1975; Miura 2002), Cu-Zn-Ga (Delaey and Warlimont 1966; Wayman 1983), Cu-Zn-Ni (Sathish et al. 2014), and Cu-Zn-Mn (Chandrasekaran and Miodownik 1979). Among them, Cu-Zn-Al SMAs have become more popular and studied extensively due to their good shape memory behavior, high processing performance, and being quite economical to use in the applications (Najah Saud Al-Humairi 2020; Özkul et al. 2019).

2.4.2 Cu-Zn-Al SMAs

Cu-Zn-Al alloys were the first ternary Cu-based shape memory alloys developed as an economical alternative to Ni-Ti-based SMAs due to their low cost of the raw materials and ease of fabrication using conventional melting and processing apparatus. Pops and Ridley (1970) investigated the influence of Al-doping on the thermoelastic martensitic transformations of β -phase Cu-Zn alloys to validate the stress-induced martensitic transformations property, called pseudoelasticity (PE). Figure 2.3 shows a pseudo-binary phase diagram of Cu-Zn-Al_{6wt.%}, which also presenting a plot and its functional relationship for the reverse martensitic transformation temperature (A_s) and is depends on both Zn and Al contents. Rapacioli and Ahlers (1977) studied the DO_3 -type ordering of parent austenitic phase and Singh et al. (1978) calculated the critical temperature for DO_3 -type ordering formation in Cu-Zn-Al SMAs. They discovered that the DO_3 -type ordering temperature is highly depending on alloying compositions, i.e., reducing sharply with increasing both Zn and Al contents. Dutkiewicz and Morgiel (1986) investigated the effect of DO_3 -type ordering on the austenite (β_1) \rightleftharpoons martensite (β'_1) transformations in Cu-Zn-Al SMAs and is responsible for the shape recovery behavior.

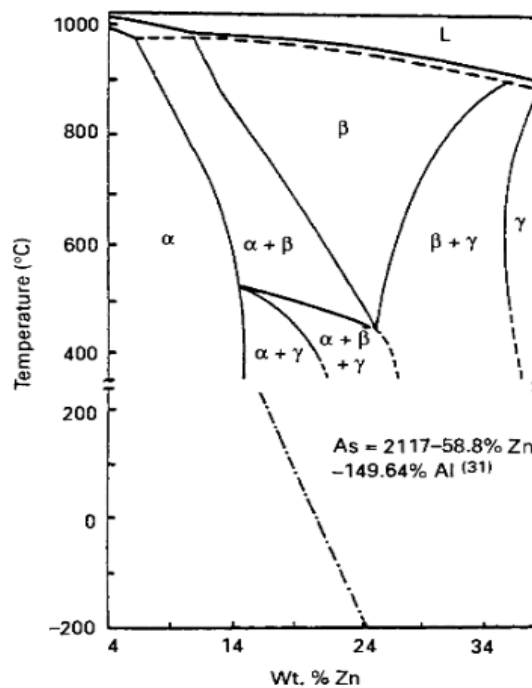


Figure 2.3 Pseudo-binary Cu-Zn-Al₆ phase diagram (Duerig et al. 1990).

Researchers (Guilemany and Gil 1990, 1992; Perkins 1974) have prepared and investigated the PE/SME characteristics of ternary Cu-Zn-Al SMAs by varying its elemental compositions, i.e., 62 - 76 wt.% of Cu, 12 - 37 wt.% of Zn, and 1 - 16 wt.% of Al, which yields phase transformation temperatures in the range of -100 to 100 °C. It was also revealed that increasing the Zn and Al elements-doping lowers the transformation temperatures. The alloys containing around 70 - 75 wt.% of Cu, 15 - 25 wt.% of Zn and 6 - 8 wt.% of Al have the phase transformation temperatures close to room temperature and possesses small thermal/stress hysteresis (Bundara et al. 2000; Guilemany and Gil 1990; Humbeeck et al. 1978), consequently exhibits good SME/PE. However, the use of SMAs in applications are restricted due to the prime limitations, such as coarse grain size leads to intergranular brittle failure (Melton and Mercier 1979) and rapid strain hardening causes some structural damages like retained/stabilized martensite plates/needles, slip defects, and plastic deformation by generated dislocations, which leads to high residual deformation in both martensitic- and austenitic-phase Cu-Zn-Al SMA samples (Janssen et al. 1979; Li and Ansell 1983; Perkins and Muesing 1983). This high residual deformation/strain retained with mechanical cycling limits repeatability of the phase transformations, i.e., $\beta_1 \leftrightarrow \beta'_1$, indicating deterioration in the pseudoelasticity of Cu-Zn-Al SMAs.

2.4.3 Cu-Al SMAs

Cu-Al alloys, like Cu-Zn alloys, undergo thermoelastic martensitic transformations and are noticed from the research work by Greinger (1939). Later, the scientists Nagasawa and Kawachi (1971) have found SME in the alloy Cu-Al₂₅ (at.%). Figure 2.4 depicts the relevant part of the binary Cu-Al phase diagram, which also shows a plot for the martensite start temperature (M_s) and is a dependent function of aluminium content. It is observed that binary Cu-Al alloys containing around 19 - 28 at.% (i.e., 9.1 - 14.1 wt.%) of Al shows the martensitic transformations (Swann and Warlimont 1963). The high-temperature β -phase of Cu-Al alloys containing more than 22.4 at.% of Al has BCC structure, which first undergoes the DO_3 -type ordering to form β_1 -phase and then completely transforms to martensite phase (i.e., $\beta'_1, \beta'_1 + \gamma'$ or γ') by rapid quenching to room temperature. The crystal structure of β_1, β'_1 , and γ' were found from the X-ray Diffraction and Transmission Electron Microscopy analysis by

(Kwarciak et al. 1986; Nishiyama and Kajiwara 1963; Swann and Warlimont 1963). The DO_3 -type ordered β_1 -phase possess FCC structure and has a composition of Cu_3Al . The martensite β'_1 -phase consist of an orthorhombic ($18R$) structure and γ' -phase has a hexagonal close-packed (HCP) structure. Further, it is noticed that the martensitic $Cu-Al_{25}$ (at.%) alloy has shown nearly complete reverse martensitic transformation, $\beta'_1 \rightarrow \beta_1$, at high M_s temperatures, i.e., above $340^\circ C$, and the formation of cubic structured γ_2 -phase precipitate particles of composition Cu_9Al_4 causes brittleness in the alloy (Murray 1985). Hence, binary Cu-Al alloys are not practically applicable owed to no SME/PE near to room temperature and poor mechanical properties that restricts their commercial developments for applications.

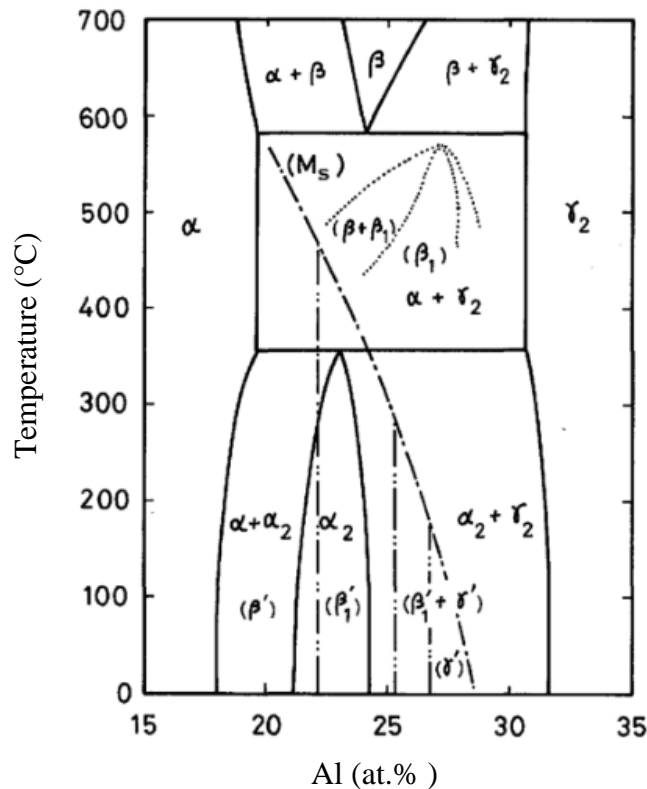


Figure 2.4 Binary Cu-Al phase diagram (Kuwano et al. 1977).

From the existing literature, as discussed in the preceding paragraph, it is discerned that β -phase structure of water quenched Cu-Al binary alloy may not be retained, since the alloy β -phase and its ordered β_1 -phase decomposes to the stable phases. Therefore, a ternary element, namely Zn, Ni, Mn, Be, etc., was doped in the

Cu-Al binary alloys to stabilize phases β and β_1 , and improving the functional and mechanical properties. The literature review is presented in the proceeding sections.

2.4.4 Cu-Al-Ni SMAs

The addition of ternary nickel (Ni) element to copper-aluminium (Cu-Al) alloy efficiently decelerates the diffusion of Al and Cu contents and overwhelms the formation of Cu_9Al_4 (γ_2 -phase) intermetallic precipitates (Duerig et al. 1990; Lojen et al. 2005; Tadaki 1998). In addition, the domain of β -phase shifts toward higher Al contents and is presented in the pseudo-binary phase diagram of 4 wt.% Ni-doped Cu-Al alloys system, as depicted in Figure 2.5. The solid- and dotted-lines of Figure 2.5 shows the equilibrium diagram of the phases and the phase transformation temperature (M_S), respectively, for Cu-Al-Ni alloys. The Ni-doping into β -type Cu-Al alloy as a ternary element efficiently benefits to decrease the phase transformation temperatures. Consequently, detected the strain and/or thermal induced reversible martensitic transformations near to room temperature (Chen 1957; Kurdyumov and Khandros 1949; Otsuka and Shimizu 1969). Later, the shape memory responses have been studied in Cu-Al-Ni ternary alloys, i.e., PE/SE at room temperature (Otsuka et al. 1974; Rachinger 1958; Yang et al. 1977) and SME near to room temperature (Otsuka and Shimizu 1970; Sarma et al. 1972).

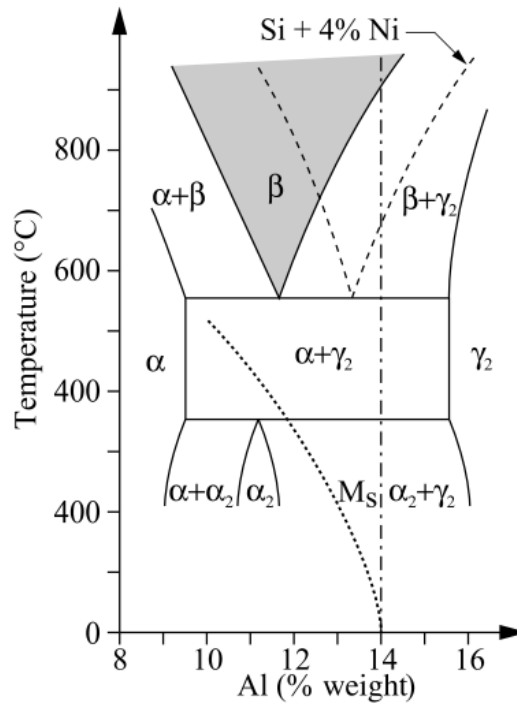


Figure 2.5 Pseudo-binary Cu-Al-Ni₄ phase diagram (Lexcelent 2013).

Kurdyumov and Khandros (1949) have first investigated thermoelastic martensitic transformations in β -type Cu-Al_{14.5} (wt.%) alloys with 1.0 to 1.5 wt.% of Ni-doping, and detected nearly complete reversible transformations without hysteresis loop in the temperature range of 0 to 10 °C. This investigation results stimulated further new interest in the research in the area of Cu-Al-Ni ternary alloys. In Cu-Al_{14.5}-Ni_{1.5} (wt.%) alloy the martensite (γ') phase was observed on cooling to the temperature of about -35 °C. Upon subsequent heating, the reverse transformation from γ' -phase to parent austenite (β_1) phase started at -10 °C and finished at 35 °C (Chen 1957). In addition, a thermal hysteresis of 25 °C was detected during the reverse $\gamma' \rightarrow \beta_1$ transformation, and hence exhibits nearly complete β_1 -phase recovery. Initially, Rachinger (1958) and Otsuka et al. (1970) observed PE/SE in Cu-Al_{14.5}-Ni₃ (wt.%) monocrystalline alloy and SME in Cu-Al_{14.2}-Ni_{4.3} (wt.%) polycrystalline alloy, respectively. Further, the researchers (Friend 1989; Malimánek and Zárubová 1995; Otsuka et al. 1979; Recarte et al. 1999; Sakamoto et al. 1987; Shimizu et al. 1978) discovered the various types of martensite phases (structures), such as β'_1 (18R), γ'_1 (2H) and α'_1 (6R) and that can be transformed from the parent austenite phase, β_1 (DO₃)

of Cu-Al-Ni alloys, and these are primarily depending on chemical composition, applied stress and temperature.

A few researchers (e.g., Agafonov et al. 1988; Oishi and Brown 1971; Otsuka et al. 1976; Recarte et al. 2002, 2004) investigated PE/SE and SME in Cu-Al-Ni SMAs by varying alloy compositions ranging between 13 - 15 wt.% of Al, 2 - 5.5 wt.% of Ni and remaining weight percentage of copper. They have found that the addition of both aluminium and nickel contents let down the phase transformation temperatures and which yields the phase transformation temperatures ranging from -150 to 210 °C. Consequently, detected that Cu-Al-Ni SMAs containing 14.5 ± 1 wt.% of Al, 3.5 ± 1 wt.% of Ni, and balanced wt.% of Cu, exhibits phase transformation temperatures around the room temperature and unveils good PE/SME. Nonetheless, these SMAs are not widely employed in applications because higher concentrations of Al and Ni generates brittle γ_2 -phase particles at grain boundaries, that embrittles the parent austenitic phase alloys and hampers martensitic transformations (Husain and Clapp 1987a; Svirid et al. 2017; Tadaki 1998).

Pérez-Landazábal et al. (2006), Kannarpady et al. (2009) and López-Ferreño et al. (2020) have developed the high-temperature Cu-Al-Ni SMAs by choosing lower weight percentage of Al and Ni contents. This alloy provides an improvement in the thermal stability, forward and reverse transformations to the martensite phase with a small hysteresis, and thus exhibits good strain recovery at higher operating temperatures, i.e., up to 200 °C. Hence, these high-temperature shape memory alloys (HTSMAs) possibly can be used as actuators, sensors or dampers to fulfill the requirements for higher operational temperature locations, particularly in many applications, such as thermal switching, control and protection devices, aerospace and automotive industries (Duerig et al. 1982; Jani et al. 2014). However, Cu-Al-Ni polycrystalline SMAs show poor ductility, unsatisfactory mechanical strength and intergranular fracture without the formation of brittle-type secondary phase precipitates. Due to their large grain-size microstructure coupled with high elastic anisotropy under loading, which causes high stress-concentration at the grain boundaries (Miyazaki et al. 1981; Sarı and Kırındı 2008; Svirid et al. 2017). These shortcomings of Cu-Al-Ni shape memory alloys limit the applications.

2.4.5 Cu-Al-Mn SMAs

Manganese (Mn) as a ternary-doped element into Cu-Al alloys, improves their ductility and lowers the phase transformation temperatures (Kainuma et al. 1995; Matsushita et al. 1985). Added Mn operated as a stabilizing constituent for the phases β and β_1 of Cu-Al alloy. It is also widens the domain of β -phase to either side of Al contents, as shown in Figure 2.6. It is seen that the critical transition temperatures allied with two types of order-disorder phase transitions, i.e., $\beta(A2) \rightarrow \beta_2(B2)$ and $\beta_2(B2) \rightarrow \beta_1(L2_1)$, decreases with reducing Al content (denoted by red color dotted-line). Alloying Mn into Cu-Al alloys system drops down the eutectoid decomposition temperature to 410 °C (Bublei and Titov 1990; Köster and Gödecke 1966), implying that the β -phase in Cu-Al-Mn SMAs possess more resistance to diffusional decomposition compared to other Cu-based alloys. Consequently, it creates a great interest in the development and investigation of Cu-Al-Mn alloys.

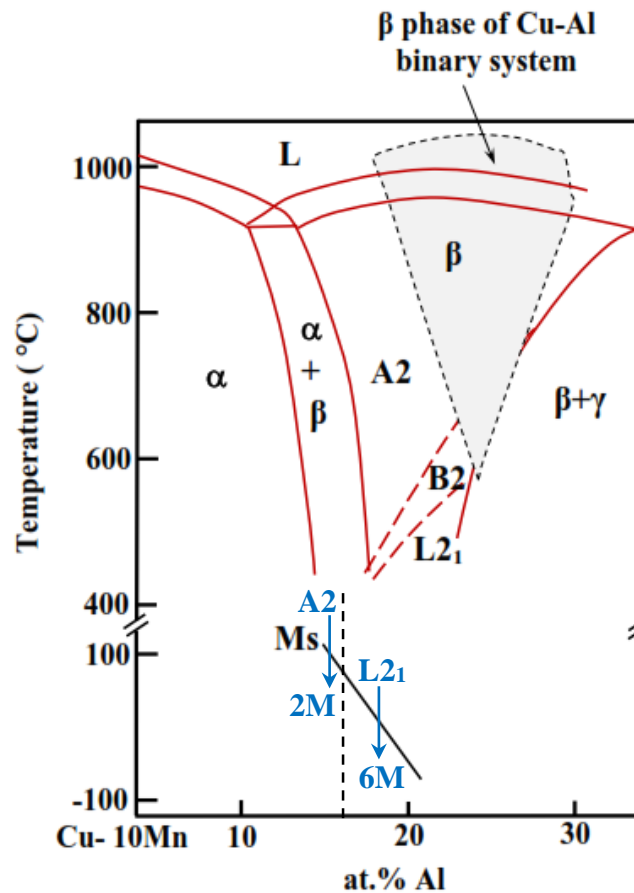


Figure 2.6 Pseudo-binary Cu-Al-Mn₁₀ phase diagram (Sutou et al. 1999).

West and Thomas (1956) have first studied the martensitic phase transformation behavior on Cu-Al-Mn ternary SMAs, and further investigation was carried out by the German scientists Köster and Gödecke (1966). Later in the 20th Century, the researchers (Agapitova et al. 1996; Blazquez et al. 1989; Bublei and Titov 1990; Dutkiewicz et al. 1991; Lopez Del Castillo et al. 1986; López Del Castillo et al. 1987; Mallik and Sampath 2008; Zak et al. 1996) studied the influence of 8 – 15 wt.% of Al, 1 – 12 wt.% of Mn, and remaining copper contents-doping on thermoelastic martensite phase transformation characteristics of ternary Cu-Al-Mn SMAs. The results of the experiments unveiled that the phase transformation temperatures of ternary Cu-Al-Mn SMAs are becoming lower than those of binary Cu-Al alloys. The higher additions of aluminium and manganese contents decreased the transformation temperatures and yield in the range of -200 to + 250 °C by varying the chemical composition of the alloys. Figure 2.6 presents two types of martensitic transformations for shape recovery behavior in Cu–Al–Mn SMAs based on their aluminium concentration, i.e., (i) in the high aluminium concentration range above 16 at.% Al, the ordering transformation takes place from the parent β_1 ($L2_1$) to $6M$ monoclinic β'_1 ($18R$) martensite, and (ii) in the low aluminium concentration range below 16 at.% Al, the ordering, $A2 \rightarrow L2_1$ can be suppressed by rapid quenching and the martensitic transformation takes place from disordered BCC structure of β ($A2$) to $2M$ disordered FCC structure of α' ($3R$).

A study by Matsushita et al. (1985) noted that alloying 1.0 wt.% of Mn to Cu-Al system lowers the martensitic temperature (M_s) by approximately 30 °C and also preventing the supercooled β -phase from precipitation to stable phases. Further, López Del Castillo et al. (1987) observed an increase in 1 wt.% Mn and Al into Cu-Al-Al alloys system gives rise to a reduction in M_s of around 42-51 °C and 126 °C, respectively. It was also found that a simple linear relationship between M_s and alloys composition over a relatively narrow composition range of Al (Sutou et al. 1999) and Mn (Zheng et al. 2007). Kainuma et al. (1995) initially discovered that Cu–Al–Mn alloys with a higher manganese content (Mn > 8 at.%) and a lower aluminium content (Al < 18 at.%) possess low degrees of order in the parent β_1 ($L2_1$) phase, and thus shows good ductility, SME, and PE responses. However, the PE strain recovery in these alloys is still limited to the range below 2% and is not suitable for practical use in many

applications. Further, the investigators (Dasgupta et al. 2018; Jain et al. 2016; Kainuma et al. 1996; Sutou et al. 2002) discovered that Cu-Al-Mn polycrystalline shape memory alloys with higher Al concentrations and ordered (β_2 or β_1) structure are remain brittle and have extremely low fatigue strengths. Brittleness in these polycrystalline alloys arises from coarse grain-size microstructure, high elastic anisotropy during loading, high degree-of-order in the parent phase with a $B2$, DO_3 , or $L2_1$ structure, and the grain boundary segregation of secondary phase precipitates/impurities. Besides, Kainuma et al. (1996) and Sutou et al. (2008) reported that ductility of Cu-Al-Mn can be improved with low weight percent of Al-doping (i.e., 16 - 17 at.%) by minimizing the degrees of order in the BCC structure of β -phase. Although these alloys possess higher transformation temperatures and shape recovery decreases with the presence of disordered parent $\beta(A2)$ phase comparative to ordered parent $\beta_1(L2_1)$ phase.

2.4.6 Cu-Al-Be SMAs

The ternary alloying element beryllium (Be) in a small weight percentage alters the equilibrium phase diagram of the Cu-Al alloys system. Figure 2.7 presents that the eutectoid plateau temperature is lowered, and all the transition temperatures curve of the quasi-binary phase diagram of 0.47 wt.% Be-doped Cu-Al alloys system is brought down. The addition of beryllium, unlike nickel, has no impact on the chemical composition of the alloy or temperature of the T-T-T (time-temperature-transformation) diagram at low concentrations (Lexcelent 2013). Nickel (1957) initially showed that Be-doping as a ternary element in the Cu-Al binary alloy extended the domain of β -phase towards the lower aluminium side. Prawdzik et al. (1966) detected that ternary beryllium element doping to binary Cu-Al system drastically reduces the phase transformation temperatures to ambient temperature or below. This feature enables the prior alloy to be used in intermediate and low-temperature vibration damping applications. Higuchi et al. (1982, 1986) and Belkahla et al. (1991, 1993) have investigated the relationship between martensitic transformation temperature (M_s) and composition in the ranges, 9 – 11.5 wt.% of Al and 0.59 - 0.86 wt.% of Be, and 10 - 12.5 wt.% of Al and 0.3 - 0.65 wt.% of Be, respectively. From the investigations, the results revealed that the martensitic transformation temperatures of Cu-Al-Be ternary alloy lowers by approximately 900 °C per 1 wt.% Be-doping. In addition, it was found

that the weight concentration of beryllium affects 12 times greater than the weight concentration of aluminium. When a small weight percentage of beryllium is added to the eutectoid Cu-Al alloy composition close to Cu_3Al causes a sharp reduction in the martensitic transition temperatures, with no changes in chemical composition.

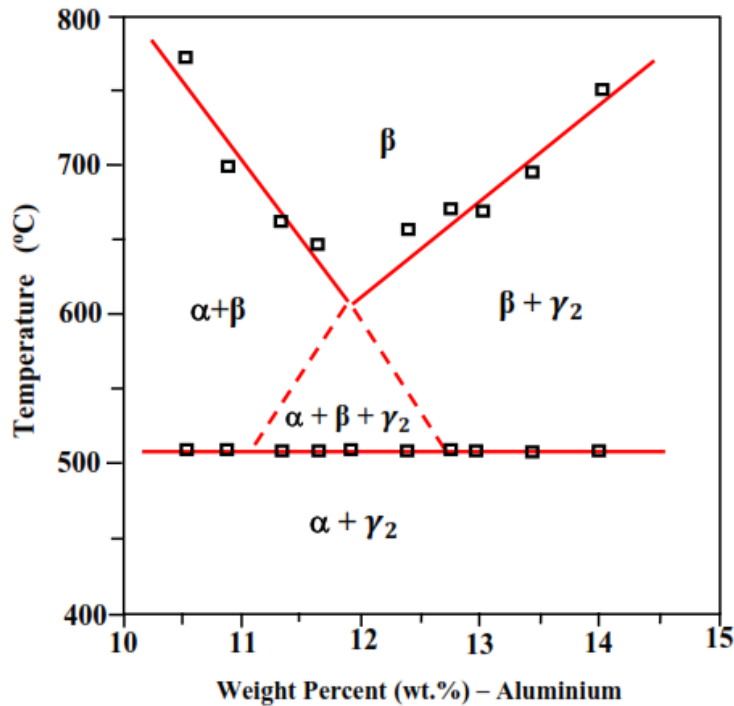


Figure 2.7 Quasi-binary Cu-Al-Be_{0.47} phase diagram (Belkahla et al. 1993).

Zúñiga et al. (1991, 1995) reported that homogenized and water-quenched Cu-Al_{11.9}-Be_{0.5} (wt.%) alloys are in the single austenitic β -phase region. This β -phase exhibits good resistance to high temperature ageing, i.e., more than 100 h at 350°C. Jurado et al. (1995, 1997, 1998) noticed a unique type of disorder-order phase transition in Cu-Al-Be alloys on cooling, i.e., from a disordered $\beta(A2)$ to an ordered $\beta_1(DO_3)$ structure starts at about 530 °C. Upon further cooling, $\beta_1(DO_3)$ structure of austenite phase transforms martensitically at a lower temperature, and these are strongly depends on alloy composition. A high temperature parent β_1 -phase of DO_3 structure was observed in Cu-Al_{12.3}-Be_{0.52} (wt.%) alloy system from the studies by Moreau et al. (1995). In addition, it is observed that thermoelastic martensite transformation starts by cooling or deformation, which produce a $\beta'_1(18R)$ martensite phase and is reversible.

This martensitic transformation ($DO_3 \leftrightarrow 18R$) is responsible for the shape memory characteristics exhibited by Cu-Al-Be alloy system.

Researchers (Balo and Ceylan 2002; Belkahla et al. 1993; Ergen et al. 2013; Flores Zúñiga et al. 1991, 1996; Montecinos et al. 2006; Rios-Jara et al. 1991a; b) detected the changes in transformation temperatures, phase structures, shape memory effect or pseudoelasticity on Cu-Al-Be ternary SMAs by varying Al from 11.4 to 12.0 wt.% and 0.31 to 0.86 wt.% of Be, yielding transformation temperatures ranging from -250 to +200 °C and as the temperature change does not modify the nature of thermoelastic martensitic transformations ($DO_3 \leftrightarrow 18R$) during strain recovery responses, and exhibits good PE/SME. Though ternary Cu-Al-Be SMAs exhibits good PE/SME behavior, the primary limitations of these SMAs are coarse grain-size microstructure (Hsu et al. 2009; Montecinos et al. 2006, 2015) leads to intergranular failure, poor ductility, unsatisfactory mechanical strength, and susceptible to martensite hyperstabilization, which increases thermal/stress-induced transformation hysteresis and that resulting to a lower strain recovery (Kustov et al. 2004b; a; Montecinos and Cuniberti 2008; Torra et al. 2015). As a result, restricts their commercial usage in the applications.

As a whole, the existing literature reveals that the ternary Cu-Zn-Al and Cu-Al-X (where, X=Ni, Mn, Be) SMAs possess coarse grain-size microstructure and that causes a rapid-brittle-failure in applications. Consequently, the poor mechanical properties and brittle fracture of these SMAs limit their commercial usage without material/process modifications. To overcome these limitations, the scientists have investigated various techniques/approaches to improve the grain refinement, strength, ductility and shape recovery properties of the alloys, as discussed in the proceeding sections.

2.5 GRAIN REFINEMENT

As literature discussed in the preceding sections present the applications of Cu-based SMAs as well as their limitations primarily including the intergranular brittle failure and is owing to coarse grain-size microstructure. Further, it is evident from the literature discussed in the proceeding sections that the grain refining process increases

grain boundary area, which suppresses brittle failures and enhances the strength as well as ductility of the alloys. Therefore, the grain-size refinement was shown to be a critical factor in achieving improved functional and mechanical properties of Cu-based SMAs comparable to that of Nitinol-based SMAs (Ziółkowski 2015). Many efforts are being undertaken by numerous researchers to investigate the various techniques for grain-size refinements, such as heat treatments that includes annealing/ageing at various temperatures range and time-periods, quenching media and processes, quaternary alloying/inoculation of less-soluble elements called grain refiners, and the advanced secondary processing methods *viz.* severe plastic deformation (SPD) and melt spinning.

2.5.1 Heat Treatments

Betatization is another heat treatment method employed to modify the grain size and vacancy concentration, which in turn affects the resistance of shape memory alloy to intergranular fracture (Lu et al. 1996). The following literature by several researchers has described the properties of shape memory alloys connected with grain size: Gann (1982) detected an increase in grain size with increasing solution treatment temperature. Besides, an increase in the grain size with increasing temperature and time of solution treatment has been reported in the Cu-based SMAs without and with grain refiners doping (Adnyana 1986; Lee and Wayman 1986a; b; Sure and Brown 1984). Gil et al. (1991, 1993) discovered the grain growth relationships for different heat treatment temperatures (750 – 900 °C) and times (3 – 60 minutes) and observed an exponential-type increase in the grain size with increasing temperatures and times. Lai et al. (1996) achieved fine grain size microstructure with lower vacancy concentrations to create defects for a shorter betatizing time of 10 minutes.

Asanovic et al. (2002) investigated the effect of solution treatment temperatures (400, 450, 500 and 550 °C), times (1, 2, 4, 8, 16, 32, 64 and 128 minutes), and followed by room temperature water quenching on Cu-Zn_{18.05}-Al_{5.35} (mass%) alloy grain-sizes that was initially solution treated at 850 °C for 10 minutes and iced-water quenching. They found an increase in the grain size with increasing both temperatures and times of the solution treatment. Sarı and Kırındı (2008) observed a slow increase in the grain size of Cu-Al_{11.92}-Ni_{3.78} (wt.%) SMAs with increasing temperatures and times of the

betatization/annealing treatments, followed by iced-water quenching. In addition, forms the precipitates during low-temperature annealing at 650 °C for 40 minutes. Montecinos et al. (2008) evaluated the influence of annealing heat-treatment time on Cu-Al_{11.4}-Be_{0.5} (wt.%) alloy grain sizes of cylindrical, tensile, and flat-type samples at various time-periods, i.e., 0 – 15min at 800 °C. They found that the grain size increased with increasing time and cylindrical-type samples have shown good grain size refinement compared to all other types. Zhang et al. (2009) investigated the effect of heat treatment on Equal Channel Angular Pressing (ECAP) Cu-Al_{11.42}-Be_{0.35}-B_{0.18} (wt.%) alloy by selecting two sets of specimens: (i) the specimens reheated for 10 minutes at various temperatures ranging from 350 to 700 °C, (ii) the specimens reheated at 600 °C for different times ranging from 10 to 70 minutes and followed by oil-quenching. It was shown that the alloy microstructure did not modify substantially after quenching at a temperature below 600 °C, whereas the average grain sizes remained smaller than 50 microns after quenching at a temperature of 600 °C, and further individual grain coarsening ensued at a temperature above 650 °C. With a holding time of more than 30 minutes, grains grow larger and become more inhomogeneous. As a result, the appropriate optimal procedure was chosen for reheating at 600 °C for 10 – 30 minutes holding time, and followed by oil cooling. Montecinos et al. (2009) observed γ_2 and α' precipitates and that formed from the decomposition of β -phase of the Cu-Al-Be polycrystalline alloys under slow cooling rates, i.e., slower than 100 °C/min, and thus no solid-state transformation occurs during phase transformations.

Jiao et al. (2010) investigated the solution treatment of Cu-Al_{7.66}-Mn_{9.52} alloys for 15 minutes at different temperatures ranging from 700 to 900 °C, followed by water quenching, and found no significant changes in the grain size. Though there are α -phase particles and no martensite phase in the alloy specimen solution treated at 750 °C when the solution treatment temperature was raised to 800 °C, the α -phase particles disappeared and the spear-like martensite appears. Further, higher solution treatment temperatures ($T \geq 825$ °C) resulted in thicker martensite plates. Montecinos et al. (2010) investigation results revealed that the β -phase of Cu-Al_{22.60}-Be_{3.26} (at.%) polycrystalline alloy rapidly decomposes into γ_2 -phase precipitates during an isothermal treatment at temperature around 550 °C, and rises with increasing time.

While, the formation of α' -phase precipitates followed by the eutectoid ($\alpha' + \gamma_2$) decomposition is seen at temperatures ranging from 400 to 500 °C. In addition, the β -phase of alloys remained in the betatized samples for 5 minutes heating at 800 °C and followed by rapid water quenching at room temperature. The investigation results of Montecinos et al. (2012) revealed an increase in the grain size with increasing betatization times of β -type Cu-Al_{11.41}-Be_{0.50} (wt.%) alloy samples at 800 °C and followed by rapid water quenching at room temperature. Canbay and Karagoz (2013) investigated the influence of annealing temperatures ranging from 700 to 850 °C for 1 hour and detected an increase in the average grain sizes as temperatures raised. Haidar et al. (2018) examined quaternary Cu-Al-Ni-Co SMAs at two different annealing temperatures (400 and 500 °C) and times (1 and 3 hours) and discerned that the addition of cobalt element forms a new Co-rich γ_2 -phase precipitates, which have a composition of Al₅Co₂₂Ni₃, and the formation of precipitates rises with increasing time. Payandeh et al. (2021) studied the effect of solution treatment and ageing temperatures ranging between 200 and 900 °C for 8 – 180 minutes on Cu-Al₁₃-Ni₄ (wt%) polycrystalline SMAs. It was shown that the existence of γ_2 -phase precipitates with a composition of Cu₉Al₄ up to 800 °C, while martensite is detected at 900 °C. The crystallization of martensitic phase without precipitates occurs following solution treatment for 20 minutes at 900 °C, and subsequent ageing at 350 °C, increases the volume fraction of β' -type martensites.

2.5.2 Grain Refiners

2.5.2.1 Boron

Boron element attracts wide interest in alloying both Ni-Ti-based and Cu-based SMAs for substantial grain refinement, beneficial in improving strength and ductility (Han and Kim 1987; Suzuki et al. 1998; Yang and Mikkola 1993). Boron-dope acts as an effective grain refiner and the smaller grain sizes for Al (Antonio and Lfo 1971; Mohanty et al. 1995; Wang et al. 2011), Ti-Ni-Pd (Yang and Mikkola 1993), Ti-Td-Ni (Suzuki et al. 1998), Cu (Lozovoi and Paxton 2008; Balart et al. 2015), Mg (Suresh et al. 2009), Ti-Al (Cheng 2000; Li et al. 2017), and Cu-Al (Davis and Committee 2001; Birol 2012) alloy systems. The extensive grain refinement with boron-dope owing to

higher heterogeneous nucleation sites in the cast alloys. The addition of boron (B) enhances the heterogeneous nucleation rate by providing additional driving force and/or dominant free-growth barrier due to large constitutional-supercooling/undercooling during solidification (Greer et al. 2000, 2003; Tamirisakandala et al. 2005). Improvements in the mechanical properties with B-doping attributes to its advantages like (i) small atomic radius (Lozovoi and Paxton 2008), which acts as an interstitial and/or substitutional solid solution element, and (ii) de-embrittling element (Balart et al. 2016; Laporte and Mortensen 2009), which enhances the cohesive strength of grain boundaries. Boron chemically combines with other metals and generates metal borides, namely AlB_2 , TiB_2 , and ZrB_2 (Birol 2012; Jones and Pearson 1976), which origins heterogeneous nucleation sites to a greater extent and thus enhancing grain refinement in B-doped alloys.

Lee and Wayman (1986b) revealed that the average grain size of $920\ \mu\text{m}$ in a B-free Cu-Zn_{25.7}-Al_{3.58} alloy and that was refined to $250\ \mu\text{m}$ by the addition of 0.051 wt.%B. Morawiec et al. (1990) added Ti and B together as grain-refiners in Cu-Zn-Al alloys and observed the grain size to $100\ \mu\text{m}$. Morris (1991, 1992) investigated Cu-Al₁₂-Ni₄-Mn₃ alloy with various addition of boron, i.e., 0.04 – 0.4 wt.% of B for grain refinement and achieved grain-size refinement of around ranging from 100 to $140\ \mu\text{m}$. Sampath (2006) observed the formation of bulky precipitates in Cu-Zn_{30.36}-Al_{2.19} alloy with 0.2 wt.% of B-doping and that inhibits the martensitic transformations. Further, Sampath and Mallik (2009, 2015) unveiled grain-size refinement of Cu-Al-Mn alloy with 0.05-0.2 wt.% of B-doping, i.e., the grain-size reduction around ranging 340 - $100\ \mu\text{m}$. Besides, they reported a decrease in strain recovery by SE and SME with adding boron elements to Cu-Al-Mn SMAs and is owing to precipitates pinning effect, which restricts the movement of austenite as well as martensite during phase transformations. Zhang et al. (2009, 2010, 2011) studied the effect of 0.18 wt.%B-doping in grain refinement of Cu-Al_{11.42}-Be_{0.35} SMA under the equal channel angular pressing (ECAP) process and discerned a significant reduction in grain sizes of two microns with uniform dispersal precipitates after 8 passes, which had an adverse effect on the mechanical and shape recovery properties of SMAs due to precipitation formation. Aydogdu et al. (2016) investigated Cu-Al₂₄-Mn₆-B_X (X = 0, 1, 2, 3, 4) and observed the precipitates

formation, loss of ductility, and a decrease in strain recovery by SME and SE with increasing B-doping. Zhang et al. (2019) observed that adding boron elements ranging 0.25 – 2.0 wt.%B to Cu-Al₁₃-Ni₄ SMA results in good grain refinement and also enhances the mechanical properties. Hussain et al. (2019) observed that Cu-Al₁₂-Ni₄ alloys with the additions of 0.1 and 0.3 wt.% of boron exhibit substantial enhancements in ductility and shape recovery properties.

2.5.2.2 Chromium

Miki et al. (1989) studied the influence of various quaternary alloying elements to Cu-Al₁₄-Ni₃ SMA and chromium-dope shown reduced β grain-sizes with fine precipitates. Besides, it is noticed that good ductility with Cr-dope compared to other dopants. Sutou et al. (2001) observed the reduction in parent β -phase grain sizes of Cu-Al₁₇-Mn₁₀ (at.%) SMA with increasing chromium additions, i.e., from 0.5 to 2 at.% of Cr. The quaternary alloying of chromium element, i.e., 0.9 – 3.0 wt.% of Cr into Cu-Al-Mn SMA by (Mallik and Sampath 2009) unveiled grain-size refinement with fine-size secondary phase precipitates in the alloys β -phase owing to the limited solubility of chromium in the alloy matrix. In addition, it was shown that the shape recovery by superelasticity (SE) decreases because of solid solution or precipitation hardening in the parent β -phase. Cu-Al_{11.8}-Be_{0.6} SMA with smaller concentrations up to 0.5 wt.% of Cr addition exhibits significant grain refinement. A maximum refinement size of 100 μ m was achieved with the addition of 0.5 wt.%Cr and is approximately 20 times smaller than the Cr-free alloy (Candido et al. 2012). Teixeira et al. (2015) noticed a reduction in grain size of Cu-Al-Ni alloys with an increase of chromium-doping, i.e., 0.74 – 2.26 wt.% of Cr. Dasgupta et al. (2015) obtained a complete martensite microstructure without precipitation by adding 0.185 wt.% of Cr to Cu-Al_{12.12}-Mn_{4.22} alloy. Yang et.al (2017) investigated the effect of Cr concentrations on the characteristics of Cu-Al-Mn SMA and detected grain size reduction with a small density of dispersive precipitates. The volume fraction of precipitates increases as Cr content rises, which improves the compressive strength while deteriorating superelastic properties.

2.5.2.3 Nickel-Niobium

A few researchers (e.g., Melo et al. 2009; Albuquerque et al. 2010a; b) have studied the addition of Niobium (Nb) - Nickel (Ni), and detected a reduction in the average grain size of Cu-Al-Be SMAs, i.e., from 1950 to 100.77 μm . Besides, an enhancement in strength from 350 to 750 MPa and ductility from 6.9 to 8.2%. This strengthening attributes to the existence of Nb-rich precipitates, which hinders the grain growth by pinning effect. Santiago et al. (2019) examined the addition of Ni-Nb master alloy to Cu-Al_{11.8}-Be_{0.58} (wt.%) alloy and discerned that increasing weight percentage of the refiner improved the grain-size refinement with enhanced tensile strength.

2.5.2.4 Zirconium

Lee and Wayman (1986a; b) investigated Zr-doped Cu-Zn-Al and Cu-Al-Ni SMAs and the results revealed that grain growth rates were suppressed effectively in Zr-doped alloys compared to other refiners. It was also discovered that a very low grain growth exponent of Zr, inhibits grain growth effectively. Further, revealed a fracture mode transition from intergranular to transgranular with Zr-doping. Chung et al. (1998) observed that grain size reduction in the Cu-Zn₂₁-Al₆ (wt.%) SMA by four times with 0.5 wt.% of Zr-doping. Kim et.al. (1990, 1991) have reported that the fine grain-size microstructure of Zr-doped hot rolled Cu-Al-Ni SMA exhibits a significant increase in tensile properties with a complete ductile fracture mode. Bhattacharya et al. (1993) investigated Cu-Al_{13.3}-Ni_{4.3} alloy and observed a significant grain-size refinement with 0.3 wt.% of Zr-doping. Hsu and Wang (1996) have studied the superplastic forming behavior on Zr-doped Cu-Zn-Al alloy and detected that the grain size decreases as the solution treatment temperature lowers over five minutes of annealing time. Gil et al. (1999) had noticed a very slow grain growth rate for the β -type Zr-doped Cu-Zn-Al alloys in comparison with Si, Co and Mn-doped alloys subjected to different heat treatment schedules. Sampath et al. (2005, 2006, 2009) studied the influence of Zr-dopant on microstructure, mechanical and shape recovery properties of Cu-Al-based SMAs and the outcomes revealed an effective grain refinement by the addition of Zr content. They revealed that the grain size reduction ratio of 60% in Cu-Al-Ni, 85% in Cu-Zn-Al, and 25% in Cu-Al-Mn alloys with 0.2 wt.% of Zr-doping. They also noticed a significant enhancement in mechanical and shape recovery properties with increase

in the weight percentage of Zirconium element, excluding Cu-Al-Mn alloys. The adverse effect in Cu-Al-Mn alloys owed to pinning effect caused by precipitate particles.

Since the last decade, a few researchers have demonstrated a method of grain refinement by different inoculant-doping, *viz.* $\text{Cu}_{51}\text{Zr}_{14}$ and CuZr in Cu-Al-X (X = Mn, Ni) SMAs. In addition to grain refinement, many properties such as damping capacity, shape memory effect, hardness, tensile, and fracture mode can be changed. Yang et al. (2016) studied the influence of $\text{Cu}_{51}\text{Zr}_{14}$ inoculant doping on tensile and low-frequency damping properties of Cu-Al_{11.9}-Mn_{2.5} SMAs, and the results reveal that refined grain size with a significant improvement in damping, ultimate tensile strength and ductility properties. They also noticed a higher density of deeper dimples with an increase in the weight percent of inoculants up to 0.9%, which indicates ductile fracture. Jiao et al. (2018) have observed refined grain size in the CuZr inoculant-doped Cu-Al_{11.85}-Mn_{2.47} SMAs with controlled precipitation, in turn, significant improvement in hardness and damping. Besides, they reported that the shape recovery decreases with increasing precipitates. Ding et al. (2019) investigated the addition of $\text{Cu}_{51}\text{Zr}_{14}$ inoculant and discerned a substantial refinement in the grains as well as the improved damping properties of Cu-Al_{13.2}-Ni₄ SMAs.

2.5.2.5 Rare earth elements

The following literature presents that minor additions of Rare Earth Elements (REE), such as Cerium (Ce), Gadolinium (Gd), and Yttrium (Y) acts as effective grain refiners and thus show good grain-size refinement in the Cu-based SMAs. Bhattacharya et al. (1993) observed an excellent grain-size refinement of Cu-Al-Ni alloy with the addition of rare-earth metals, Yttrium and Mischmetal. The China scientist Xu (2008) investigated Cu-Zn₂₆-Al₄ alloy doped with 0 – 0.2 wt% of Gd and observed a significant reduction of the grain sizes. Yang et al. (2009) added 0.1 – 0.43 mass percentage of Mischmetal into Cu-Zn₂₆-Al₄ alloy and observed a substantial grain-size refinement, *i.e.*, from the coarse grain-size of 1000 μm to the finer grain-size of 30 μm with alloying 0.43 mass% of Mischmetal. Besides, they detected that the fracture strength and ductility enhances significantly with increasing the mass percentage of Mischmetal. Fracture morphology revealed that the addition of Mischmetal to Cu-Zn-Al alloy

effectively transforms intergranular cleavage to transgranular dimple fracture and is attributed to smaller grain sizes. Lu et al. (2009) investigated the effect of cerium -dope on Cu-Al₁₂-Mn₅ SMA and found that Ce-doping refines the grain sizes and thus enhances the damping capacity, tensile strength and ductility of SMAs. Zhang et al. (2016) investigated Cu-Al₁₃-Ni₄ alloy doped with 0 – 6 wt.% of Gd contents and observed that Gd-doping refines the grains and improves the mechanical as well as shape recovery properties of SMAs.

2.5.3 Severe Plastic Deformation

Severe plastic deformation techniques, such as Equal Channel Angular Pressing (ECAP), Equal Channel Angular Rolling (ECAR), and Accumulative Roll Bonding (ARB) are the advanced secondary processing methods for grain-size refinement to improve mechanical properties, as described in the following literature:

Zhang et al. (2009, 2010, 2011) investigated the effect of ECAP and post-deformation annealing heat treatment on Cu-Al_{11.42}-Be_{0.35}-B_{0.18} SMA and the results unveiled that grain size refined effectively from 300 to 2 μm with diminutions in ultimate strength from 460 to 312 MPa, and ductility from 2.7 to 0.4% after eight passes. The ECAP processed fine-grained SMA had a lower shape recovery ratio than that of the as-cast Cu-Al-Be-B alloy. Further, ECAP processed Cu-Al-Be-B alloy reheated at 600 °C for 10 minutes and followed by room temperature oil-quenching, which coarsen the grains of around 50 μm with ultimate strength and ductility enhancements of 703 MPa and 3.2%, respectively. However, the adverse effect on shape memory properties was observed due to precipitation formation. Moghaddam et al. (2014, 2017) examined the effects of ARB, ECAR, and post-deformation annealing heat treatment on two groups of Cu-Al-Mn SMAs. It is discerned that 5-pass ARBed specimens after successive annealing at 700°C for 150 seconds and followed by water-quenching, forms zig-zag morphology of martensitic phase for the grain size of approximately 20 – 40 μm with a tensile strength of 430 MPa and ductility of 8.5% is observed. Further, extended annealing at 700 °C for 5 minutes possesses grain coarsening of sizes ranging about 100 – 200 μm with improved tensile strength of 780 MPa and ductility of 11%, and the fracture surface showing deep dimples. Whereas,

the shape recovery characteristics deteriorate because of the larger density of dislocations accumulated by phase transformations cycling. For the 5-pass ECARed specimens, controlling the annealing time of 105 seconds at 890 °C, resulted in more uniformity and smaller grain sizes with the coexistence of martensitic and bainitic phases with superior mechanical properties. Finally, Severe Plastic Deformation (SPD) techniques are impractical for bulk shape memory alloys (Zhang et al. 2009a).

2.5.4 Melt Spinning

Matsuoka et al. (1983) investigated on grain size and mechanical properties of the Cu-Al-Ni ribbons prepared using the melt-spun (rapid solidification) technique and found that this technique is highly favorable for reducing the grain sizes. However, the Cu-Al-Ni SMA ribbons with fine grain structures remain brittle. Eucken et al. (1988) achieved various grain-size microstructures of Cu-Al-Ni SMA ribbons by varying the wheel speed, ejection pressure, and angle between the nozzle and the wheel of melt spinning. Lara-rodriguez et al. (2006) studied the influence of melt spinning unit wheel speed on grain sizes and transformation temperatures in the rapidly solidified Cu-Al_{11.83}-Be_{0.48} (wt.%) alloy ribbons. They discovered that the wheel speeds ranging from 24 to 36 m/s effectively refine the grain sizes. The transformation temperatures (M_f, M_s, A_s, A_f) decreases with increasing wheel speed and is owed to grain-size refinement. Ergen et al. (2013) observed that a rise in beryllium content with a constant wheel speed of melt spun unit reduces the grain sizes and also lowers the transformation temperatures of Cu-Al-Be SMAs. On the other hand, the rapid solidification processing (melt spinning) has the disadvantage of introducing internal stresses into the alloy, which can inhibit the growth of the martensitic plates. This effect implies deterioration in the shape memory characteristics of the alloy processed by melt spinning. Moreover, the melt spun processing is not a commercially attractive technique for bulk production of alloys (Agrawal and Dube 2018).

2.6 PHASE TRANSFORMATION TEMPERATURES

The phase transformation temperatures are essential constraints in the selection of shape memory alloys for use in applications at the requisite operating zone. The

existing literature indicates that alloying quaternary elements improve the mechanical properties, despite the changes in the phase transformation temperatures. Further, varying the heat treatment procedures can increase/decrease the phase transformation temperatures, and the pertinent literature is as presented below:

2.6.1 Quaternary Alloying Elements

Sutou et al. (2001) investigated Cu-Al-Mn alloys with quaternary dope elements, *viz.* 0.1 – 1.0 wt.% of vanadium (V) and 0.5 – 2.0 wt.% of chromium (Cr). They observed a reduction in the phase transformation temperatures with increasing the weight percent of V and Cr contents owing to fine grain sizes. Sampath and Mallik (2009a; b) studied the effect of quaternary alloying elements (B, Cr, Fe, Mg, Ni, Pb, Si, Ti, Zn and Zr) on Cu-Al-Mn SMAs, and noticed the lowering of phase transformation temperatures with raising the addition of Cr, Fe, Mg, Si and Ti, whereas B, Ni, Zn and Zr shifts the phase transformation temperatures toward a higher temperatures side. Lu et al. (2009) examined the addition of 0.05 – 0.15 wt.% Ce (REE) to Cu-Al₁₂-Mn₅ SMA and discerned a reduction in the phase transformation temperatures initially up to 0.10 wt.% of Ce, and a further increase in the weight percent of Ce-doping rises the phase transformation temperatures. Melo et al. (2009) and Albuquerque et al. (2010a) detected that Nb- and Ni-doping forms Nb-rich precipitates into the matrix of the Cu-Al-Be polycrystalline alloy, which increases the phase transformation temperatures.

Candido et al. (2012) observed Cr-rich precipitates, which causes the depletion of beryllium (Be) content from Cu-Al-Be alloy matrix with 0.1 – 0.5 wt.% of Cr-doping and thus rises the phase transformation temperatures. Canbay et al. (2014) have measured the variations in transformation temperatures on Cu-Al-Mn SMA doped with quaternary elements, *viz.* 0.45 – 0.73 wt.% of vanadium (V), and 0.60 – 0.43 wt.% of cadmium (Cd) and observed that V- and Cd-doping lowers the transformation temperatures. Further, it was discovered that Cd-doping is more efficient in lowering the phase transformation temperatures than that of V-doping. Saud et al. (2014, 2015b; a) investigated the effects of quaternary elements, such as Co, Mn and Ti on martensitic transformation temperatures of Cu-Al-Ni SMA and detected that the addition of Co, Mn and Ti rises the martensitic transformation temperatures. Besides, it was noted that

Co-doping is more efficient in rising the transformation temperatures compared to others, and is due to the existence of Co-rich precipitates. Aydogdu et al. (2016) examined the changes of transformation temperatures on Cu-Al-Mn SMA by the addition of 1 – 4 at.% of boron (B) and discerned that an increase in the B-doping effectively rises the phase transformation temperatures. Zhang et al. (2016) discerned a reduction in the phase transformation temperatures of Cu-Al_{13.0}-Ni_{4.0} alloys with increasing the addition of rare earth element gadolinium (Gd) up to 0.9 wt.%, and further higher additions of Gd slightly increases the phase transformation temperatures. Stipcich and Romero (2017) have observed higher phase transformation temperatures of Cu-Zn-Al SMA doped with 0.65 at.% Zr and is owed to the existence of precipitates. Yang et al. (2017a; b) studied the influence of Cr- and V-doping on transformation temperatures of Cu-Al-Mn SMAs. From the investigation results, it was shown that an increase in the additions of Cr and V to Cu-Al-Mn SMAs decreases and increases the transformation temperatures, respectively.

Ding et al. (2019) studied the influence of combined additions of grain-refiners, *viz.* Cu₅₁Zr₁₄ inoculant and Ti element on the reversible characteristic transformation temperatures of Cu-Al-Ni SMA and noticed a reduction in the reversible characteristic transformation temperatures with a rise in refiners-doping due to smaller average grain size. Santiago et al. (2019) investigated the addition of Nb-Ni master alloy on phase transformation temperatures of Cu-Al_{11.80}-Be_{0.58} alloy. They observed that an increase in the phase transformation temperatures with increasing refiners-doping *i.e.*, up to 0.65Nb-0.35Ni (wt.%) master alloy and further higher addition of master alloy lowers the phase transformation temperatures. Zhang et al. (2019) studied the influence of boron-doping on transformation temperatures of Cu-Al_{13.0}-Ni_{4.0} alloy and discerned a reduction in the phase transformation temperatures with the cumulative addition of boron contents.

2.6.2 Effect of Thermal Treatments

The phase transformation temperatures of SMAs can be modified by varying the thermal treatment parameters, *i.e.*, time-periods and temperatures of annealing

(betatization/solution treatment), as well as cooling rate and quenching media have been studied by numerous researchers and the literature is as follows:

The researchers (Adnyana 1986; Han and Kim 1987; Jiao et al. 2010; Montecinos and Cuniberti 2012) observed a rise in the phase transformation temperatures with increasing betatization/solution treatment temperatures and time-periods of Cu-based SMAs without or with refiners-doping and is attributed to larger grain size. Dong et al. (1994) and Chung et al. (1998) investigated low temperatures ageing effects on the phase transformation temperatures of Cu-Al-Be-X (X = B, Cr, Ti, Zn) and Cu-Zn-Al-X (Mn, Zr) SMAs, respectively. Their investigation results show that the phase transformation temperatures slightly decrease with an increase in the ageing temperatures below 200 °C, and is owed to reduced vacancy concentrations and changes in the chemical composition of the parent phase. Further, higher ageing temperatures (≥ 200 °C) and times (> 10 minutes) lead to the formation of secondary phase precipitates, which restricts the twin boundary movements and thus increases the phase transformation temperatures (Kozlova and Titenko 2006; Payandeh et al. 2021; Saud et al. 2015b; Suresh and Ramamurty 2008). Cuniberti et al. (2009) observed that a slow cooling rate forms γ_2 -phase precipitates, and consequently raises the phase transformation temperatures. The scientists (Leu and Hu 1991; Shafeeq et al. 2016) have studied the effects of different quenching media and observed the lowering of the phase transformation temperatures with direct quenching (DQ) to water at room temperature due to the existence of pure austenitic/martensitic phase without precipitates.

2.7 PSEUDOELASTIC BEHAVIOR

Heller et al. (2009) suggest a pseudoelastic/superelastic SMA as one of the simplest representations of the damper for vibration damping applications. The researchers (DesRoches and Delemont 2002; Hartl and Lagoudas 2007; Montecinos et al. 2008, 2011; Qian et al. 2016; Sharabash and Andrawes 2009; Song et al. 2006; Sutou et al. 2005, 2013; Wang et al. 2017; Zhang et al. 2008) have investigated the selection of pseudoelastic shape memory alloys for vibration damper and isolator applications based on their performance parameters such as critical stress to start the stress-induced

martensite transformation from the parent austenitic phase, work hardening rate after yielding, transformation hysteresis loop, reversible strain, residual strain, stiffness, loading-unloading speed, and energy dissipation capability. They reported that the effectiveness of pseudoelastic SMA dampers on vibration mitigation has the characteristics of good energy dissipation capability, high stiffness for small displacements, excellent self-centering capability, great versatility, long-term reliability, high reversible strain without significant deterioration in the pseudoelasticity or permanent plastic deformation, lesser residual strain, and high strength and ductility to prevent catastrophic brittle failure of the structures subjected to large deformations.

The main characteristic features of pseudoelastic behavior, as discussed in the preceding paragraph, are primarily dependent on the morphology and microstructural properties of SMAs, such as crystalline type, grain size, texture, structure change of phase transformations mechanism, precipitates, etc. From the existing literature (Kaouache et al. 2004; Kato et al. 1999; Sade et al. 2015; Siredey-Schwaller et al. 2009; Suresh and Ramamurty 2007; Yawny et al. 2000), it is observed that monocrystalline ternary Cu-based SMAs have shown superior pseudoelastic strain recovery compared to Ni-Ti-based SMAs (Ammar et al. 2017; Xiao et al. 2016). On the other hand, the preparation of single-crystal particularly for large-size production of bulk alloys is difficult (Xie et al. 2015). Consequently, the focus was concentrated on polycrystalline ternary Cu-based SMAs because polycrystalline technology is usually simpler and less costly than that of monocrystals. However, the utilization of pseudoelastic Cu-based polycrystalline alloys is limited in many potential applications, such as efficient energy dissipation and recentering dampers due to their shortcomings, *viz.* low pseudoelastic strain recovery, high brittleness, unsatisfactory mechanical strength, short life cycle, poor cold-workability, and easy intercrystalline crack initiation and propagation. These shortcomings of polycrystalline Cu-based SMAs are attributed to their high elastic anisotropy in the parent phase and coarse grain-size microstructure (Fu et al. 2016; Kaouache et al. 2006; Miyazaki et al. 1982; Montecinos et al. 2006; Sedláč et al. 2005; Sutou et al. 2009; Tadaki 1998; Xu et al. 2011; Zhu et al. 2009). Consequently, the poor functional and mechanical properties of these SMAs limit their commercial usage without material/process modifications.

Montecinos et al. (2008, 2011) observed that the martensitic transformation temperatures diminished and forward transformation ($A \rightarrow M$) stresses increased with a decrease in grain size of the heat-treated Cu-Al_{11.4}-Be_{0.5} alloys. Sade et al. (2014) presented that as grain size decreases, the pseudoelastic properties of Cu-Al-Be polycrystalline SMAs enhances. (Sutou et al. 2002, 2004, 2005, 2013) investigated the grain size and texture dependency of pseudoelastic behavior on Cu-Al-Mn-based SMAs. From the investigation results, it is apparent that the critical stress for stress-induced martensitic (SIM) transformation and work-hardening rate ($d\sigma_{PE}/d\varepsilon$) after yielding enhances with reduction of grain size. A maximum pseudoelastic strain recovery is obtained in the $\{112\}\langle 110 \rangle$ textured direction of sheet specimen with a large relative grain size. Dutkiewicz (1999) observed good superelasticity with $\beta_1(DO_3) \leftrightarrow \beta'_1(18R)$ transformations and a deterioration of the superelasticity caused by the formation of $\gamma'_1(2H)$ martensite rather than $\beta'_1(18R)$ martensite. Cuniberti et al. (2009) observed the formation γ_2 -phase precipitates on Cu-Al_{22.66}-Be_{2.98} (at%) polycrystalline SMA by slow cooling from 800 °C to the temperature (T_Q) ranging from 580 to 530 °C, and followed immediately by rapid water quenching at room temperature. The volume fraction γ_2 -phase precipitates increases as T_Q lowers, which causing deterioration in the pseudoelastic strain recovery. The scientists (Kozlova and Titenko 2006; Sutou et al. 2009) have studied low-temperature ageing on Cu-Al-Mn-based SMAs and detected that deterioration in the pseudoelasticity with increasing ageing time owed to the existence of precipitates. Yang et al. (2019) observed an excellent superelasticity on Cu-Al_{13.96}-Mn_{9.84} SMA with the addition of 0.51 wt.% of tungsten (W). The researchers (Sampath and Mallik 2009; Yang et al. 2017a; b) investigated the influence of minor additions of grain refiners on Cu-based SMAs and observed excellent grain-size refinement with improved PE shape recovery properties. Besides, it was shown that higher addition of grain refiners i.e., solid solubility limit forms secondary phase precipitates, does have an adverse effect on grain-size refinement as well as PE shape recovery properties (Ding et al. 2019; Jones and Pearson 1976; Yang et al. 2017a).

2.8 IDENTIFICATION OF THE PROBLEM

The efficient energy dissipation and recentering characteristics of dampers are much necessary for vibration damping/isolation applications of structures that require higher PE strain recovery and longer functional life without significant degradation or permanent plastic deformation, along with high stiffness, strength, and ductility. All of these properties required for the utilization of SMA dampers in civil and structural applications are primarily dependent on the elemental composition and heat treatments employed in the preparation and processing of alloys.

Ni-Ti-based shape memory alloys are used in many applications and already had a commercial presence due to their superior advantages, such as high strain recovery and long functional life. Nevertheless, these are restricted to their vast usage due to shortcomings like processing difficulties and high cost. Cu-Al-based SMAs are selected as a prime alternative to Ni-Ti-based SMAs owing to their ease of manufacture and economical. All ternary Cu-based polycrystalline SMAs have shown poor mechanical properties and rapid brittle failure in the application, owing to the coarse grains. The addition of different grain refiners (i.e., B, Cr, Ti, V, Zr, and REE, etc.) and thermal treatments (betatization) modifies the grain sizes, grain boundaries, phase transformation temperatures, and the phases as well as their structures of the ternary base alloys. It is observed that the identical refiner behaves differently in two distinct ternary alloys depending on metal characteristics and treatments.

Among the family of Cu-based polycrystalline SMAs, these alloy dampers and isolators are limited their usage in practical applications because; (i) Cu-Zn-Al SMAs undergoes rapid strain hardening by stabilized martensites at room temperature, (ii) Cu-Al-Ni SMAs hinders martensitic transformations and fails brittle owing to the existence of secondary phase precipitates along the grain boundaries, and also possess high transformation temperatures, (iii) Cu-Al-Mn SMAs with higher wt.% of Al remains brittle and have extremely low fatigue strength, whereas lower weight percentage of aluminium does have high transformation temperatures, preventing pseudoelasticity at room temperature, and, and (iv) Cu-Al-Be SMAs with lower wt.% of Al has a wide range of transformation temperatures, i.e., from -200 to +200 °C and also shown good

pseudoelasticity at room temperature. However, the parent austenitic phase of Cu-Al-Be SMAs possesses a coarse-grained microstructure that is inherently brittle.

2.9 RESEARCH GAPS

From the literature survey, it is observed that beryllium (Be) as a ternary element is now often added into Cu-Al alloys to develop pseudoelastic SMAs at room temperature, as very small changes in weight percentage of the beryllium can cause drastic differences in phase transformation temperatures. In general, the addition of 0.1 wt.%Be to the Cu-Al alloy reduces phase transformation temperatures by approximately 90 °C. The unique characteristics of polycrystalline Cu-Al-Be SMAs, such as pseudoelasticity (PE), shape memory effect (SME), and damping effect are enhanced by refining the grain size. However, grain refinement can be restricted to a minimal extent by various methods of thermal treatment. The addition of solutes/inoculants is a simple and efficient technique of grain refinement in bulk alloys and is also beneficial in improving strength and ductility. However, the influence of grain refiner elements boron and zirconium has not been reported on the pseudoelastic behavior of Cu-Al-Be SMAs. This has motivated us to investigate the influence of quaternary elements, boron- and zirconium-doping into Cu-Al-Be polycrystalline SMAs to improve the strength, ductility, and pseudoelastic strain recovery without significant martensite stabilization or permanent plastic deformation at ambient work temperature. On the basis of the preceding discussion, the present research objectives were designed and presented in the proceeding section.

2.10 OBJECTIVES

The objectives of the present research work drawn from the study are as follows:

- To investigate the role of alloying additions on phase transformations, mechanical and pseudoelastic properties of Cu-Al-Be SMAs.
- To investigate the influence of grain refiner elements boron and zirconium on morphology, microstructure, mechanical properties and pseudoelastic behavior of parent austenitic phase Cu-Al-Be SMAs.
- To examine the effect of extended pseudoelastic cyclic loading and unloading on the change of transformation mechanism including SMA response stabilization, and suitability for use as vibration damping material.
- To examine the microstructural modifications and characterize the defects generated by pseudoelastically deformed SMAs.

2.11 CLOSURE

This chapter presented a detailed overview of the comprehensive literature on shape memory alloys and their types. Besides, the literature connected to the numerous techniques and investigations to the enhancement of grain-size refinement, variations in phase transformation temperatures, mechanical and pseudoelastic shape recovery characteristics was provided. Based on the existing literature, the problem and research gaps were identified, and further objectives were defined. The next chapter discusses the complete details of metals and their elemental compositions used in the present investigation. Besides, the methodology for producing shape memory alloys as well as the standards used for alloy characterization are presented.

CHAPTER 3

MATERIALS AND METHODS

3.1 INTRODUCTION

This chapter presents a detailed discussion of metals and variations in their elemental composition range used in the investigation of SMAs and the methodology for preparing and processing the alloys/specimens in three sections. The first section discusses the metals, master alloys, and their purity. The second section discusses the methodology used for the preparation of SMAs and the specimens/samples for characterization studies. The third section discusses the procedures and ASTM standards used for X-ray diffraction, microstructure, grain size, morphology, transformation temperatures, uniaxial tensile test for mechanical properties, and cyclic tensile test for pseudoelastic response studies.

3.2 ELEMENTAL COMPOSITIONS

In the present study, Cu-Al-Be ternary SMAs were selected as the base/nominal alloys. Four different combinations of nominal alloys investigation are carried out between hypoeutectoid and hypereutectoid compositions. Further, boron and zirconium are selected as grain refiners to improve the grain refinement of SMAs. Table 3.1 presents the elemental composition range of the elements considered for the preparation of the shape memory alloys.

Table 3.1 Elements and their weight percentages.

Sl. No.	Metal	Range (wt.%)
1.	Copper (Cu)	Remaining
2.	Aluminium (Al)	11.00 - 11.80
3.	Beryllium (Be)	0.50 - 0.60
4.	Boron (B)	0.05 - 0.20
5.	Zirconium (Zr)	0.05 - 0.30

3.3 METALS AND PURITY

The raw materials used in this investigation are high purity copper, aluminium and the different master alloys including CuBe_4 , CuB_2 , and $\text{Cu}_{51}\text{Zr}_{14}$ are as presented in Figures 3.1 – 3.5. Aluminium is used in the form of small buttons. Copper and all master alloys were sliced into small pieces from the respective ingots using a shear cutting machine. The purity of raw materials is given in Table 3.2.

Table 3.2 Type of metals and their purity.

Sl. No	Metals	Purity (%)
1.	Copper	99.95%
2.	Aluminium	99.90%
3.	Copper Beryllium - CuBe_4	99.99%
4.	Copper Boron - CuB_2	99.99%
5.	Copper Zirconium - $\text{Cu}_{51}\text{Zr}_{14}$	99.99%



Figure 3.1 Copper.

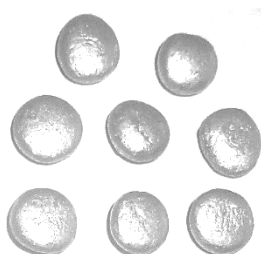


Figure 3.2 Aluminium buttons.

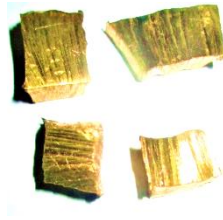


Figure 3.3 CuBe₄ master alloy.

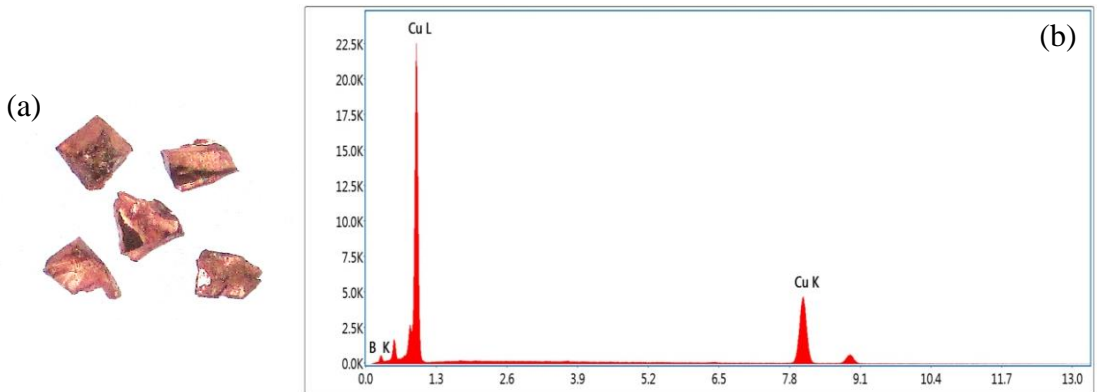


Figure 3.4 (a) Photograph of CuB₂ inoculant and (b) EDS of CuB₂ inoculant.

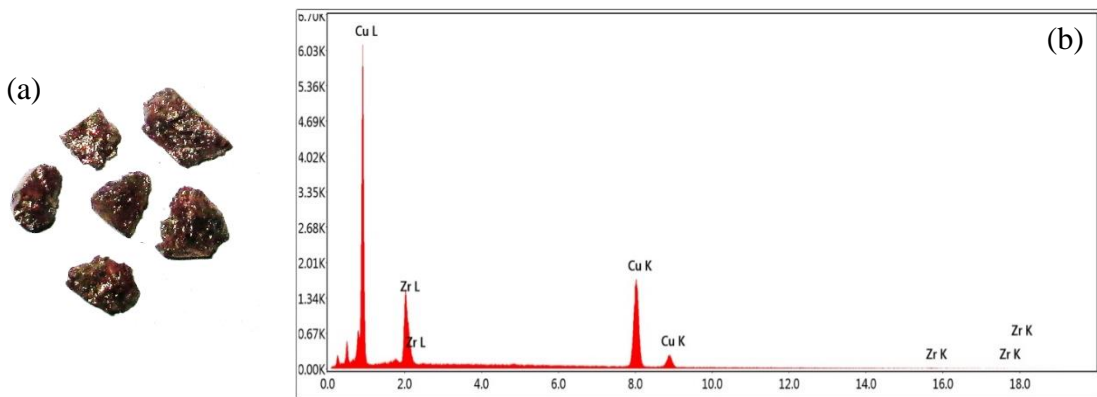


Figure 3.5 (a) Photograph of Cu₅₁Zr₁₄ inoculant and (b) EDS of Cu₅₁Zr₁₄ inoculant.

3.4 METHODOLOGY

The experimental methodology as shown in Figure 3.6 was carried out in the present investigation. This includes experimental procedures carried out for preparing alloys for the investigation of phases/precipitates, morphology, microstructure, transformation temperatures, tensile properties, fractography, pseudoelastic hysteresis behaviors and microstructural modifications.

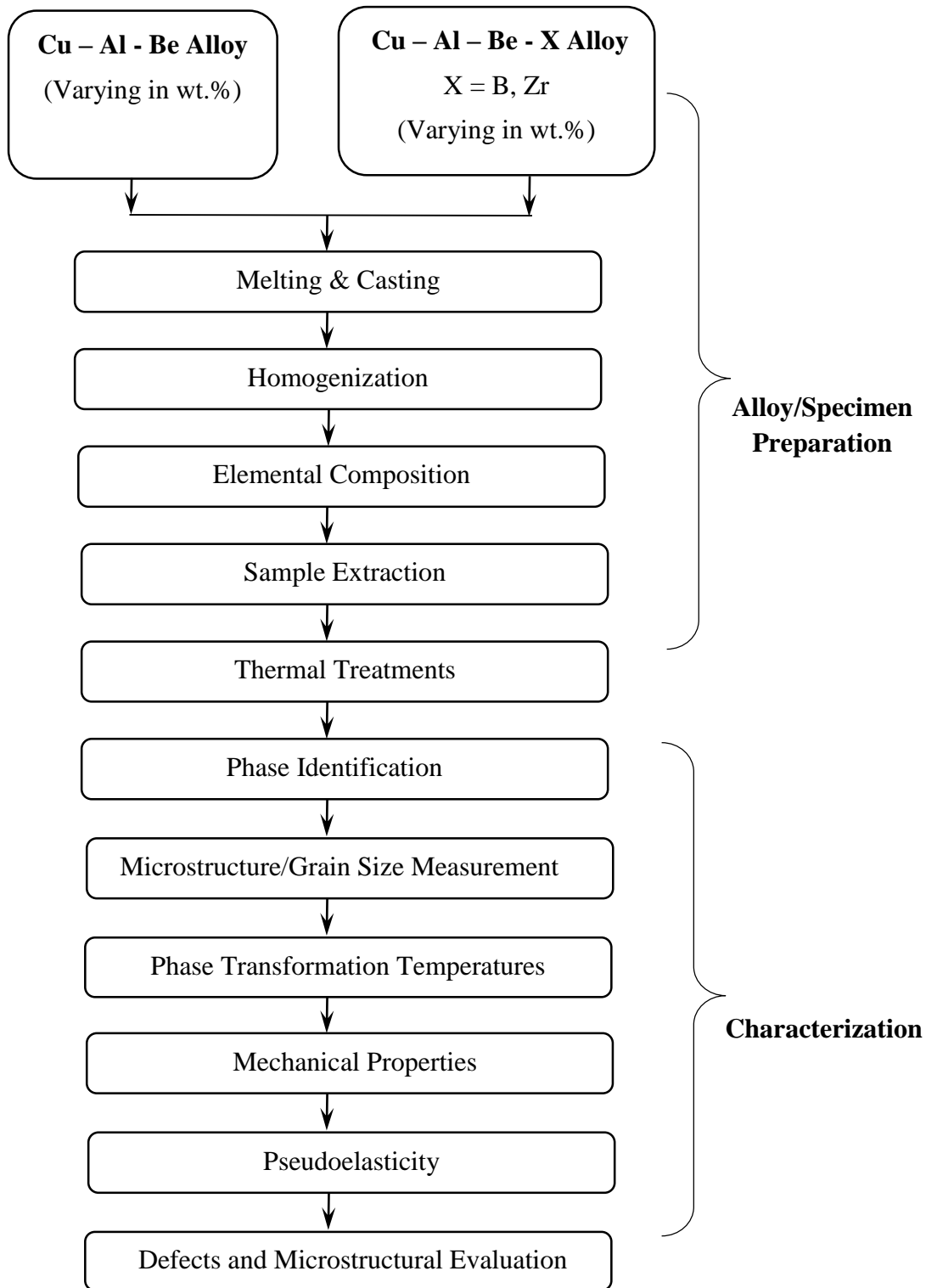


Figure 3.6 Flow chart of methodology.

3.4.1 Alloy Preparation

In the following subsequent sections, the details of experimental procedures carried out for preparing alloys and samples have been discussed.

3.4.1.1 Melting and casting

Initially, small pieces of raw materials were weighed accurately as per the nominal compositions of the alloy elements in terms of weight percentage (wt.%) using a four-decimal digit display weighing machine. The mixture of 250 grams of raw materials was melted in an isostatic graphite crucible sited in an induction furnace heating-coil chamber under an argon protective atmosphere (99.999% Ar purity) and is shown in Figure 3.7(a). Melt was thoroughly stirred and then poured into the preheated die steel molds with a cavity size of 100×100×2.5 mm, and allowed to solidify. Further, the cast alloys were remelted twice to ensure better homogeneity and cast was made in the form of a plate, as shown in Figure 3.8(a).

3.4.1.2 Homogenization

The solidified cast plates were homogenized at 850 °C for four hours in a muffle furnace (Figure 3.7b) under an argon protective atmosphere to ensure homogeneous distribution of alloying elements in the matrix, and then air-cooled to ambient temperature to prevent cracking (Davis and Committee 2001).

3.4.1.3 Sample preparation

The alloy specimens for the investigations were extracted from homogenized cast plates using a wire electrical discharge machine (WEDM) for microstructural, tensile, and pseudoelastic response studies and a low-speed diamond cutting machine for differential scanning calorimetry (DSC) test to measure the phase transformation temperatures of the alloys.

3.4.1.4 Betatization

The alloy specimens extracted from WEDM were betatized/annealed at 850 °C for 10 minutes under an argon protective atmosphere to avoid oxide formation and then rapidly quenched into water at room temperature.

Several stages involved in the fabrication and processing of Cu-Al-Be-based SMA specimens are illustrated schematically in Figure 3.9.

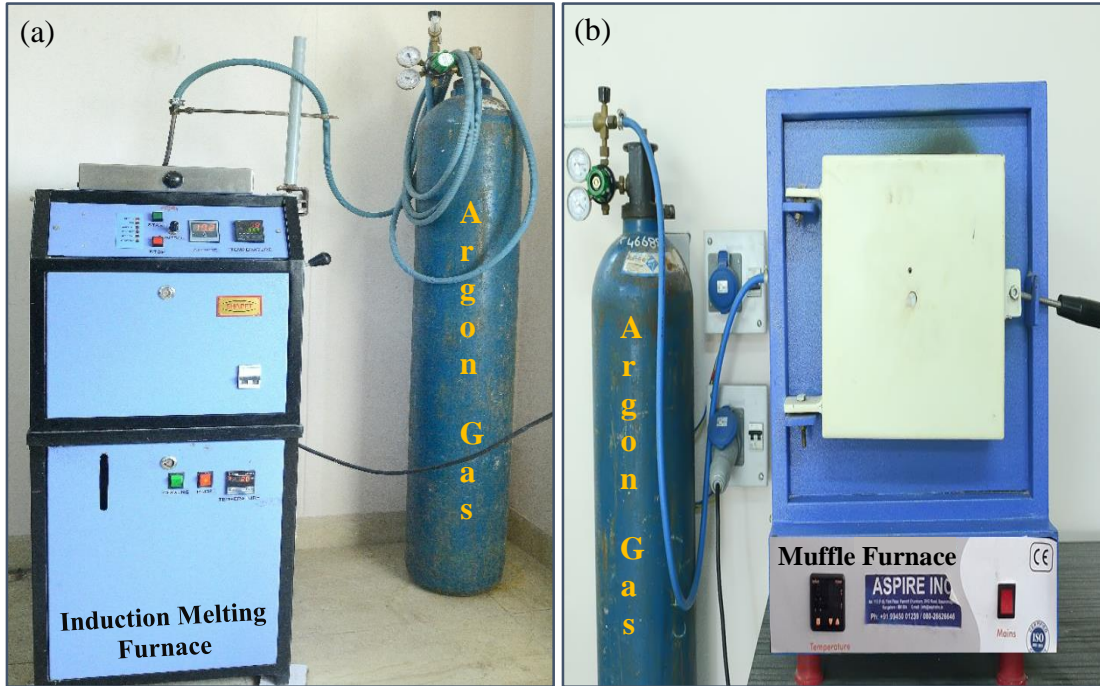


Figure 3.7 Photographs of (a) Induction melting furnace with argon gas setup and (b) Muffle furnace with argon gas setup.

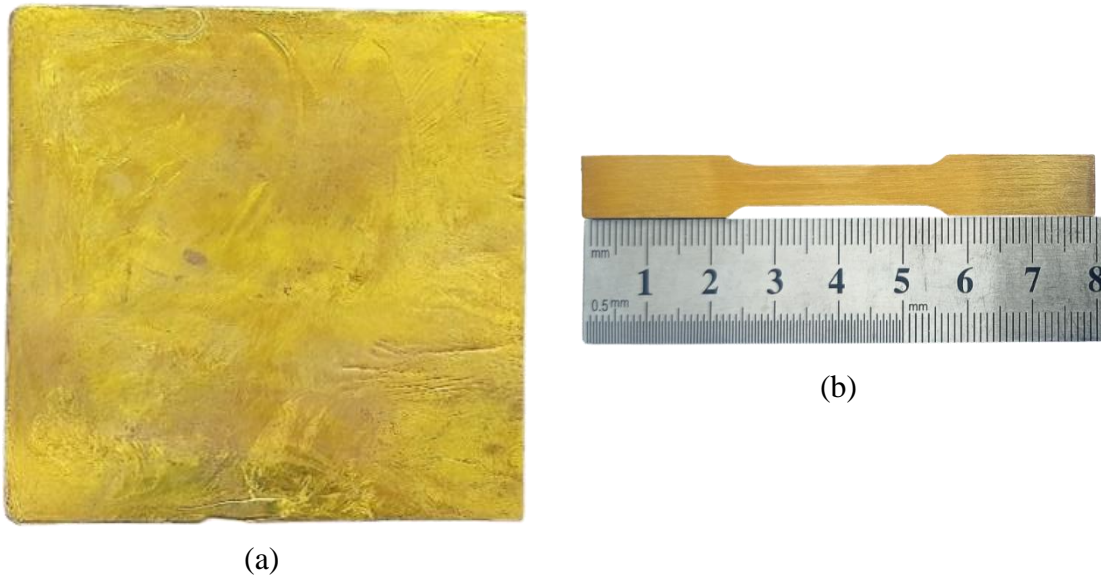


Figure 3.8 Photographs of (a) Alloy plate and (b) Tensile specimen.

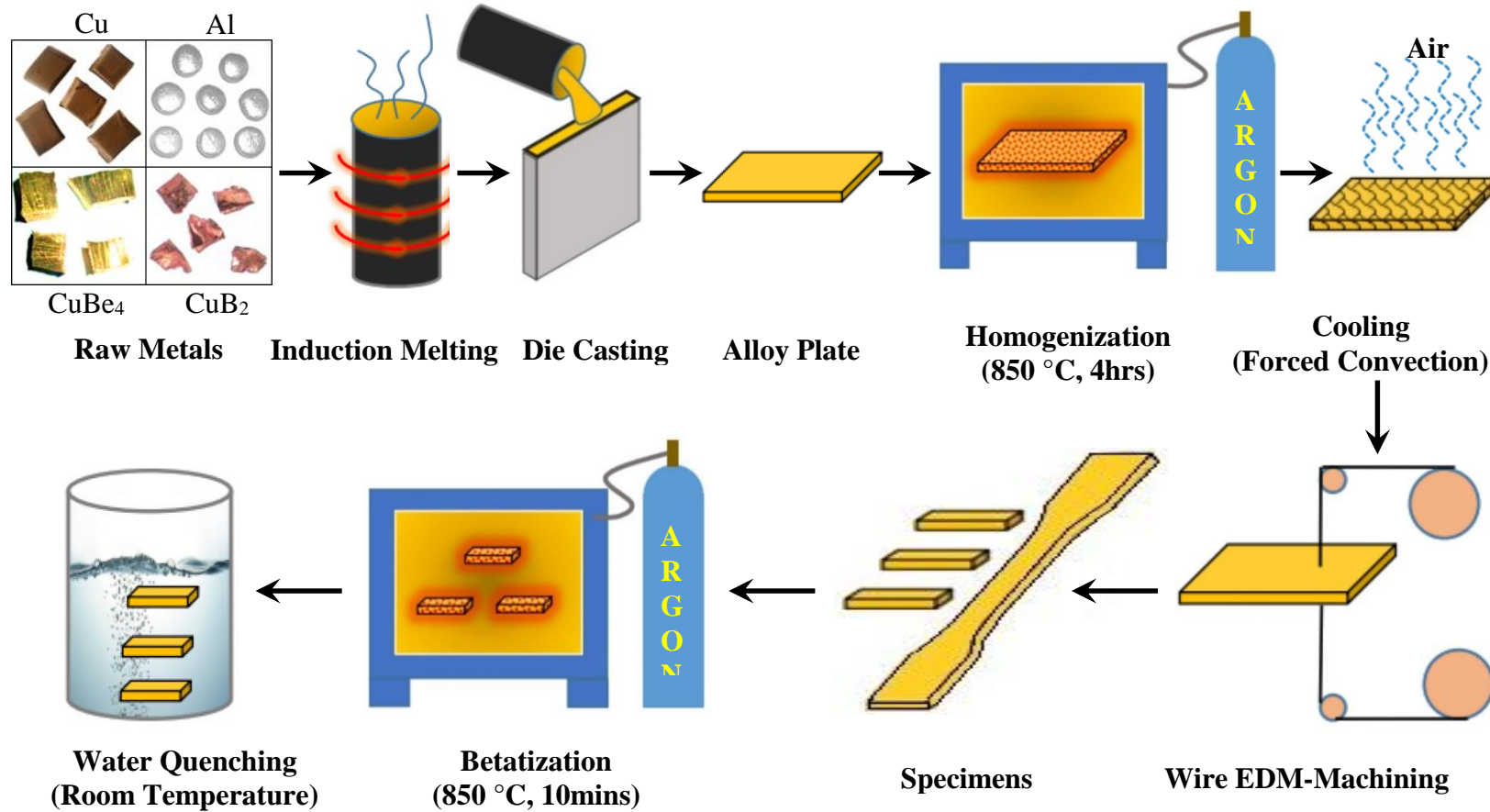


Figure 3.9 Stages of the preparation and processing of Cu-Al-Be-based SMAs.

3.4.2 Characterization

Betitized and quenched alloy specimens were investigated for phase identification, morphology, microstructure, phase transformation temperatures, mechanical properties, fractography, pseudoelastic hysteresis responses using various apparatuses, and procedures for average grain size and main characteristic features of pseudoelastic hysteresis plot. These are discussed in detail in the proceeding sections.

3.4.2.1 Elemental composition

The actual/elemental composition of SMAs was determined using AMETEK make spark discharge-based optical emission spectrometer (Model: MAXxLMF04). The spark was ignited at three distinct spots on the homogenized SMA plate. Therefore, each outcome is the average of three measurement readings. Agilent make inductively coupled plasma optical emission spectrometer (ICP-OES, Model: Agilent-5100) was employed to measure the actual composition of boron elements. Alloy samples for the ICP-OES test were digested in 10 ml reverse aqua regia solution (i.e., 8 ml HCl+2 ml HNO₃) and then diluted in distilled water (dilution factor: 0.1). These diluted samples were tested at wavelengths of 249.677, 313.107, 396.153 and 327.393 nm for boron, beryllium, aluminium and copper, respectively.

3.4.2.2 X-ray diffraction - Phase identification

Phases exist in the betitized and quenched SMAs, and their crystal structures were analyzed using Rigaku make X-ray Diffractometer (XRD, Model: Miniflex 600). The alloy specimen was placed in a rectangular-shaped aluminium holder with an adhesive tape backing and then laid on the sample stage. The copper anode was then rotated from $2\theta=20^{\circ}$ – 90° at a scan speed of $2^{\circ}/\text{min}$ under monochromatic $\text{CuK}\alpha_1$ radiation of wavelength, $\lambda = 1.54056 \text{ \AA}$ at 40 kV and 15 mA.

3.4.2.3 Specimen preparation – Morphology and microstructure

To investigate the microstructure and surface morphology of SMAs, the betatized and quenched specimens were initially polished by mechanical grinding with a typical sequence of coarse- to ultrafine-grit abrasive papers (i.e., 80, 120, 400, 800, 1000, 1500, 2000 and 2500 grit), and then final polishing was carried out using velvet cloth with alumina slurry (1 μm size Al_2O_3 powder and distilled water). After ensuring a scratch-free surface by final polish, etched with a solution of 2 g of FeCl_3 + 2 ml of HCl + 95 ml of methanol. The etched surface is thoroughly cleaned with distilled water and dried out to assess the morphology and microstructure.

- **Morphology**

The surface morphology, secondary phase precipitates, and its elemental composition were studied using Zeiss make field emission scanning electron microscope (FESEM, Model: Gemini-300) equipped with energy dispersive spectroscopy (EDS, Model: EDAX - AMETEK).

- **Microstructure**

The microstructural changes of SMAs were captured using Zeiss make optical microscope (OM, Model: Axiocam-105 color).

3.4.2.4 Grain size measurement

The average grain size of the SMAs was measured from the optical micrographs by adopting the linear intercept method as per ASTM E1382 standard - automatic and semiautomatic image analysis tools.

3.4.2.5 Phase transformation temperatures

The phase transformation temperatures were obtained using a differential scanning calorimeter (DSC, Model: Perkin, Elmer-6000) equipped with a liquid nitrogen environment. SMA specimens with a weight between 35 to 45 milligrams were extracted from the alloys using a low-speed diamond cutter and sealed in a DSC pan with a covering

lid. The sealed DSC pan was inserted into the chamber and heated at a scan rate of 10 °C/min from -50 to 100 °C, then cooled to -50 °C. DSC testing consists of three cycles: heating, cooling, and heating. DSC curves/thermograms were recorded from the first cooling and second heating cycle. Phase transformation temperatures of the martensite (M_s, M_f) and austenite (A_s, A_f) were determined from DSC thermograms by adopting the baseline tangent method, and enthalpy change (ΔH) was measured from the area under the phase transformation cycles of the DSC curve, as shown in Figure 3.10. Enthalpy is the chemical energy required for phase transformations, and the enthalpy change in SMAs comprises of two reactions: endothermic and exothermic. As the name implies, “ $\Delta H_{M \rightarrow A}$ ” occurs when the heat energy is added for martensite to austenite transformation and is preceded with a positive sign, i.e., an endothermic reaction, while “ $\Delta H_{A \rightarrow M}$ ” takes place when the heat energy is removed from austenite to martensite transformation and is preceded with a negative sign, i.e., an exothermic reaction.

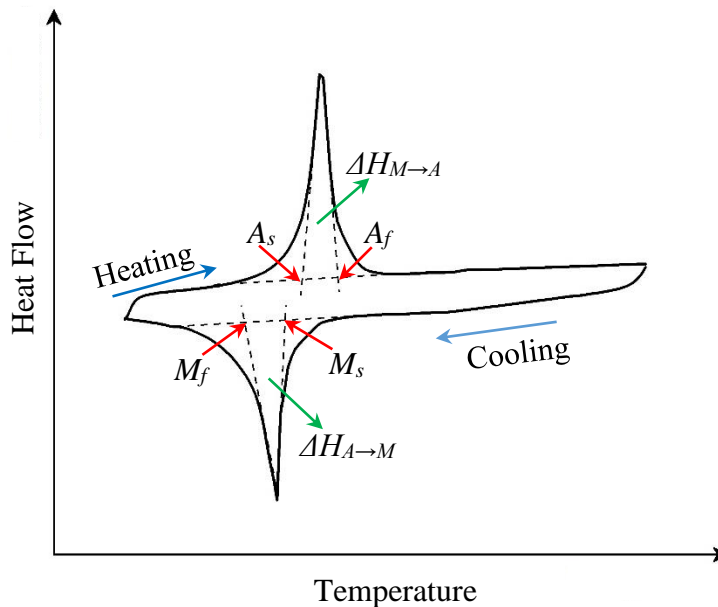


Figure 3.10 Schematic of the measurement for phase transformation temperatures from DSC curves.

3.4.2.6 Mechanical properties – Uniaxial tensile test

Uniaxial tensile tests were performed on the SMA samples using a universal testing machine (Make: Shimadzu, and Model: AG-X Plus, 100 kN) to assess the mechanical properties, such as ultimate stress and ultimate strain. Figure 3.8(b) depicts the photographic image of betatized and quenched tensile specimen. Flat dog-bone-shaped specimens were prepared as per ASTM E8/E8M standard for 25 mm gauge length, and tests were carried out with a loading rate of 1 mm/min at room temperature (i.e., parent austenite state).

3.4.2.7 Fractography

Tensile fracture modes were analyzed using a field emission scanning electron microscope (FESEM, Make: Zeiss, Model: Gemini-300).

3.4.2.8 Pseudoelastic behavior – Cyclic tensile test

The pseudoelastic behavior of SMAs was studied by performing a cyclic tensile test consisting of mechanical loading in the first half-cycle up to the selected deformation strain, and then unloading in the next half-cycle, as schematically illustrated in Figure 3.11. All the cyclic tests were set to a constant cross-head speed of 0.1 mm/min to record hysteresis of stress-induced shape recovery at an ambient temperature, i.e., above the austenite finish temperature (A_f). For all the hysteresis tests, a flat dog-bone-shaped specimen was subjected to a single cycle or extended cycles of loading and unloading.

Hysteresis plot features denote the main characteristics of pseudoelastic behavior (Montecinos et al. 2008; Sade et al. 2014; Sutou et al. 2013), namely critical stress (σ_{CS}) for the transformation of parent austenite (DO_3) to stress-induced martensite ($18R$), pseudoelastic transition slope ($d\sigma_{PE}/d\varepsilon$), stress hysteresis ($\Delta\sigma$), and residual strain (ε_r). The procedure to assess plot features is as follows, the first linear segment of the pseudoelastic loading curve indicates the elastic regime of the austenite phase, whereas the linearity deviation is related to the start of austenite to martensite transformation. Consequently, the stress at the end of the first linear segment is denoted as σ_{CS} . The

progression of martensite transformation exhibit nearly constant stress (σ) – strain (ε) path, and the work-hardening rate defined by the slope, i.e., $d\sigma_{PE}/d\varepsilon$ after yielding and is called pseudoelastic transition slope. On releasing the applied load, martensite retransformation into austenite forms a hysteresis loop, and show nearly constant σ – ε path at relatively lower stress levels than that of martensite transformation path; thus, “ $\Delta\sigma$ ” is a measure of stress difference between the martensite transformation and retransformation paths, i.e., $\Delta\sigma = (\sigma_{PE})_{\text{Loading}} - (\sigma_{PE})_{\text{Unloading}}$, and this was determined at median of the selected deformation strains (ε_d). Residual strain, ε_r is defined as the irreversible strain that remains permanently in the alloy after complete unloading. Finally, the microstructural modifications and defects generated after the pseudoelasticity tests were examined using both optical microscopy and XRD studies.

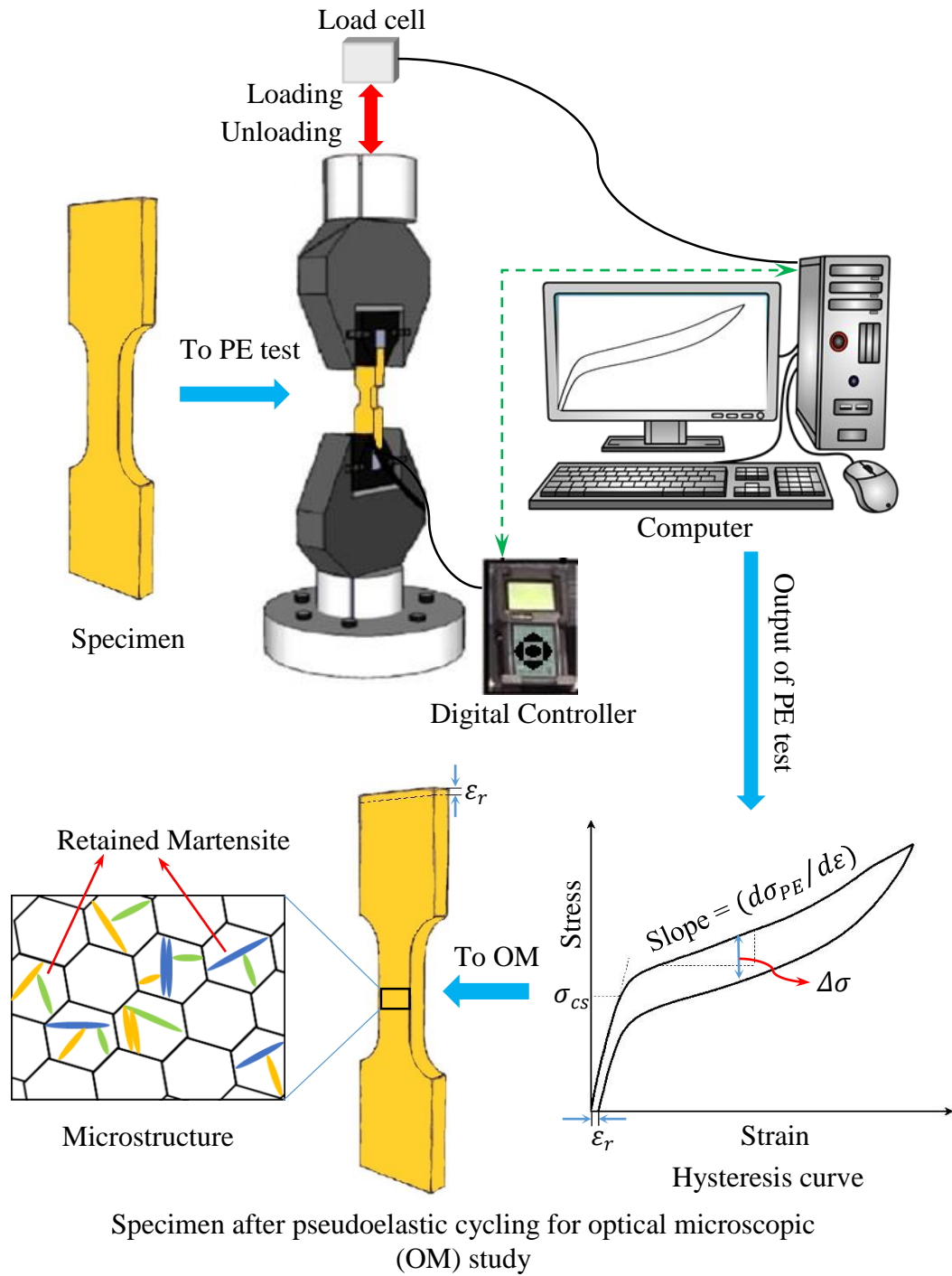


Figure 3.11 Schematic of the pseudoelasticity (PE) test.

3.5 CLOSURE

This chapter presented a detailed description of the metals used in the investigation, including their purity and the range of elemental compositions. In addition, the methodologies for the preparation and processing of alloys as well as specimens for the present characterization studies, namely, X-ray diffraction, morphology, microstructure, grain size, DSC test, and uniaxial and cyclic tensile tests have been reported. The proceeding chapter presents experimental investigation results and discussion on the influence of ternary- and quaternary-doped elements on the properties of SMAs and their mechanisms.

CHAPTER 4

RESULTS & DISCUSSION

4.1 INTRODUCTION

This chapter presents the details of the elemental compositions of Cu-Al-Be-X (X=B, Zr) shape memory alloys used in the present investigation. The role of ternary and quaternary elements on metallurgical, mechanical, and pseudoelastic behavior of the SMAs has been examined. The mechanisms of phase modifications, grain-size refinement, precipitate formations, variations in phase transformation temperatures, changes in tensile properties, and the pseudoelastic shape recovery response of the evaluated alloys have been discussed. Section 4.2 shows the results of ternary Cu-Al-Be polycrystalline shape memory alloys. Sections 4.3 and 4.4 presents the results of quaternary added elements, i.e., boron- and zirconium-doped SMAs, respectively. The closure of this chapter provides suitable alloying elements and their optimal compositions for developing a damper for vibration damping applications.

4.2 TERNARY Cu-Al-Be SMAs

In the present investigation, four sets of ternary Cu-Al-Be polycrystalline SMAs were prepared by varying the weight percentage of aluminium, $11.0 \leq \text{Al} \leq 11.8$ wt.%, and beryllium, $0.5 \leq \text{Be} \leq 0.6$ wt.%. The actual (as-cast) elemental composition of Cu-Al-Be SMAs are tabulated in Table 4.1 and denoted as A_{1-4} , where, A denotes the alloy and the number placed in subscript indicates the alloy type.

Table 4.1 Elemental compositions of Cu-Al-Be SMAs.

Sl. No.	Alloy	Actual composition (wt.%)		
		Cu	Al	Be
1.	A ₁	87.6	11.08	0.458
2.	A ₂	87.2	11.53	0.497
3.	A ₃	86.7	11.98	0.55
4.	A ₄	86.3	12.23	0.57

4.2.1 X-ray Diffraction (XRD) – Phases Identification

The prepared ternary Cu-Al-Be SMA samples were betatized and then rapidly quenched into water at room temperature, as discussed in Section 3.4.1.4. The phases that exist in the evaluated alloys are analyzed by XRD and X'Pert HighScore software and are presented in Figure 4.1.

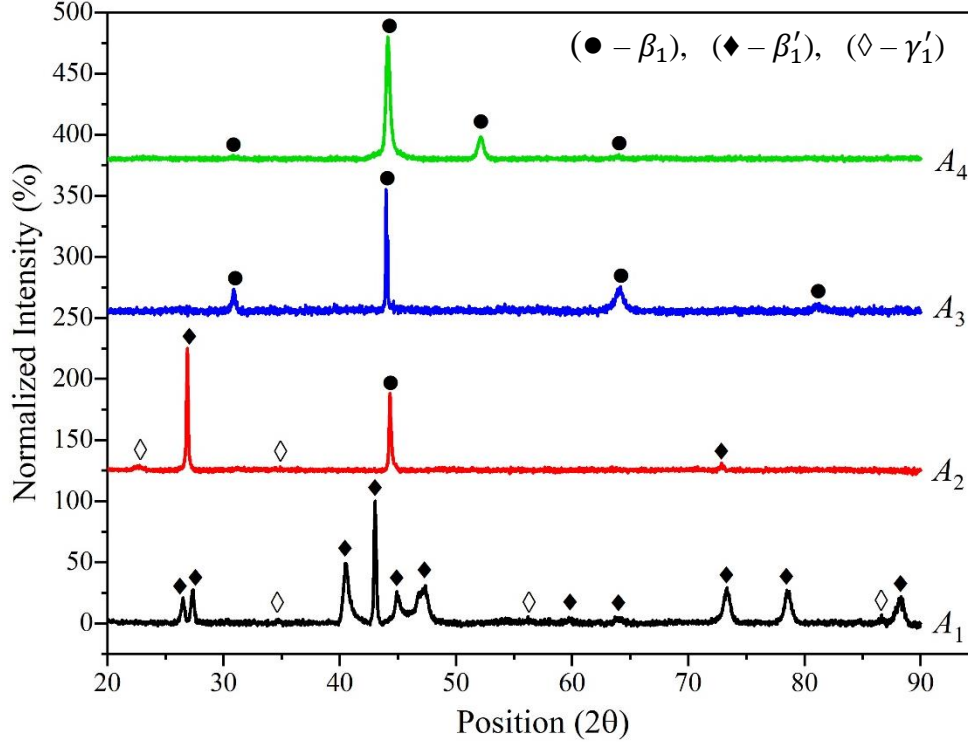


Figure 4.1 Normalized X-ray diffractograms of Cu-Al-Be SMAs.

X-ray diffractograms of Cu-Al-Be SMAs shown in Figure 4.1, confirms the phases and structures of the alloys by varying wt.% of aluminium and beryllium. Diffractogram of the alloy A_1 reveals the presence of complete martensite phase of orthorhombic ($\beta'_1 - 18R$) and monoclinic ($\gamma'_1 - 2H$) structures are denoted with the symbol (\blacklozenge) and (\diamond), respectively. The higher additions of Al and Be to A_2 exhibit a mixture of both austenite (\bullet) and martensite phases. Furthermore, the increase of Al and Be into A_3 and A_4 process a pure austenite phase of cubic ($\beta_1 - DO_3$) structure.

4.2.2 Microstructure – Grain Size

The optical micrographs were captured from Cu-Al-Be SMA samples and the microstructures are presented in Figure 4.2. From this Figure, it is observed that all the ternary Cu-Al-Be alloys consist of equiaxed and coarse grains in both longitudinal and transverse directions. The measured average grain size of the SMAs is $1134 \pm 29 \mu\text{m}$.

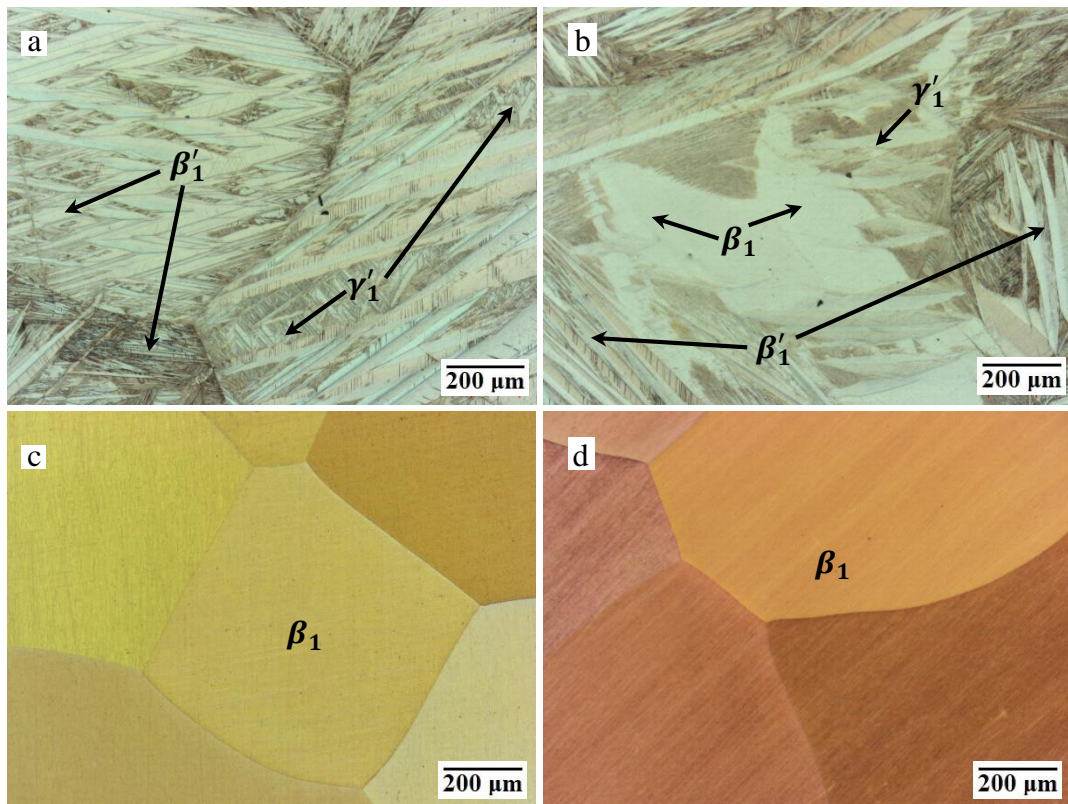


Figure 4.2 Microstructures of Cu-Al-Be SMAs: (a) A_1 , (b) A_2 , (c) A_3 and (d) A_4 .

The prime phase of A_1 alloy as depicted in Figure 4.2(a), consists of fine and sharp needles of β'_1 -type and coarse plates of γ'_1 -type martensites. It is also confirmed with an X-ray diffractogram and from Sari et al. (2006, 2008). A_2 alloy micrograph is shown in Figure 4.2(b) unveiled the coexistence of austenite and martensite phases, i.e., $\beta_1 + \beta'_1 + \gamma'_1$. Figures 4.2(c and d) depicted that SMAs A_3 and A_4 possess complete austenite (β_1) phase.

4.2.3 Phase Transformation Temperatures

The phase transformation temperatures, enthalpies, and thermal hysteresis of Cu-Al-Be SMAs are determined using heating and cooling cycles of DSC curves. The transformation temperatures (M_f , M_s , A_s , A_f) were measured by adopting the baseline-tangent method and enthalpy (ΔH) from the area under the DSC curve. The results are presented in Figure 4.3 and Table 4.2.

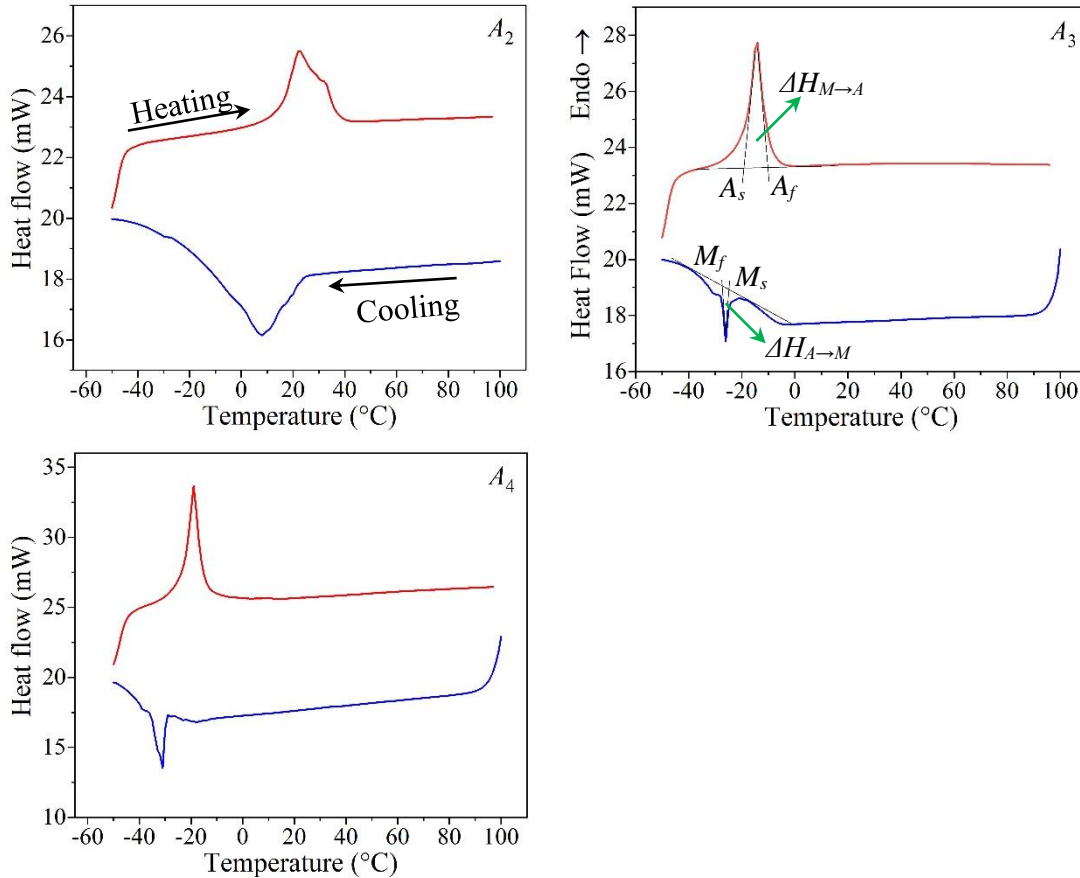


Figure 4.3 DSC curves of Cu-Al-Be SMAs.

Table 4.2 Phase transformation temperatures ($^{\circ}\text{C}$), enthalpies (J/g), and thermal hysteresis ($^{\circ}\text{C}$) of Cu-Al-Be SMAs.

Alloy	M_f	M_s	$\Delta H_{A \rightarrow M}$	A_s	A_f	$\Delta H_{M \rightarrow A}$	$(A_f - M_s)$
A_2	-3.86	20.28	-11.71	14.42	37.14	6.97	16.86
A_3	-27.96	-25.13	-1.45	-18.95	-10.40	6.01	14.73
A_4	-34.08	-30.12	-4.71	-22.71	-15.12	8.23	15.00

From the results, it is worth to be noted that an increase in the weight percentage of both aluminium and beryllium decreases the transformation temperatures. Besides, the effect of beryllium-doping on the transformation temperature of Cu-Al-Be ternary alloy is much stronger than that of aluminium (Belkahla et al. 1993; Mañosa et al. 1998). From Figure 4.3, it is also observed that the alloy A_2 exhibit a much broader peak, indicating higher thermal energy needed for transformation, whereas A_3 and A_4 SMAs show a sharp peak, which indicates the rapid transformations of the phases austenite and martensite due to the elemental composition of Al near to the eutectoid (Belkahla et al. 1993).

4.2.4 Mechanical Properties and Fracture Morphology

At room temperature, uniaxial tensile tests were carried out on the mechanical properties of ternary Cu-Al-Be SMAs, such as tensile strength, ductility, and fractography analysis, as discussed in Sections 3.4.2.6 and 3.4.2.7. The measured engineering stress-strain plot is the average of three test data as depicted in Figure 4.4(a), and the results of ultimate tensile stress (σ_{max}) and ultimate tensile strain (ε_{max}) are presented in Figure 4.4(b). The tensile strength, σ_{max} and ductility, ε_{max} of the alloy A_2 are 194.68 ± 16.79 MPa, and $10.67 \pm 0.32\%$, respectively. Furthermore, increased wt.% of both Al and Be into A_3 and A_4 resulted in the enhancements of tensile strength, 216.39 ± 30.17 and 220.48 ± 11.81 MPa, owing to the presence of austenite phase (Figueroa et al. 2020; Prashantha et al. 2014). However, the coarse austenite grains cause a loss of ductility, 9.24 ± 0.66 and $8.34 \pm 0.35\%$, with increasing strength because the austenitic phase of SMAs is harder and more rigid than the martensitic phase (Fernandes et al. 2011; Shimoga et al. 2021).

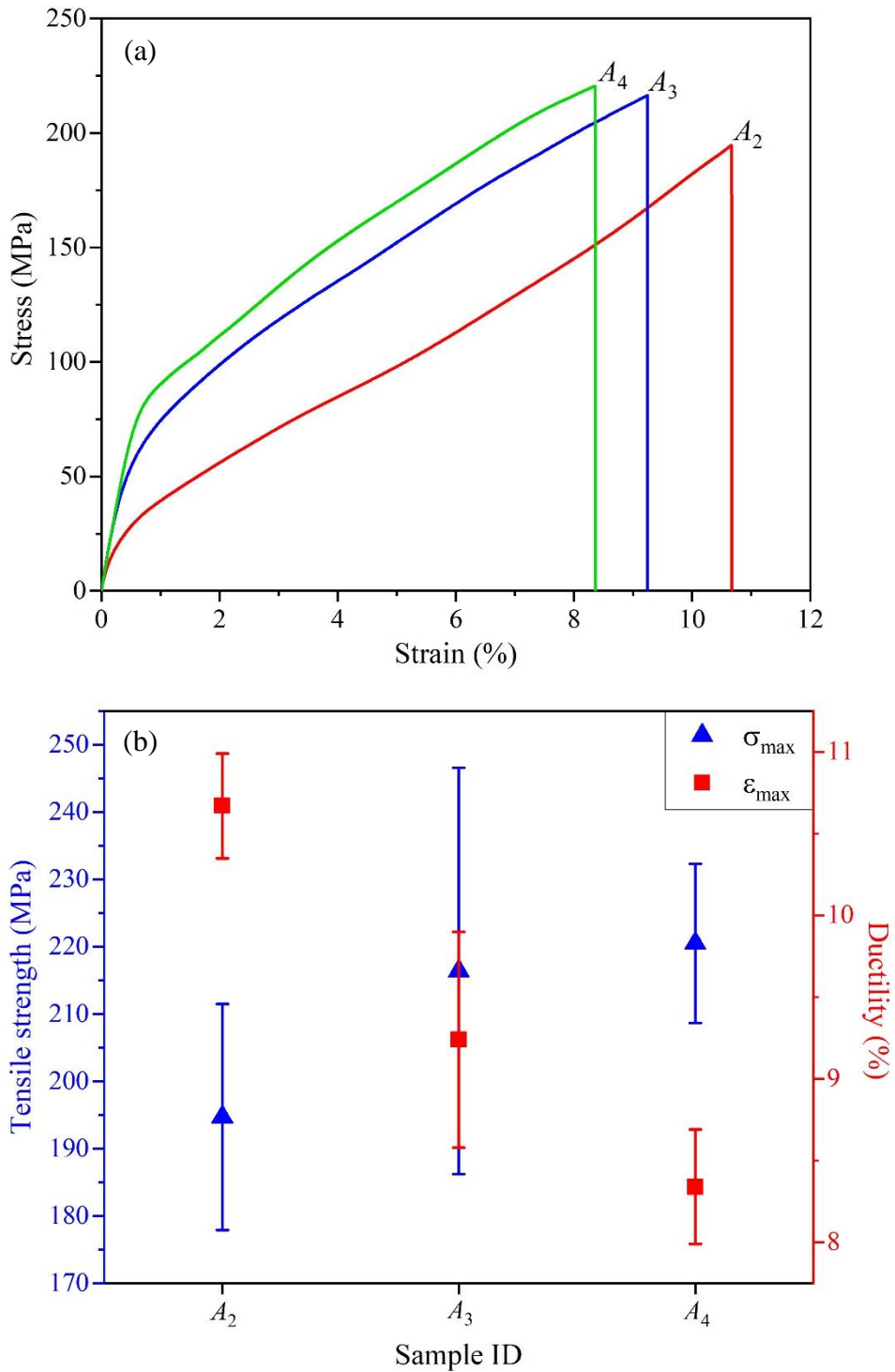


Figure 4.4 Tensile properties of Cu-Al-Be SMAs: (a) engineering stress-strain plots and (b) ultimate tensile stress (σ_{max}) and ultimate tensile strain (ϵ_{max}).

The fracture morphology as shown in Figures 4.5(a-c) indicates that all SMAs fail in an intergranular brittle fracture mode, i.e., separation of coarse grains occurs along crystallographic planes, due to low cohesive strength, and high-stress concentration at the grain boundaries (Husain and Clapp 1987b).

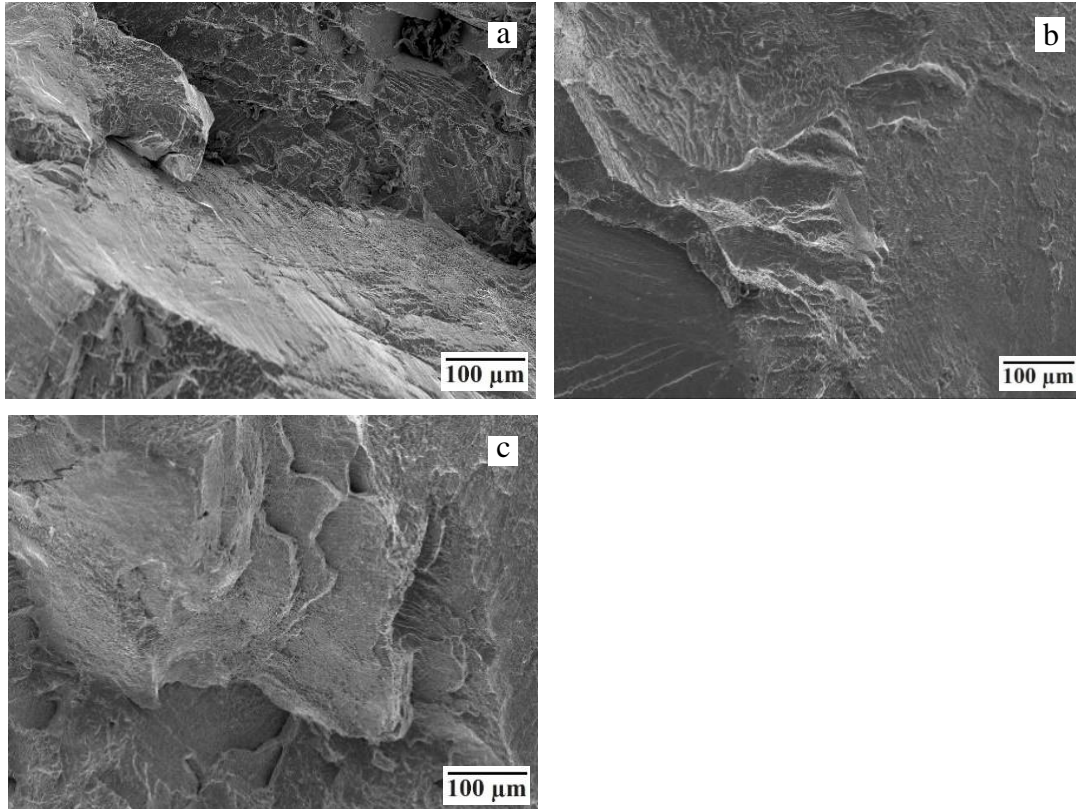


Figure 4.5 FESEM images of the fracture surface of Cu-Al-Be SMAs: (a) A_2 , (b) A_3 and (c) A_4 .

4.2.5 Pseudoelasticity and Microstructural Modifications

The pseudoelasticity tests were performed on A_3 SMA using cyclic tensile tests because that exhibits a complete austenitic phase at room temperature, smaller energy differences (ΔH) between austenite and martensite, and good mechanical properties at room temperature. The results are presented and discussed in Section 4.3.5.

4.3 QUATERNARY Cu-Al-Be-B SMAs

Based on the literature survey, the minimal addition of boron, i.e., 0.02 - 0.19 wt.%, as a quaternary-doped element exhibits a good grain refinement with improved mechanical properties (Han and Kim 1987; Morris 1991; Sampath and Mallik 2009; Zhang et al. 2010). This section presents the influence of B-doping, i.e., 0.05 - 0.2 wt.% to Cu-Al_{11.5}-Be_{0.57} SMA, and its impact on phases, morphology, microstructure, phase transformation temperatures, mechanical properties, and pseudoelastic behavior. The actual elemental composition of (Cu-Al_{11.5}-Be_{0.57})-B_x (x = 0.05, 0.1, 0.15, 0.2) alloys are tabulated in Table 4.3, B_i denotes the boron-doped alloy where, subscript, *i* = 1, 2, 3 and 4 for 0.05, 0.1, 0.15 and 0.2 wt.% of B, respectively.

Table 4.3 Elemental compositions of Cu-Al-Be-B SMAs.

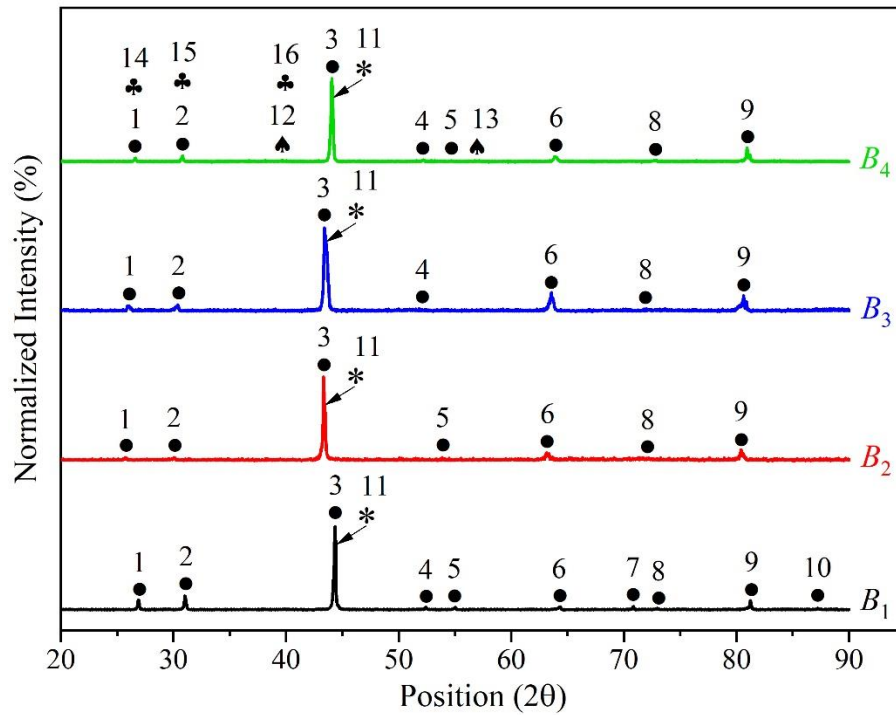
Sl. No.	Alloy	Actual composition (wt.%)			
		Cu	Al	Be	B
1.	B ₁	86.7	11.94	0.54	0.047
2.	B ₂	86.7	11.87	0.55	0.092
3.	B ₃	86.5	11.89	0.55	0.145
4.	B ₄	86.6	11.85	0.53	0.186

4.3.1 Phases and Morphology

The phase identification of Cu-Al-Be-B SMAs has been made through the XRD and X'Pert HighScore software. X-ray diffraction (XRD) profiles of the betatized and quenched SMA samples as shown in Figure 4.6, confirms the phases and crystal structures of the matrix parent phase, β_1 and secondary phase precipitates, AlB₂, Al_{1.35}Cu_{1.17}B_{52.5}, and Al_{8.67}B₁₇₆Be_{13.48}.

The XRD profiles of the B-doped alloys, viz. B₁, B₂ and B₃ reveals that the existence of a predominant β_1 -phase peaks along with AlB₂ phase peak. The presence of a parent β_1 -phase (Cu₃Al) denoted with a symbol (●), i.e., the austenite phase with ordered DO₃

structure (Chentouf et al. 2010). The structure of the AlB_2 phase (*) is a hexagonal crystal symmetry (space group: P6/mmm). The alloy B_4 exhibits two additional phase peaks, i.e., precipitates of $\text{Al}_{1.35}\text{Cu}_{1.17}\text{B}_{52.5}$ (♠) and $\text{Al}_{8.67}\text{B}_{176}\text{Be}_{13.48}$ (♣), in addition to β_1 and AlB_2 phases. The phases, $\text{Al}_{1.35}\text{Cu}_{1.17}\text{B}_{52.5}$ and $\text{Al}_{8.67}\text{B}_{176}\text{Be}_{13.48}$ are associated with rhombohedral (space group: R-3m) and tetragonal (space group: P43212) crystal structures, respectively.



● – β_1 : 1(1 1 1), 2(0 0 2), 3(0 2 2), 4(1 1 3), 5(2 2 2), 6(0 0 4), 7(1 1 3), 8(0 2 4), 9(2 2 4), 10(1 1 5); * – AlB_2 : 11(0 1 1); ♠ – $\text{Al}_{1.35}\text{Cu}_{1.17}\text{B}_{52.5}$: 12(2 2 6), 13(2 0 14); ♣ – $\text{Al}_{8.67}\text{B}_{176}\text{Be}_{13.48}$: 14(1 0 4), 15(3 1 2), 16(3 3 2).

Figure 4.6 Normalized XRD profiles of the betatized and quenched Cu-Al-Be-B SMAs.

FESEM-EDS studies were performed on the alloy B_4 and are, as presented in Figure 4.7. FESEM image, as shown in Figure 4.7(a) depicts the morphology of B_4 SMA and EDS spectrums of the alloy of B_4 provides the elemental composition of coarse secondary phase precipitates (Figures 4.7b and c) and the matrix (Figure 4.7d). From Figure 4.7(a), it is

observed that the presence of white and black spots, viz. $\text{Al}_{1.35}\text{Cu}_{1.17}\text{B}_{52.5}$ and $\text{Al}_{8.67}\text{B}_{176}\text{Be}_{13.48}$ phases, respectively, containing B-rich precipitates (Figures 4.7b and c) with very little quantity of aluminium and copper.

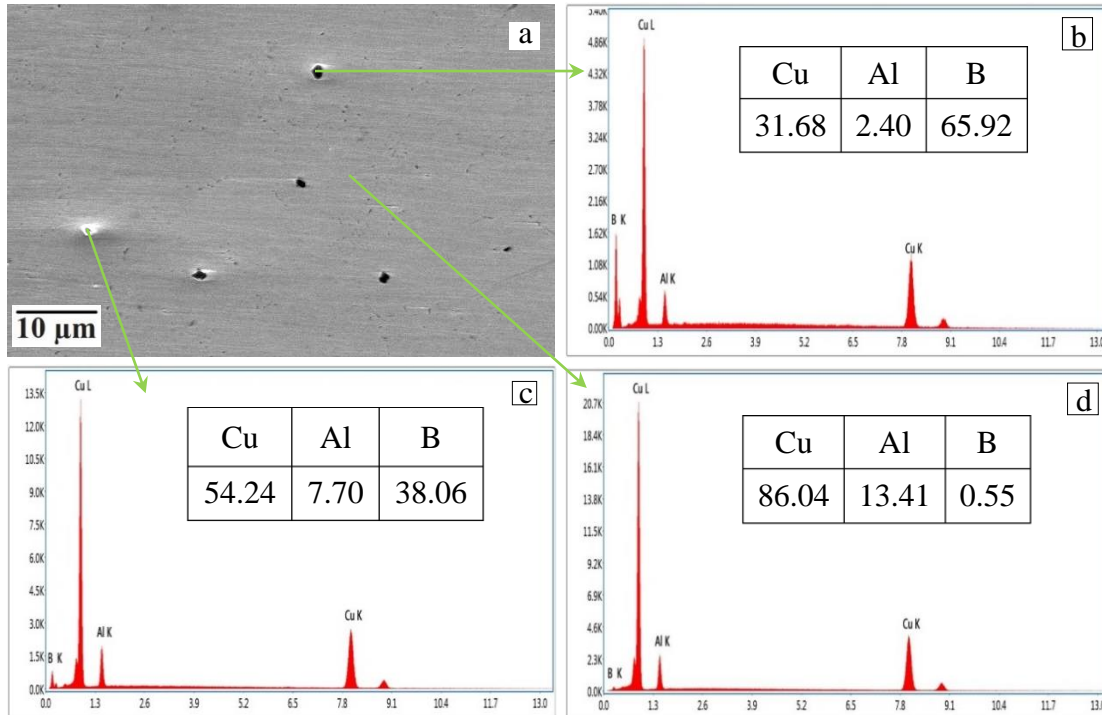


Figure 4.7 (a) FESEM image of alloy B_4 and (b)-(d) EDS spectrums of alloy B_4 .

4.3.2 Microstructure – Grain Size

The microstructure of the betatized and quenched alloys with boron-doping is shown in Figure 4.8. It is evident from the micrographs that B-doping strongly alters the β_1 -grains of polycrystalline $\text{Cu}_{87.93}\text{-Al}_{11.5}\text{-Be}_{0.57}$ shape memory alloys. Figure 4.8 shows that B-doping crystallized the microstructure of alloys and refined the average grain size by 119 ± 7 , 76 ± 3 , 50 ± 2 , and $87 \pm 8 \mu\text{m}$ for 0.05, 0.1, 0.15 and 0.2 wt.%, respectively. The newly originated microstructure of Cu-Al-Be-B SMAs, as depicted in Figure 4.8, display serrated grains (i.e., uneven size with irregular/wavy-shaped grain boundaries). These serrated grains are formed due to grain boundary segregation of AlB_2 fine-size precipitates (Wang et al. 2011). From Figure 4.8(a), it is observed that the addition of 0.05

wt.%B reduces the average grain size to 89.51%, owing to the combined effect of heterogeneous nucleation and high growth restriction factor (Balart et al. 2016; Birol 2012; Bolzoni et al. 2015; Chen et al. 2016). A further increase in B-doping up to 0.15 wt.%, shows higher grain-size refinement attributed to enhanced heterogeneous nucleation and restricted grain-growth (Greer et al. 2000; Wang et al. 2011; Yang et al. 2013). The addition of 0.2 wt.%B to the base alloy (i.e., B_4) forms coarse precipitates/clusters in the matrix as well as the interface (Figure 4.8d), owing to the limited solubility of boron (Jones and Pearson 1976; Lozovoi and Paxton 2008), and consequently, the grain size increased to $87 \pm 8 \mu\text{m}$. The existence of B-rich secondary phase coarse precipitates confirmed from FESEM-EDS studies, which contain a higher amount of boron due to larger inoculant-doping (Xu et al. 2021). These coarse precipitates of various sizes (Figures 4.7a and 4.8d) were formed by agglomeration and that had a negative impact on grain refinement (Limmaneevichitr and Eidhed 2003; Xu et al. 2021), and hence a larger grain size is seen in the alloy B_4 .

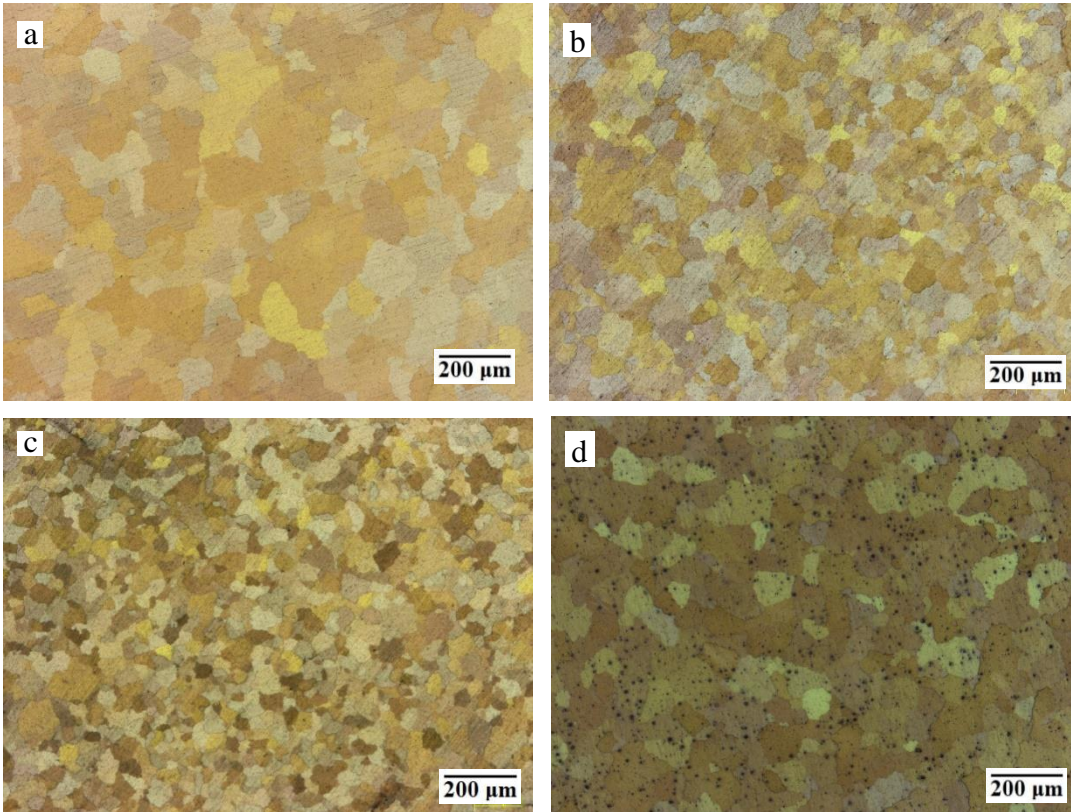


Figure 4.8 Microstructures of Cu-Al-Be-B SMAs: (a) B_1 , (b) B_2 , (c) B_3 and (d) B_4 .

4.3.3 Phase Transformation Temperatures

The phase transformation temperatures of all the betatized and quenched Cu-Al-Be-B alloys were obtained using the DSC tests and recorded thermograms were plotted based on heat flow versus temperature as shown in Figure 4.9. The measured phase transformation temperatures, enthalpies, and thermal hysteresis ($A_f - M_s$) of all the SMAs are tabulated in Table 4.4.

The variations in phase transformation temperatures are interpreted in terms of the dependent functions of alloy systems, *viz.* elemental composition, grain size, intermetallics, and secondary phase precipitates (Horiuchi et al. 2007; Jiao et al. 2018; Liu et al. 2014; Montecinos and Cuniberti 2012; Nishiyama 1978). From the thermograms of Cu-Al-Be-B SMAs, it is observed that both endothermic and exothermic peaks shifted towards a lower temperature with B-doping, indicating a slight decrease in transformation temperatures up

to 0.15 wt.%. This reduction is caused by the stability of austenite owing to chemical stability i.e., due to a change in chemical composition (Horiuchi et al. 2007; Nishiyama 1978) and grain size refinement (Montecinos et al. 2011; Montecinos and Cuniberti 2012). It is also noted that the segregation effect of AlB_2 fine intermetallic particles, alters the composition of the matrix as shown in Table 4.3. In addition, the actual composition of the alloys also varies due to burning losses, and only the grain-refining particles change the grain sizes. Figure 4.8 shows that an increased concentration of B-doping reduces austenite grain size, implying that a larger grain boundary area leads to a decrease in martensitic transformation temperatures (Montecinos and Cuniberti 2012; Nishiyama 1978; Roca et al. 2017). Further, it is observed that transformation temperatures increased with 0.2 wt.% of B-doping due to increased grain size and the existence of insoluble B-rich coarse precipitates confirmed from FESEM-EDS results. From Table 4.3, it is observed that the concentration of alloy elements depletes from the B_4 matrix and thereby agglomerates in the coarse precipitates, as shown in Figure 4.7.

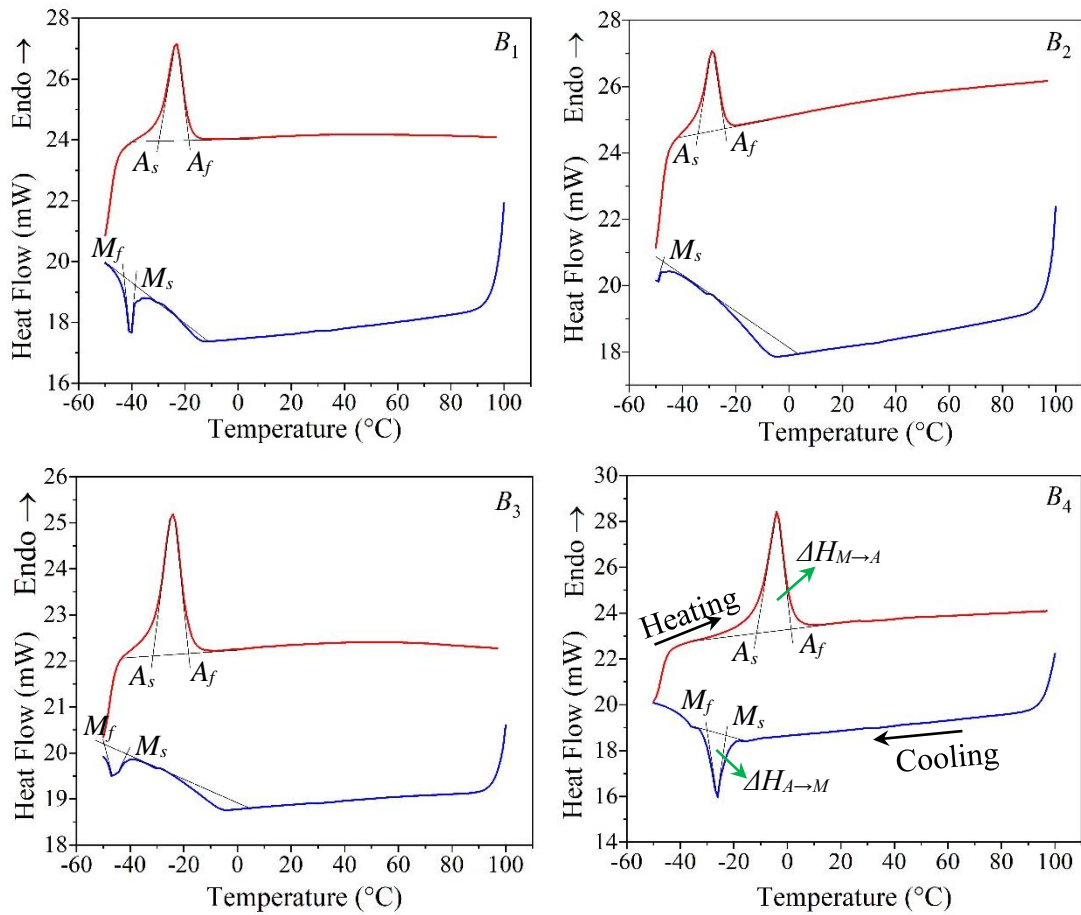


Figure 4.9 DSC curves of Cu-Al-Be-B SMAs.

Table 4.4 Transformation temperatures (°C), enthalpies (J/g) and thermal hysteresis (°C) of Cu-Al-Be-B SMAs.

Alloy	M_f	M_s	$\Delta H_{A \rightarrow M}$	A_s	A_f	$\Delta H_{M \rightarrow A}$	$(A_f - M_s)$
B_1	-42.66	-39.24	-3.10	-30.44	-18.29	5.17	20.95
B_2	---	-47.34	---	-34.04	-24.18	2.91	23.16
B_3	-49.65	-41.58	---	-31.28	-18.33	3.58	23.25
B_4	-29.27	-23.89	-3.74	-11.40	1.48	7.02	25.37

4.3.4 Mechanical Properties and Fracture Morphology

The influence of boron doping on mechanical properties of the Cu-Al-Be SMAs, i.e., tensile strength and ductility have been investigated by performing the uniaxial tensile test using the ASTM E8/E8M standard. All the tests were conducted at a loading rate of 1 mm/min to record engineering stress-strain data, and each plot is the average of three test results, as presented in Figure 4.10(a).

Figure 4.10(b) depicts the UTS properties of the boron-doped Cu-Al-Be SMAs, viz. ultimate tensile strength (σ_{max}) and ultimate tensile strain (ε_{max}). The tensile strength (i.e., σ_{max}) and ductility (i.e., ε_{max}) of the 0.05 wt.%B-doped alloy B_1 is 456.31 ± 9.66 MPa and 14.55 ± 0.26 , respectively. An increase in B to B_2 and B_3 exhibits substantial improvement in tensile strengths, 644.07 ± 23.25 and 744.65 ± 29.34 MPa, with enhanced ductility of 20.00 ± 0.87 , and $21.93 \pm 0.56\%$, respectively. This improvement in tensile strength and ductility for the B-containing Cu-Al-Be alloys are connected to grain-boundary strengthening coupled with grain-size refinement (Han and Kim 1987). The grain-boundary strengthening is caused by the segregation effect of B and AlB_2 fine-size particles/precipitates strengthening, which enhances cohesive strength at the grain boundaries (Deppisch et al. 1997; Hosseini et al. 2018; Lozovoi and Paxton 2008; Spear 1976). The fractured surface of the alloy B_1 , as shown in Figure 4.11(a), unveils highly elongated strip-like dimples. As boron-doping increases up to 0.15 wt.% (i.e., B_2 and B_3), the elongated dimples become more refined and form fine dimples (Figures 4.11b and c), implying a greater ductility. However, the tensile strength and ductility of B_4 decreases to 537.82 ± 30.33 MPa and $16.53 \pm 1.48\%$, respectively owing to B-rich coarse precipitates and the larger grain size (Hosseini et al. 2018; Lozovoi and Paxton 2008; Zhang et al. 2011). The morphology of the fracture surface (Figure 4.11d) reveals the existence of both small and large size dimples caused by the presence of both fine and coarse precipitates, and the grain size (Lozovoi and Paxton 2008; Zhang et al. 2011).

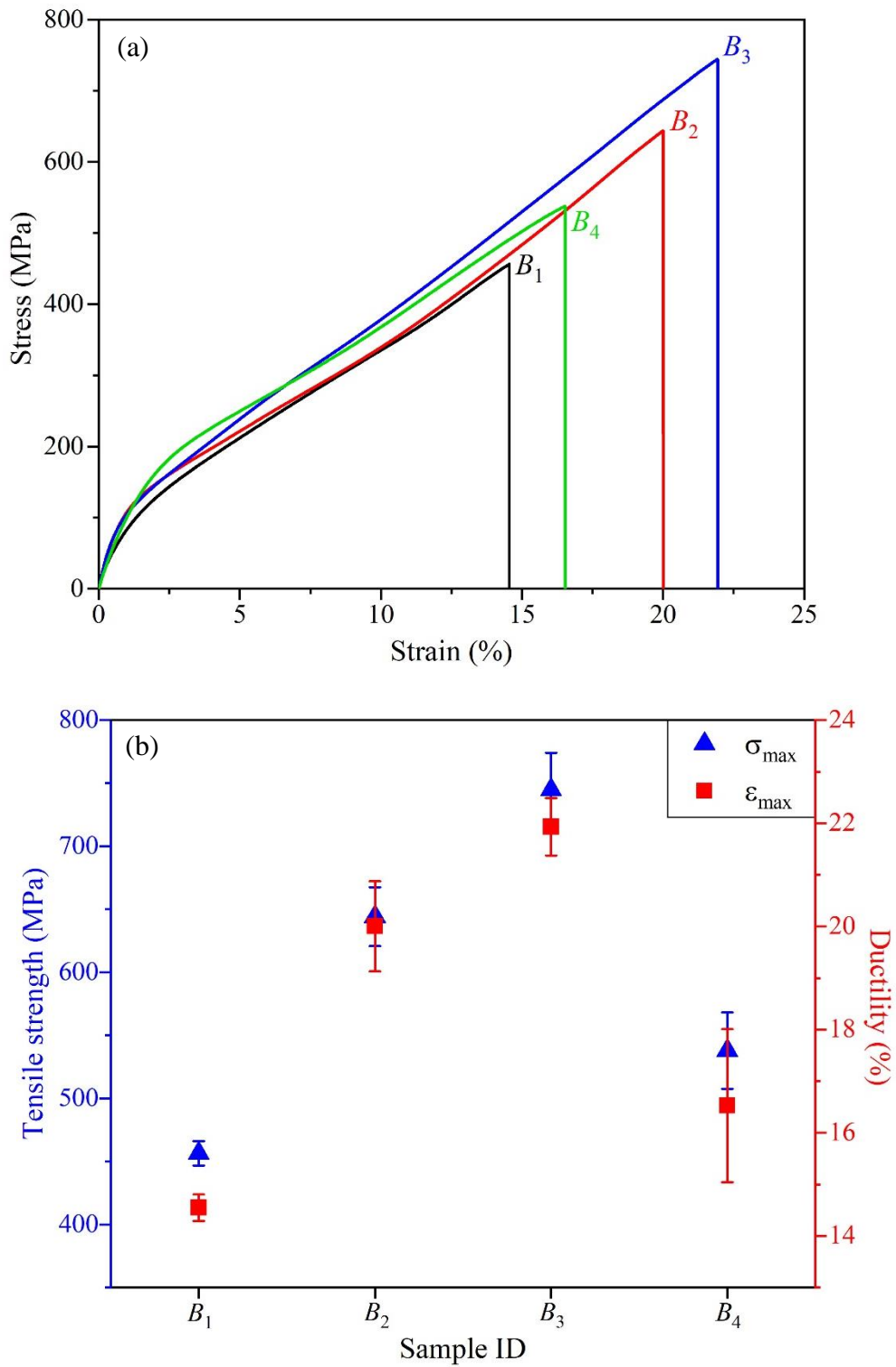


Figure 4.10 Tensile properties of Cu-Al-Be-B SMAs: (a) engineering stress-strain plots and (b) ultimate tensile stress (σ_{max}) and ultimate tensile strain (ϵ_{max}).

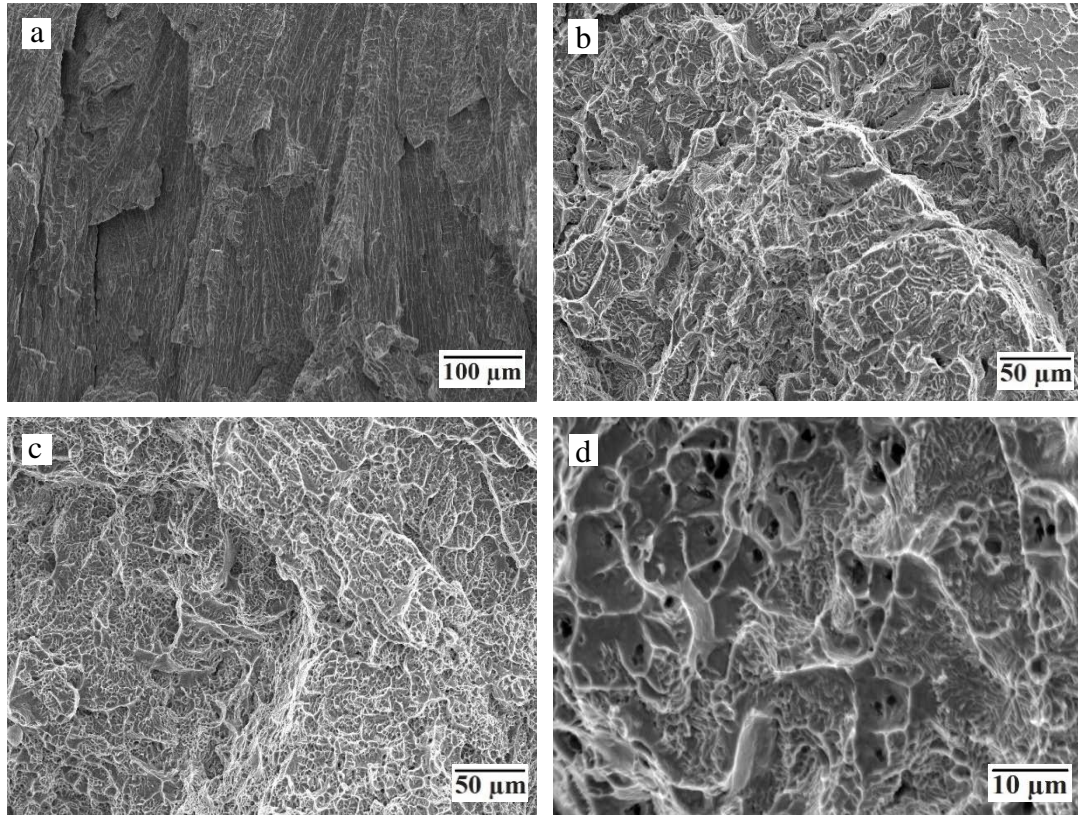


Figure 4.11 FESEM images of the fracture surface of Cu-Al-Be-B SMAs: (a) B_1 , (b) B_2 , (c) B_3 and (d) B_4 .

4.3.5 Pseudoelasticity and Microstructural Modifications

The cyclic hysteresis test was performed on SMAs to estimate their pseudoelastic behavior. All SMA specimens were subjected to a single cycle of loading and unloading for the selected maximum deformation strains (ϵ_d) of 3, 4, and 5% at room temperature, and their associated hysteresis plots are shown in Figures 4.12(a), 4.13, and 4.14, respectively. The austenite finish temperature (A_f) of all SMA samples presented here is less than the room temperature, satisfying the condition to conduct pseudoelasticity tests at room temperature (Sampath and Mallik 2009). The main plot features of pseudoelastic behavior are indicated in the hysteresis plot, as depicted in Figure 4.14. In polycrystalline SMAs, plot features such as critical stress (σ_{cs}) for the transformation of austenite ($\beta_1 -$

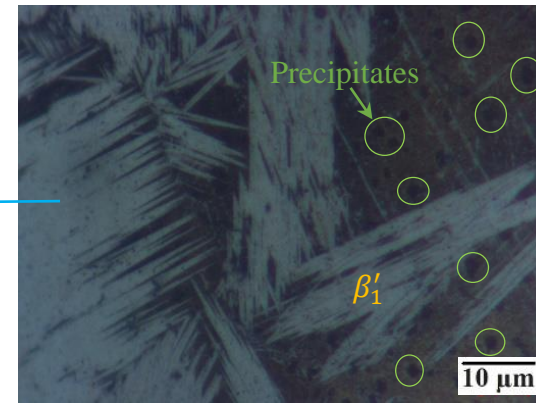
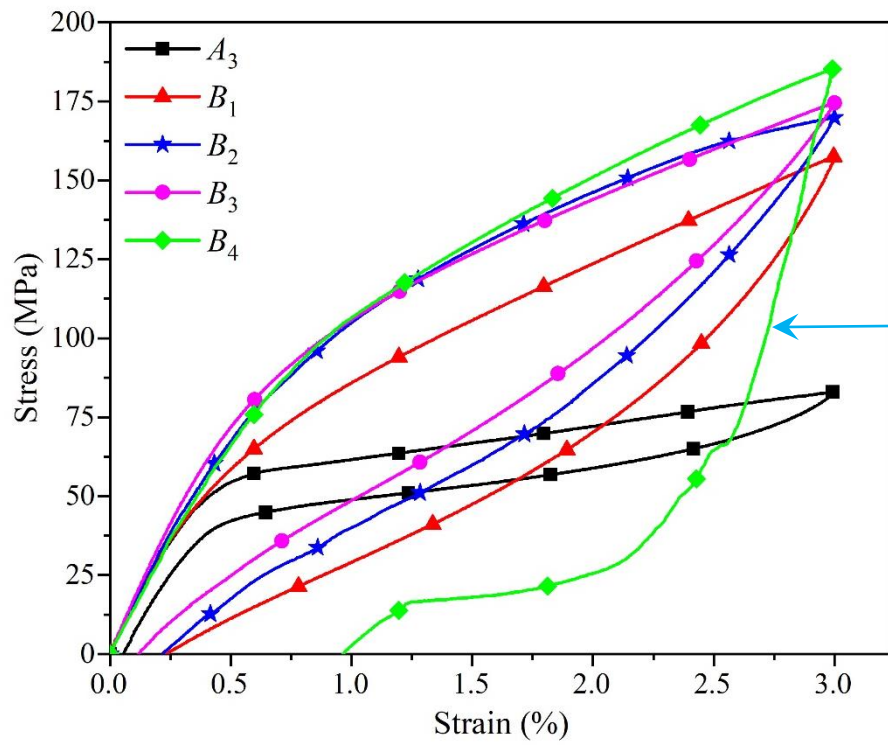
DO₃) to stress-induced martensite ($\beta'_1 - 18R$), pseudoelastic transition slope, stress hysteresis and residual strain (ϵ_r) characterize the pseudoelastic cycle (Sade et al. 2014).

From the hysteresis plots, it is noticed that B-free alloy A_3 has low critical stress of 48.43 MPa due to coarse grains, as confirmed from the existing literature (Montecinos et al. 2008; Sade et al. 2014). The increased B-doping into B_1 , B_2 , B_3 and B_4 alloys enhanced the critical stress, σ_{cs} to 62.85, 81.25, 91.64 and 87.55 MPa, respectively. The improvement in the critical stress is due to decreased phase transformation temperatures (Horiuchi et al. 2007), smaller grain size (Sade et al. 2014; Sutou et al. 2005), and increased grain boundary area (Kim et al. 2019). Due to these combined effects, the alloys require an additional driving force for β_1 (DO₃) \rightarrow β'_1 (18R) transformation. Moreover, the pseudoelastic transition slope (i.e., almost constant stress-strain slope corresponding to the progress of the stress-induced martensitic transformation) increases and the hysteresis loop enlarges in all the quaternary Cu-Al-Be-B SMAs relative to the ternary Cu-Al-Be SMA.

Figure 4.16 depicts the residual strains obtained from pseudoelastic plots for the maximum deformation strains of 3, 4, and 5%. The pseudoelastic hysteresis plots of the B-free alloy A_3 (Figures 4.12a and 4.13) exhibit nearly complete strain recovery for the applied deformation strain up to 4% owing to a pure β_1 -phase with regular grain boundary morphology, as seen in Figure 4.2(c). An increased amount of residual strain is observed in the alloy B_1 on unloading, owing to more uneven grain size and highly irregular/wavy grain boundary morphology, namely, serrated grains (Figure 4.8a). The highly irregular grain boundary induces irreversible plastic deformation of austenite and restricts complete reversible martensitic transformation on unloading (Kim et al. 2019), thereby causing a high residual strain. The alloys B_2 and B_3 (Figures 4.8b and c) discerned the presence of serrated grains with diminished irregular grain boundaries. In addition, decreased grain size dissimilarities lead to lesser residual strains. The fine-grained alloy B_3 with serrated grain boundaries has less irregularities and showed maximum pseudoelasticity up to 4% and transformation strain recovery with negligible residual strain. A pseudoelastic cycle of the alloy B_4 for the maximum deformation strain of 3% ensured an open hysteresis loop (Figure 4.12a) with a large irreversible strain. The presence of B-rich coarse precipitates inside the

parent β_1 -phase confirmed with SEM-EDS, which act as a strong barrier (pinning) for the mobility of austenite/stress-induced martensite, i.e., $\beta_1 \leftrightarrow \beta'_1$. It is also worth noting that the B-rich coarse precipitates surrounding matrix are still in β_1 -phase and little stress-induced martensite plates/needles are retained, as presented in Figure 4.12(b). This is related to the blocking/pinning effect of stress-induced martensitic growth restricted due to the dislocations generated during the plastic deformation of the austenite/martensite phase, confirmed with the existing literature (Cuniberti et al. 2009; Rodriguez et al. 1996; Sampath and Mallik 2009; Yi et al. 2019). Therefore, this mechanism causes incomplete reverse-transformation to the parent β_1 -phase, and showed no full strain recovery. Further investigation was carried out on the pseudoelastic behavior of SMAs, i.e., A_3 , B_1 , B_2 and B_3 with a deformation strain of 5% as seen in Figure 4.14. From the plot results, it is observed that the residual strains have progressively remained permanently in the SMAs on complete unloading and that can be attributed to the existence of retained stress-induced martensite (Figures 4.15a – d), plastic deformation, and/or slip defects (Montecinos et al. 2008; Montecinos and Cuniberti 2008). Hence, higher residual strains of the alloys, indicating deterioration in the pseudoelasticity of SMAs.

In view of the variations in residual strain for $\varepsilon_d = 5\%$ (Figure 4.14), it is noticed that larger residual/irreversible strain retained in the alloy A_3 is mainly due to irreversible plastic deformation by dislocations, leading to a hyperstabilization effect (Montecinos and Cuniberti 2008). As shown in the optical micrographs, the average grain size of Cu-Al-Be SMAs decreases with increased B-doping up to 0.15wt.%. The refined grain size enhances the stability of austenite by enabling larger stored elastic strain due to limited space to accommodate martensite variants, and internal friction resistance owing to the increased grain boundary area. Besides, the stored elastic strain is released on unloading, provides a reversible path for the martensitic transformation (Sade et al. 2014). However, the internal friction resistance barrier increases due to morphological irregularity of the grain boundaries. This leads to irreversible plastic deformation of austenite along with reversible martensite transformation (Kim et al. 2019), resulting in low pseudoelastic recovery strain. Therefore, smaller residual strains are retained in B-containing alloys than the B-free alloy.



(b)

Figure 4.12 (a) Stress-strain hysteresis responses of Cu-Al-Be-B SMAs for the deformation strain, $\epsilon_d = 3\%$ and (b) Optical micrograph of the pseudoelastically deformed alloy B_4 .

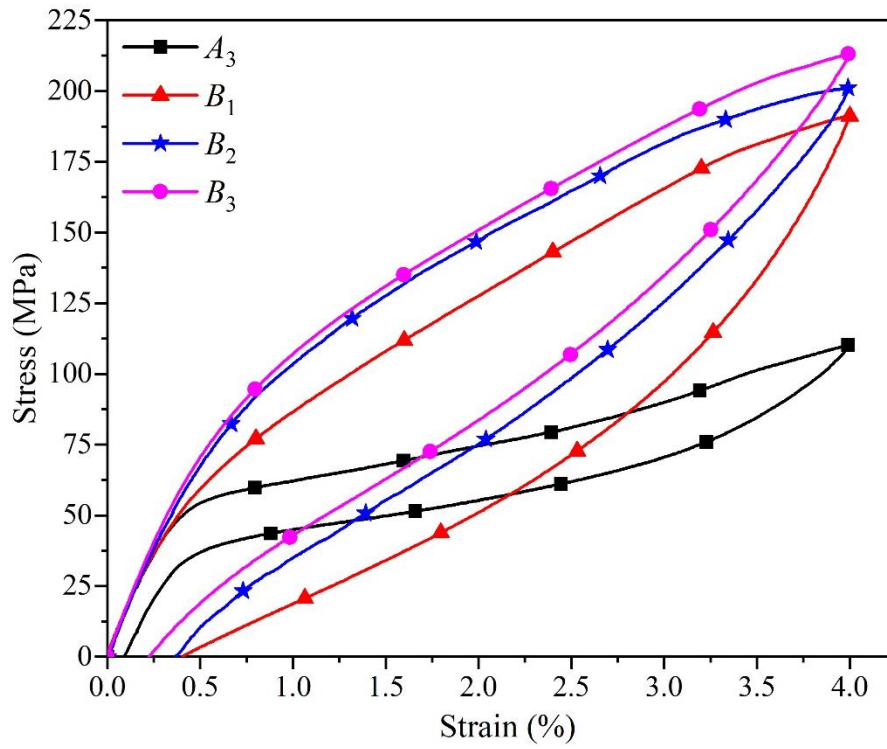


Figure 4.13 Stress-strain hysteresis responses of Cu-Al-Be-B SMAs for the deformation strain, $\varepsilon_d = 4\%$.

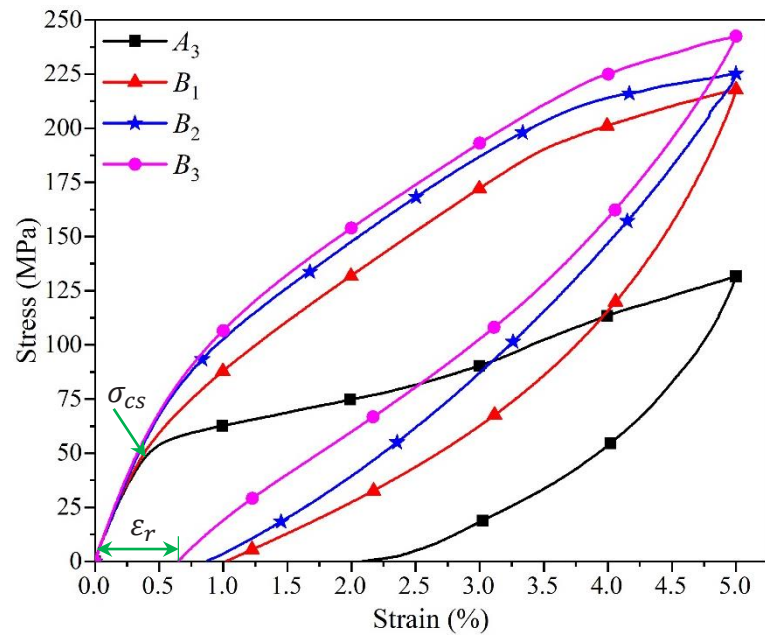


Figure 4.14 Stress-strain hysteresis responses of Cu-Al-Be-B SMAs for the deformation strain, $\varepsilon_d = 5\%$.

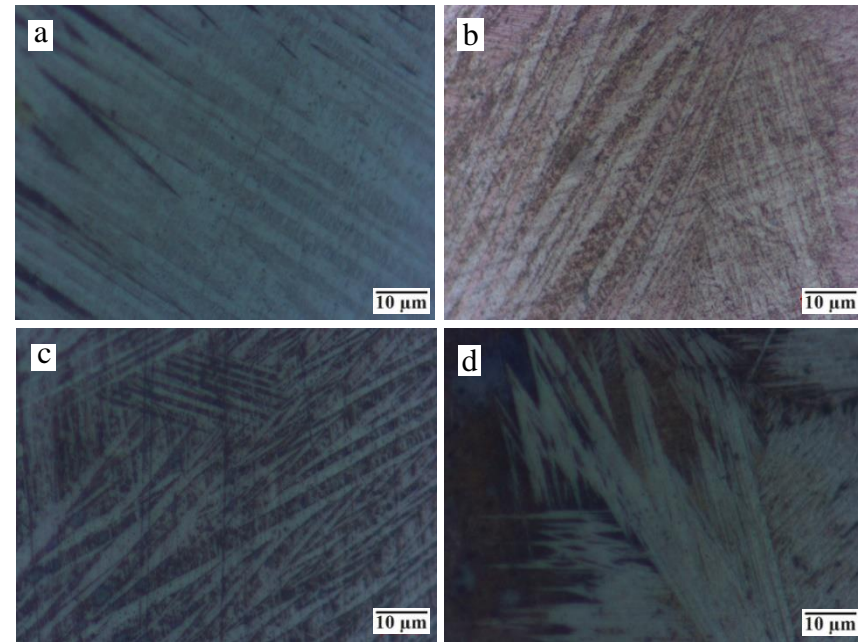


Figure 4.15 Retained martensite in SMAs: (a) A_3 , (b) B_1 , (c) B_2 , and (d) B_3 .

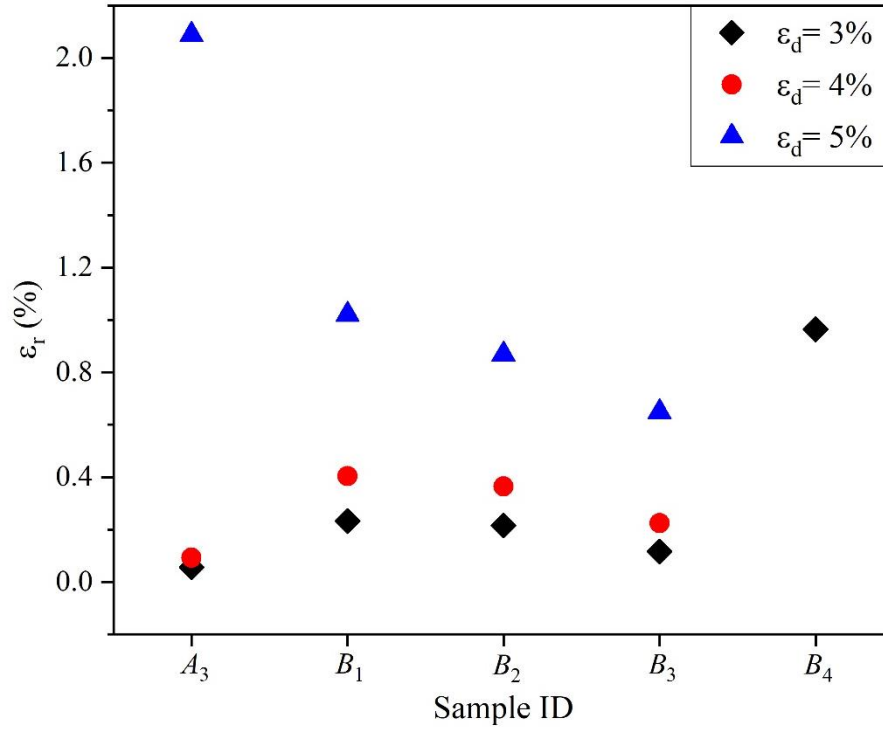
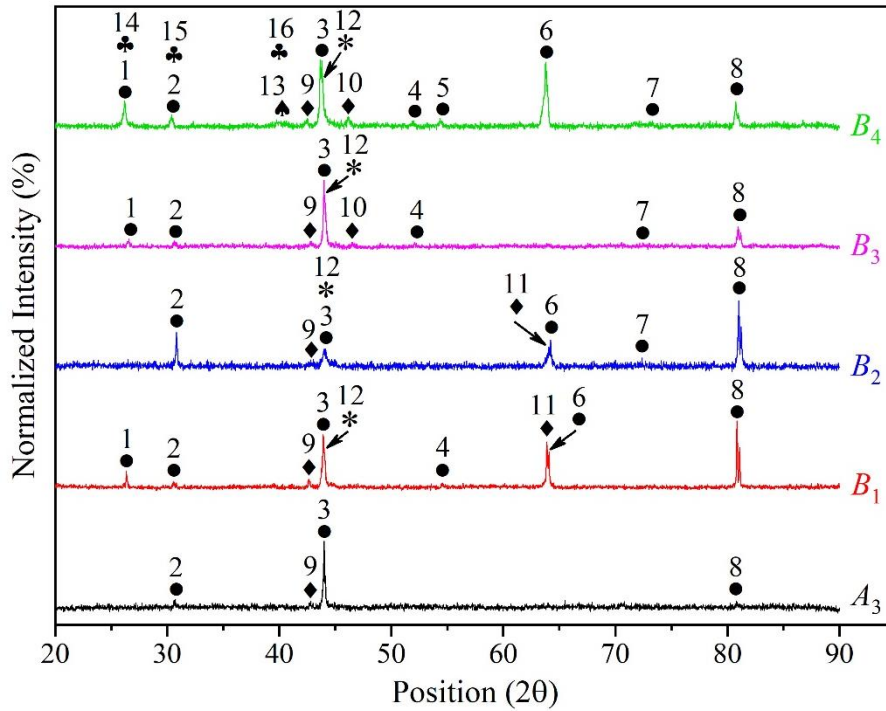


Figure 4.16 Variations in the residual strain (ϵ_r) for different deformation strains, ϵ_d .

After pseudoelastic cycling (i.e., $\epsilon_d = 5\%$ for A_3 and B_1 to B_3 , and 3% for Ψ_4), the assessment of the retained stress-induced martensite was carried out using XRD at room temperature, and the diffraction patterns are presented in Figure 4.17. Indexing the diffraction patterns revealed that all pseudoelastically deformed SMAs exhibit an additional martensite phase of β'_1 (\blacklozenge) comparative to betatized and quenched SMAs. The retained stress-induced martensite after complete pseudoelastic cycling consists of an orthorhombic martensite phase, β'_1 (Cu_3Al) with $18R$ structure, also confirmed from the literature (Sade et al. 2014). The alloy A_3 showing the minor intensity of the martensitic peak (0 0 22) confirms that some martensite needles/plates remain permanently within the β_1 -phase (Figure 4.15a), whereas a large amount of residual strain is mainly due to slip dislocations, as discussed in the preceding paragraph. The alloys B_1 and B_2 exhibited different intensity peaks associated with different orientations of the irreversible plastic deformed austenite phase. Moreover, B_1 shows high intensities of martensite phase reflections, viz., (0 0 22) and (0 3 17) relative to B_2 , this indicates an increase in the retained β'_1 -phase (Carl et al. 2016). The alloy B_3 show

no β_1 -phase peak for the (004) reflection present in the betatized and quenched alloy B_3 , and small β_1' - phase peaks noticed from the (0 0 22) and (2 0 12) reflections. The alloy B_4 has two martensitic reflections, viz. (0 0 22) and (2 0 12) with minor peak intensities, which confirms the existence of small amounts of retained martensite in β_1 -phase, as shown in Figure 4.12(b).



● – β_1 : 1(1 1 1), 2(0 0 2), 3(0 2 2), 4(1 1 3), 5(2 2 2), 6(0 0 4), 7(0 2 4), 8(2 2 4);
 ◆ – β_1' : 9(0 0 22), 10(2 0 12), 11(0 3 17); * – AlB_2 : 12(0 1 1); ♠ –
 $\text{Al}_{1.35}\text{Cu}_{1.17}\text{B}_{52.5}$: 13(2 2 6); ♣ – $\text{Al}_{8.67}\text{B}_{176}\text{Be}_{13.48}$: 14(1 0 4), 15(3 1 2), 16(3 3 2).

Figure 4.17 Normalized XRD profiles of the pseudoelastically deformed Cu-Al-Be-B SMAs.

4.4 QUATERNARY Cu-Al-Be-Zr SMAs

Based on the literature survey, the addition of zirconium acts as a very good grain refiner, and correspondingly the grain growth rates are suppressed effectively owed to the lowest grain growth exponent (Gil et al. 1999; Kim et al. 1990). This section presents the influence of alloying zirconium, i.e., 0.05 - 0.3 wt.% of Zr-dope into Cu-Al_{11.5}-Be_{0.57} SMAs and its significant effect on phases, morphology, microstructure, phase transformation temperatures, mechanical and pseudoelastic shape recovery properties. The results are investigated and presented with detailed mechanisms. The actual elemental composition of (Cu-Al_{11.5}-Be_{0.57})-Zr_x (x = 0.05, 0.1, 0.15, 0.2, 0.3) alloys are tabulated in Table 4.5 and denoted as “Zr_i”, where, “Zr” represents the zirconium-doped alloy, and subscript, i = 1, 2, 3, 4 and 5 for 0.05, 0.1, 0.15, 0.2 and 0.3 wt.% of Zr, respectively.

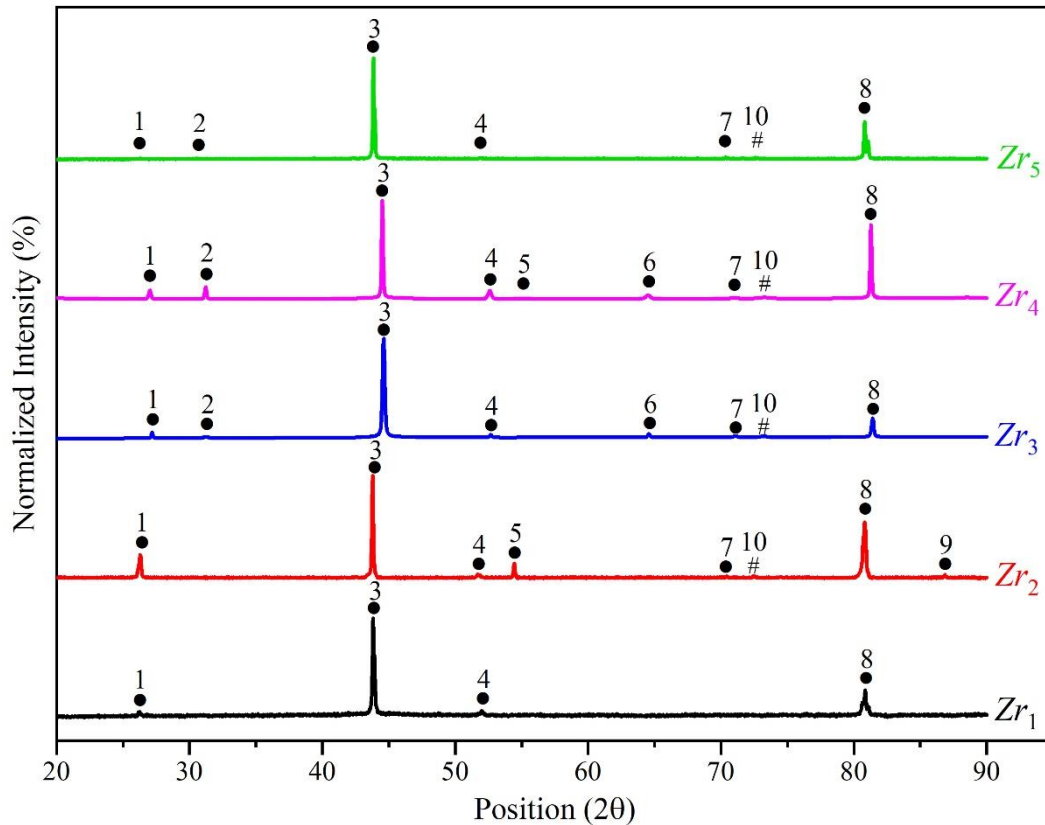
Table 4.5 Elemental compositions of Cu-Al-Be-Zr SMAs.

Sl. No.	Alloy	Actual composition in wt.%			
		Cu	Al	Be	Zr
1.	Zr ₁	86.8	11.87	0.53	0.026
2.	Zr ₂	86.9	11.75	0.54	0.056
3.	Zr ₃	86.8	11.77	0.55	0.079
4.	Zr ₄	87.2	11.50	0.54	0.113
5.	Zr ₅	87.1	11.56	0.54	0.171

4.4.1 Phases and Morphology

X-ray diffraction (XRD) was employed to assess the phases that exist in the zirconium-doped Cu-Al_{11.5}-Be_{0.57} SMAs, and the normalized X-ray diffractograms are presented in Figure 4.18. Black, red, blue, magenta and green colored lines represent zirconium addition of 0.05, 0.1, 0.15, 0.2 and 0.3 wt.%, respectively. The X-ray diffractograms were normalized at the highest intensity peak of (0 2 2) lattice diffraction (De Assis et al. 2018; Chaisan et al. 2019). In addition, all the lattice diffraction intensities were normalized to 100% at the peak value for the (0 2 2) lattice diffraction (Liang et al. 2006). Figure 4.19 depicts the FESEM-EDS results of the betatized and

quenched Cu-Al-Be-Zr SMAs. FESEM images, as shown in Figures 4.19(a-e) depicts the morphology of Zr-doped SMAs that reveals the size, shape, and volume fraction of the secondary phase precipitates. The energy dispersive spectrums (EDS) of the alloy Zr_5 provided the elemental composition of the matrix (Figure 4.19f) and the second-phase precipitates (Figures 4.19g and h).



● – β_1 : 1(1 1 1), 2(0 0 2), 3(0 2 2), 4(1 1 3), 5(2 2 2), 6(0 0 4), 7 (1 3 3), 8 (2 2 4), 9(1 1 5); # – Al_3Zr : 10(0 1 3).

Figure 4.18 Normalized X-ray diffractograms of Cu-Al-Be-Zr SMAs.

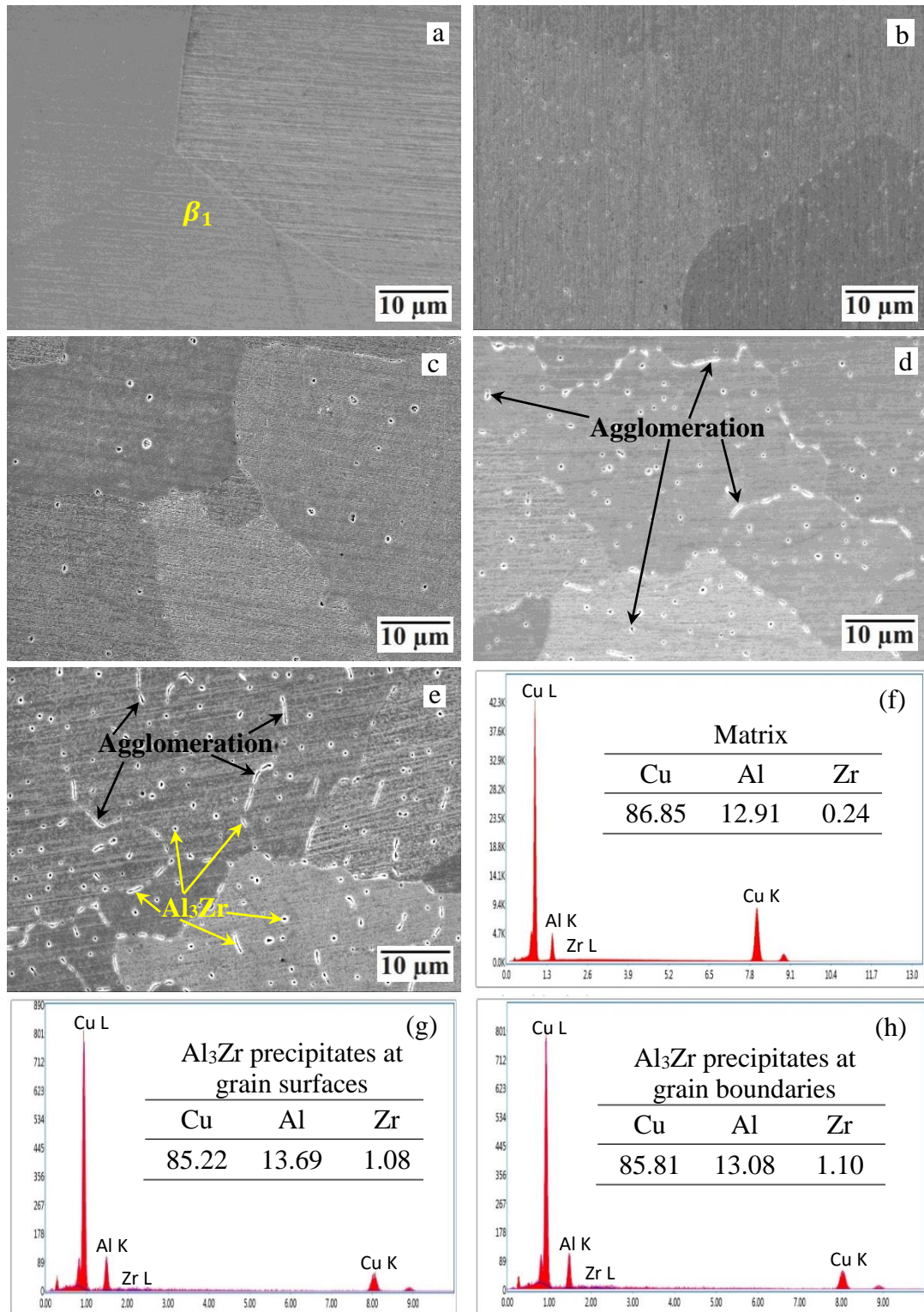


Figure 4.19 FESEM images of Cu-Al-Be-Zr SMAs: (a) Zr₁, (b) Zr₂, (c) Zr₃, (d) Zr₄ and (e) Zr₅, and (f-h) EDS of Zr₅.

From the diffractograms (Figure 4.18), it is observed that 0.05 wt.% of Zr-doped alloy possess pure austenite (β_1 - DO₃) phase peaks of cubic structure, denoted with a symbol (●). The crystal structures and associated peaks of the β_1 (Cu₃Al) confirmed the existence of an austenite β_1 -phase (Figure 4.19a), and thereby no secondary phase peak was noticed for the alloy *Zr*₁. The alloys *Zr*₂ to *Zr*₅ are of complete austenite along with the secondary phase peak of Al₃Zr (#). From Figures 4.19(b-e), it is observed that spherical-shaped precipitates correspond to the secondary phase, viz. Al₃Zr and the same were also confirmed by (Pilz et al. 2020). This precipitate formation is attributed to a strong affinity of aluminium to zirconium (Bhattacharya et al. 1993). As Zr-doping increases, the size as well as the volume fraction of precipitates increases. The surface morphology of the alloys *Zr*₄ and *Zr*₅ shown in Figures 4.19(d and e), respectively, depicted that the spherical Al₃Zr precipitates combine and are concentrated at both grain boundaries as well as inside the grains, attributed to precipitates agglomeration (Hosseini et al. 2018; Li et al. 2011). The EDS results of Figures 4.19(g and h) showed a nearly equal elemental composition that reveals the existence of Al₃Zr precipitates at both grain surfaces and grain boundaries, respectively.

4.4.2 Microstructure – Grain Size

The microstructure of the betatized and quenched alloys shown in Figure 4.20 reveals that alloying Zr promotes changes in the grain size of β_1 -type Cu-Al-Be polycrystalline SMAs. The average grain sizes of SMAs are 244 ± 18 , 126 ± 9 , 65 ± 7 , 85 ± 12 and 109 ± 13 μm for *Zr*₁, *Zr*₂, *Zr*₃, *Zr*₄ and *Zr*₅, respectively. The micrograph is shown in Figure 4.20(a) reveals that 0.05 wt.% of Zr-doping exhibits bimodal grains due to minimal addition. Moreover, the presence of regular grain boundaries (flat facets and straight edges) of pure austenite β_1 -phase was confirmed from *Zr*₁ alloy X-ray diffractogram (Figure 4.18). An increase in Zr-doping to 0.1 and 0.15 wt.% displays good grain refinement (Figures 4.20b and c) and a maximum refinement is attained with the addition of 0.15 wt.% of Zr. The grain refinement in zirconium-doped alloys are attributed to the following mechanisms: (i) very small grain growth exponent of Zr, leads to grain refining efficiency (Gil et al. 1999; Wang et al. 2015), (ii) increased heterogeneous nucleation sites caused by insoluble Zr dispersoid particles, acts as

nucleant to form a large number of smaller grains (Gil et al. 1999; Yang et al. 2016), and, (iii) very slow grain growth rate by precipitates pinning effect at the grain boundaries (Lee and Wayman 1986a; Sampath 2005). Figures 4.20(d and e) showed an increase in the average grain size of the SMAs with 0.2 and 0.3 wt.% of Zr-doping, i.e., the alloys Zr_4 and Zr_5 , respectively, and is owed to precipitates agglomeration (Yang et al. 2016), which depletes the grain refining nucleant in the matrix (Jones and Pearson 1976).

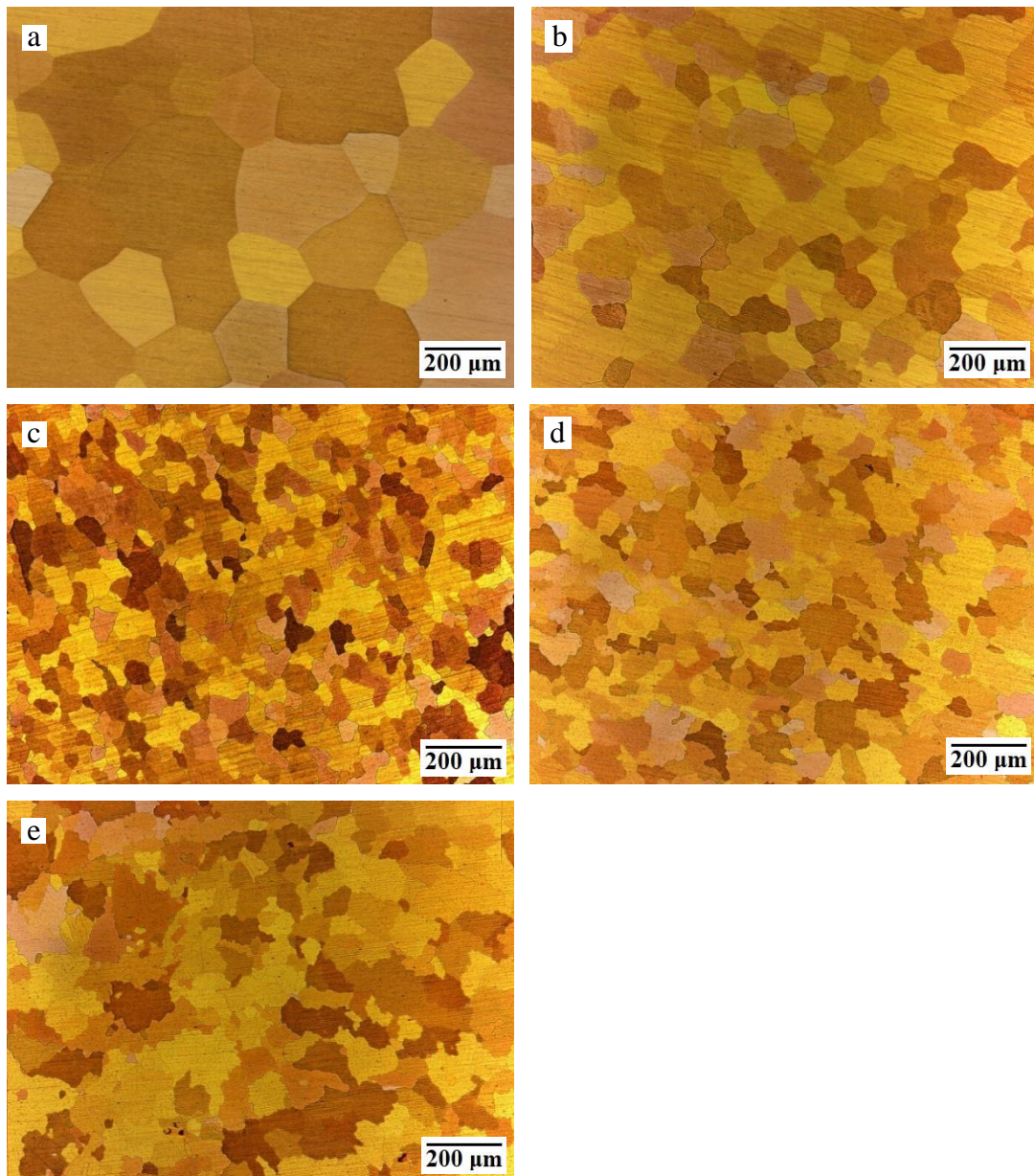


Figure 4.20 Microstructures of Cu-Al-Be-Zr SMAs: (a) Zr_1 , (b) Zr_2 , (c) Zr_3 , (d) Zr_4 and (e) Zr_5 .

4.4.3 Phase Transformation Temperatures

The transformation temperatures of Zr-doped Cu-Al_{11.5}-Be_{0.57} SMAs were determined using heating and cooling cycles of DSC thermograms, as presented in Figure 4.21. The measured transformation temperatures (A_s , A_f , M_s , M_f), enthalpies ($\Delta H_{A \leftrightarrow M}$), and thermal hysteresis ($A_f - M_s$) of the Cu-Al-Be-Zr SMAs are tabulated in Table 4.6.

Figure 4.21 and Table 4.6 depicted that the forward and reverse martensitic transformations shift towards lower temperatures up to 0.1 wt.% of Zr-doping, owed to grain refinement and reduced valence electron to atom ratio denoted by e/a (where e is the number of valence electrons and a is the number of atoms) (Ding et al. 2019; Dogan et al. 2012). Further, the higher addition of Zr increases the transformation temperatures and is mainly due to the larger size and volume fraction of the second-phase precipitates. It modifies chemical, electronic, and structural factors, such as elemental composition (Table 4.5), e/a ratio (Table 4.6), and the average grain size (Figures 4.20c-e), respectively, also confirmed with the existing literature (Sampath 2005; Sampath and Mallik 2009). A higher addition of zirconium, i.e., more than 0.1 wt.%, leads to the formation of larger size and high volume fraction of Al₃Zr precipitates as discussed in Section 4.4.1, which contain a higher amount of aluminium wt.%, as confirmed from EDS data. As a result, the concentration of aluminium in the matrix decreases and thus resulting in high transformation temperatures (Sampath and Mallik 2009). A higher e/a ratio and larger grain size also rise the transformation temperatures (Aydogdu et al. 2016; Montecinos and Cuniberti 2012). In addition, the actual composition of the alloys varies due to the burning losses, and thus modifies the transformation temperatures of shape memory alloys.

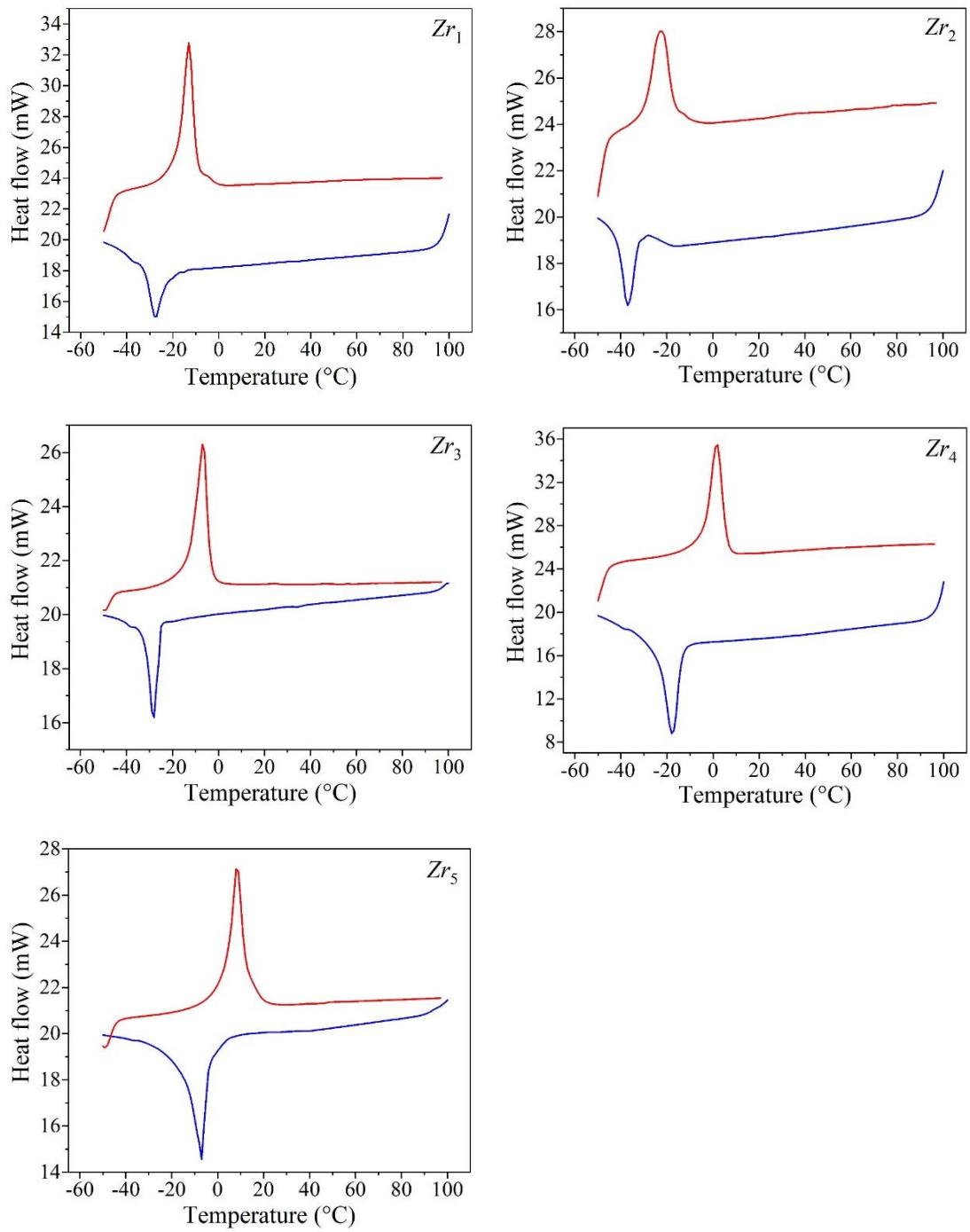


Figure 4.21 DSC thermograms of Cu-Al-Be-Zr SMAs.

Table 4.6 Transformation temperatures (°C), enthalpies (J/g), e/a ratio and thermal hysteresis (°C) of Cu-Al-Be-Zr SMAs.

Alloy	M_f	M_s	$\Delta H_{A \rightarrow M}$	A_s	A_f	$\Delta H_{M \rightarrow A}$	e/a	$(A_f - M_s)$
Zr_1	-28.30	-25.88	-5.46	-17.84	-09.78	8.47	1.5038	16.10
Zr_2	-39.09	-33.83	-3.15	-29.90	-16.92	9.37	1.5005	16.91
Zr_3	-30.86	-25.76	-3.59	-13.37	-03.80	5.28	1.5022	21.96
Zr_4	-24.97	-17.70	-6.72	-02.09	05.24	8.50	1.4926	22.94
Zr_5	-15.47	-03.09	-9.42	03.33	13.02	8.84	1.4957	16.11

4.4.4 Mechanical Properties and Fracture Morphology

Uniaxial tensile tests were performed on Zr-doped Cu-Al_{11.5}-Be_{0.57} SMAs at room temperature using UTM operated at a loading rate of 1 mm/min to assess the changes in tensile strength and ductility. Figure 4.22(a) depicts the engineering stress-strain plots, and each plot is the mean of three test results. The tensile strength (σ_{max}) and ductility (ε_{max}) plot is shown in Figure 4.22(b). The engineering $\sigma - \varepsilon$ plot of the alloy Zr_1 reveal that minimal addition of Zr, i.e., 0.05 wt.% exhibited the tensile strength of 316.28 ± 19.13 MPa and the ductility of $12.37 \pm 0.66\%$. Further, it is observed that both tensile strength and ductility of Zr-doped Cu-Al-Be SMAs improved with increased weight percent of Zr additions and reached a maximum with 0.15 wt.%. An increased Zr-doping in the alloys Zr_2 and Zr_3 yields substantial improvement in tensile strengths, 503.57 ± 4.27 and 690.12 ± 28.01 MPa, with enhanced ductility of 17.09 ± 0.22 and $21.01 \pm 0.68\%$, respectively. The improvement in the mechanical properties attributes to (i) grain refinement, increases the total area of grain boundaries, and (ii) fine-size precipitates strengthening. Thus, it provides an effective barrier to the dislocation's mobility and a high degree of plastic deformation, implying better strength and ductility before the fracture of SMAs (Hosseini et al. 2018; Roh et al. 1991; Yang et al. 2016). Furthermore, additions of Zr to Zr_4 and Zr_5 , i.e., the alloys with 0.2 and 0.3 wt.% of Zr-doping decreases the tensile strengths to 602.93 ± 18.13 and 542.14 ± 18.14 MPa with diminished ductility of 15.50 ± 0.55 and $10.37 \pm 0.52\%$, respectively, and is due to precipitates agglomeration and increase in the grain-size (Jones and Pearson 1976).

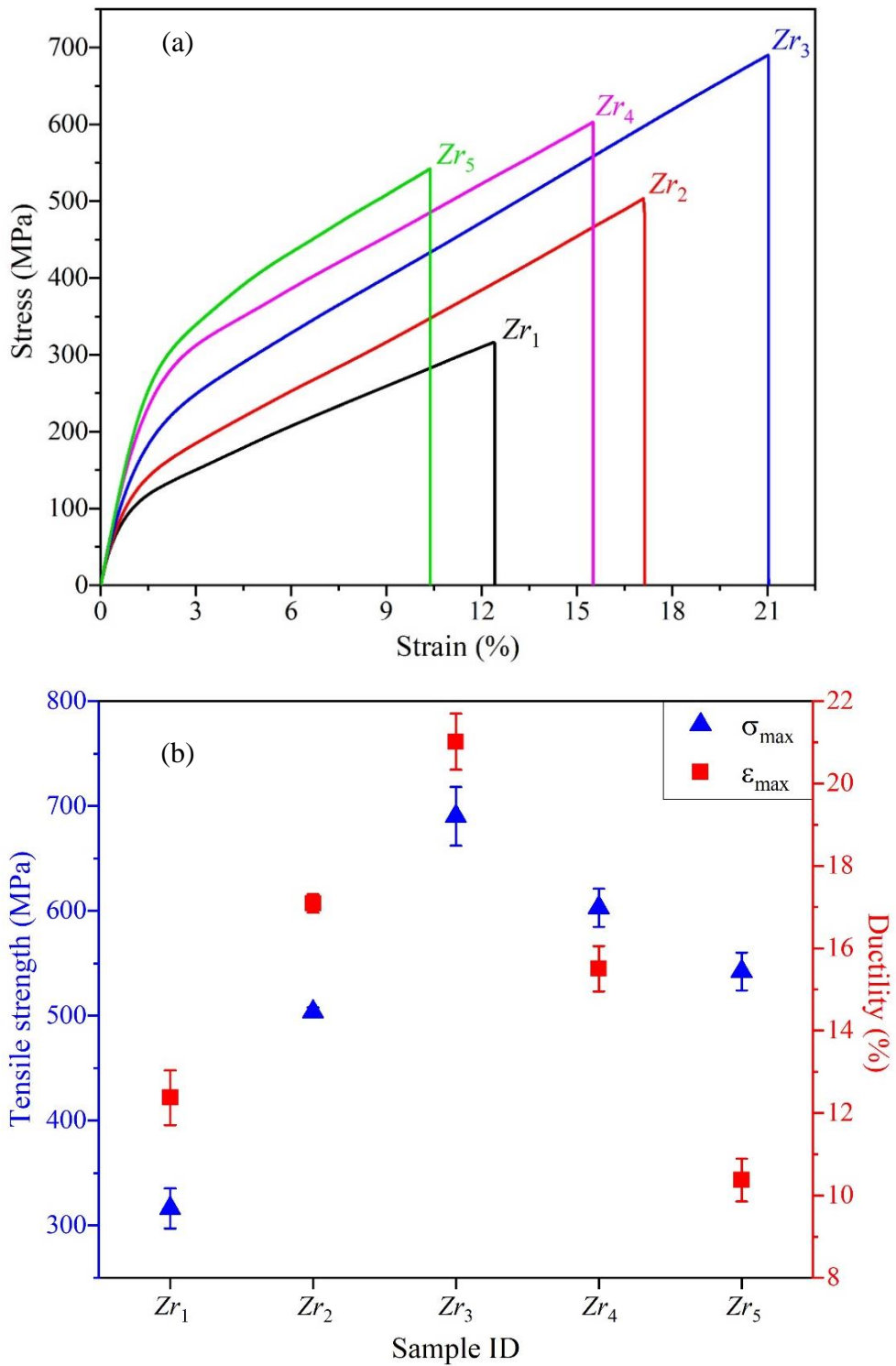


Figure 4.22 Tensile properties of Cu-Al-Be-Zr SMAs: (a) engineering stress-strain plots and (b) ultimate tensile stress (σ_{max}) and ultimate tensile strain (ϵ_{max}).

Figure 4.23 presents the FESEM images of the tensile fractured surfaces of Zr-doped Cu-Al_{11.5}-Be_{0.57} SMAs. Fracture morphology of the alloy Zr_1 (Figure 4.23a) indicates mixed-mode fracture consists of both dimples and cleavage planes due to the presence of bimodal grains, confirmed with the alloy Zr_1 micrograph shown in Figure 4.20(a). Increase of Zr-doping in the alloy Zr_2 completely transformed to ductile fracture mode with surface areas containing dimples, as shown in Figure 4.23(b), owing to the spherical fine-size precipitates and the reduced grain-size confirmed with Figures 4.19(b) and 4.20(b), respectively. Besides, a more significant number of smaller dimples are observed in Zr_3 (Figure 4.23c), attributes to a more volume fraction of precipitates within the matrix and finer grain size. However, the alloys Zr_4 and Zr_5 fail at lower stresses, and correspondingly the density of dimples decreased as shown in Figures 4.23(d and e). This is owed to increased average grain size and agglomeration of precipitates (Yang et al. 2016), which leads to a high-stress concentration at the grain boundaries (Candido et al. 2012; Zhang et al. 2011). An increased size and volume fraction of Al₃Zr precipitates by agglomeration generate secondary micro-cracks on the bottom of the dimples encircled in Figures 4.23(d and e). While, the micro-cracks initiated from the precipitates at the grain boundaries extend quickly to relieve the stress concentration (Zhang et al. 2011); hence tensile strength and ductility loss are exhibited in Zr_4 and Zr_5 SMAs.

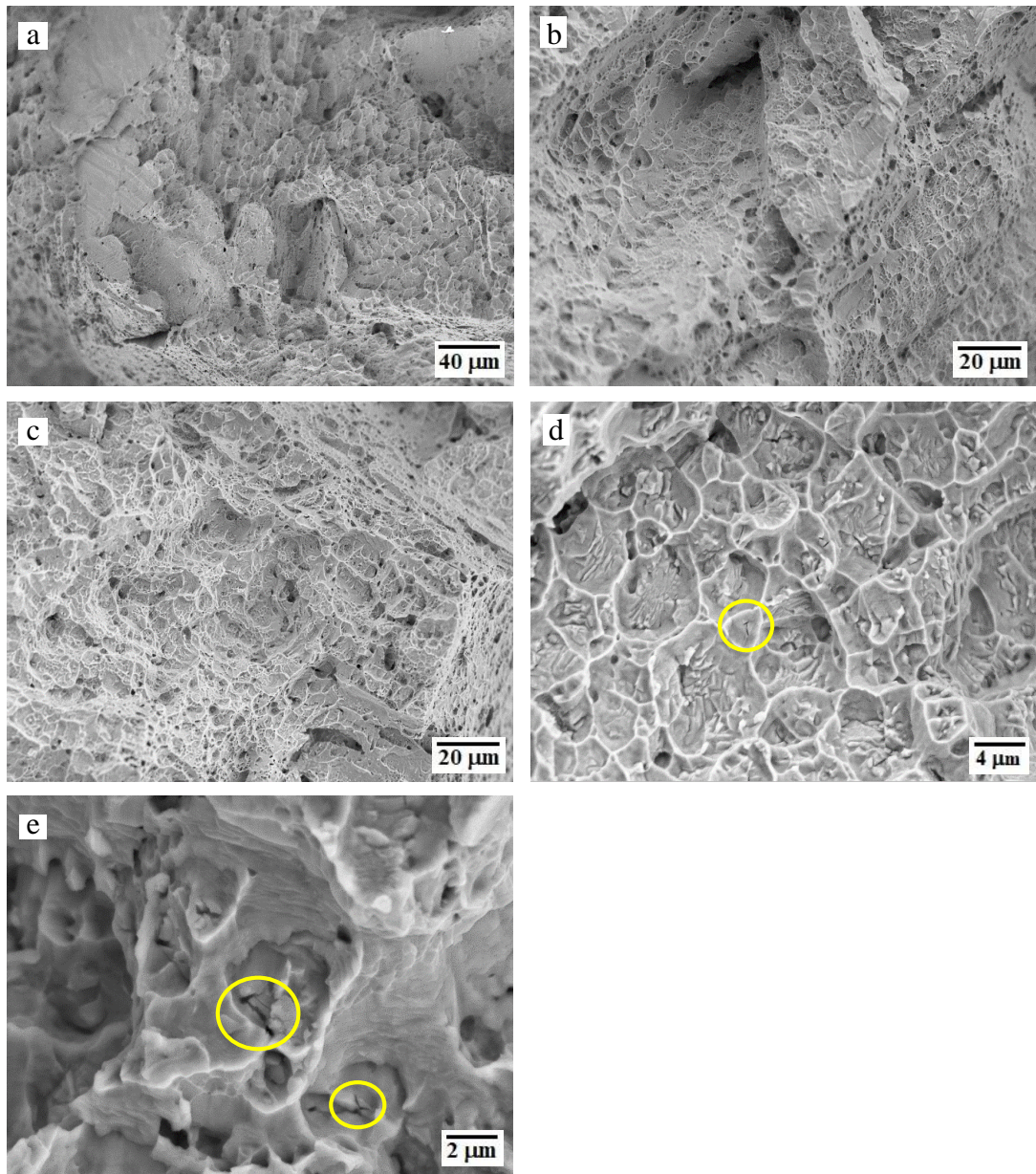


Figure 4.23 FESEM images of the fracture surface of Cu-Al-Be-Zr SMAs: (a) Zr_1 , (b) Zr_2 , (c) Zr_3 and (d) Zr_4 and (e) Zr_5 .

4.4.5 Pseudoelasticity and Microstructural Modifications

Pseudoelastic behavior of Zr-doped Cu-Al_{11.5}-Be_{0.57} SMAs was studied to evaluate the influence of grain size and second-phase precipitates on stress-induced martensitic (SIM) transformations. The pseudoelastic cycling was carried out using cyclic tensile tests with a loading rate of 0.1 mm/min at room temperature because all the evaluated SMA samples presented here have an austenite finish temperature (A_f)

lower than room temperature. Cyclic tensile tests were performed on the betatized and quenched flat dog-bone-shaped SMA specimens subjected to extended cycles of loading and unloading for the selected deformation strains (ε_d) ranging between 2 - 6%, with an increased step of 0.5% ε_d for each extended cycling. The plots of $\sigma - \varepsilon$ hysteresis are presented in Figures 4.24(a) - 4.27(a).

From the Figure 4.24(a), it is observed that the addition of 0.05 wt.% of Zr exhibited the critical stress, σ_{CS} for SIM ($\beta_1 \rightarrow \beta'_1$) transformations of 82.48 MPa and pseudoelastic transition slope ($d\sigma_{PE}/d\varepsilon$) of 1.18 GPa. Further, higher additions of Zr into Zr_2 , Zr_3 and Zr_4 alloys enhance the critical stress to 148.42, 207.47 and 247.50 MPa, and pseudoelastic transition slope, 1.77, 2.76 and 2.96 GPa, respectively. This improvement attributes to (i) decreased grain size (Celada-Casero et al. 2019; Ergen et al. 2013; Sade et al. 2014), increases the austenite phase resistance exerted by the limited space for the accommodation of stress-induced martensite, and (ii) increased size and volume fraction of the second-phase precipitates (Cuniberti et al. 2009; Sampath and Mallik 2009), acts as a barrier for the formation of stress-induced martensite, and thus require an additional driving force for SIM transformations.

The microstructural modifications accompanying after pseudoelastic cycling are shown in Figures 4.24(b) and 4.25(b) for $\varepsilon_d=6\%$ – loaded and unloaded, and Figures 4.26(b) and 4.27(b) for $\varepsilon_d=4\%$ – loaded and unloaded. Moreover, XRD analysis was carried out on pseudoelastically deformed Cu-Al-Be-Zr SMAs to assess the transformed phases and their crystal structure, and the diffractograms are presented in Figure 4.30. Indexing of the diffractograms reveals that pseudoelastically deformed alloys Zr_1 , Zr_2 and Zr_3 exhibited an additional orthorhombic, $18R - \beta'_1$, martensite phase (\blacklozenge) along with cubic, $DO_3 - \beta_1$, austenite (\bullet) and Al_3Zr precipitate ($\#$) phases. Whereas, no martensitic peak was observed in the alloy Zr_4 .

The results of residual strain (ε_r) and stress hysteresis ($\Delta\sigma$) measured from stress (σ) – strain (ε) hysteresis plots for each extended cycling of Zr-doped Cu-Al_{11.5}-Be_{0.57} SMAs, and are presented in Figures 4.28 and 4.29, respectively. This indicates that extended cycling led to an increased amount of irreversible/residual strain (ε_r), and enlarged stress hysteresis ($\Delta\sigma$). The pseudoelastic hysteresis plot of the alloy Zr_1

(Figure 4.24a) exhibits nearly complete strain recovery up to 5% deformation strain due to pure austenite phase confirmed with XRD and FESEM results of Figures 4.18 and 4.19(a), respectively. From Figure 4.24(a), it is also observed that the irreversible strain (ϵ_r) increases, but very small in magnitude for each cycling, cumulative with extended cycling (Figure 4.28) owing to the introduced slip defects (Montecinos et al. 2008). Furthermore, extended cycling, i.e., greater than 5% deformation strain, a larger ϵ_r is progressively retained due to the stabilized martensite (β'_1) and surface distortions around the grain boundaries, enclosed by a blue dotted line indicated in Figure 4.24(b). These resulted from the slip defects and plastic deformation induced by applying a large deformation strain (Montecinos et al. 2008; Montecinos and Cuniberti 2008; Sutou et al. 2013). Hence, it effectively reduces the reversible strain and correspondingly ensured an open hysteresis loop, as shown in Figure 4.24(a). Martensite phase (\blacklozenge) peaks of Zr_1 diffractogram, as depicted in Figure 4.30, consists of several intersecting variants, viz., (2 0 2), (0 0 22), (2 0 12) and (2 4 8) reflections associated with different orientations of the stabilized β'_1 -phase, caused by mutual interactions of the martensite plates (Dvorak and Hawbolt 1975). Besides, high intensities of the reflections indicated a more significant number of stabilized martensite plates remain permanently within the parent β_1 -phase (Carl et al. 2016).

The plots shown in Figures 4.25(a) – 4.27(a), unveil that deterioration in the strain recovery with further additions of Zr-inoculants. This detrimental effect is due to the blocking/pinning effect exerted by the precipitates (Sampath and Mallik 2009; Sun et al. 2019), which provides obstacles to the formation of stress-induced martensite, and also hampers the easy movements of austenite/martensite interfaces, i.e., $\beta_1 \leftrightarrow \beta'_1$. Consequently, the dislocations generated during plastic deformation, which hinders the reverse-transformations to the parent phase, and thereby showed no full strain recovery. From the Figure 4.28, it is observed that the residual strain is progressively retained with increased wt.% of Zr-doping, owed to increase in the size and volume fraction of the second-phase precipitates confirmed with FESEM images. The fine-size precipitates morphology of the alloys Zr_2 and Zr_3 (Figures 4.19b and c) exhibited a lesser amount of martensite plates on the pseudoelastically unloaded SMA sample micrographs, as encircled in Figures 4.25(b) and 4.26(b), respectively, owed to partial

SIM transformations (Yi et al. 2019). A minor intensity of the β'_1 -phase peak (0 0 22) reflection in Zr_2 and Zr_3 diffractograms also confirms that fewer martensite plates remain permanently within the parent β_1 -phase. Therefore, the larger residual strain leftovers on unloading are caused by the dislocation defects and little amount of retained martensite (β'_1). Nevertheless, the recoverable pseudoelastic strain is lower in the alloy Zr_4 (Figure 4.27a) compared with all other Zr-doped Cu-Al_{11.5}-Be_{0.57} SMAs considered here. The alloy Zr_4 morphology (Figure 4.19d) consists of very large density of precipitates within the grains as well as at the grain boundaries, which inhibits the SIM transformations completely due to strong pinning effect. Hence, no martensite plates are detected in the alloy Zr_4 micrograph as shown in Figure 4.27(b) and higher residual strains are retained (Figure 4.27a) due to plastic deformation. Moreover, Figure 4.30 indicates that no martensitic peak in Zr_4 diffractogram confirmed the absence of β'_1 -phase.

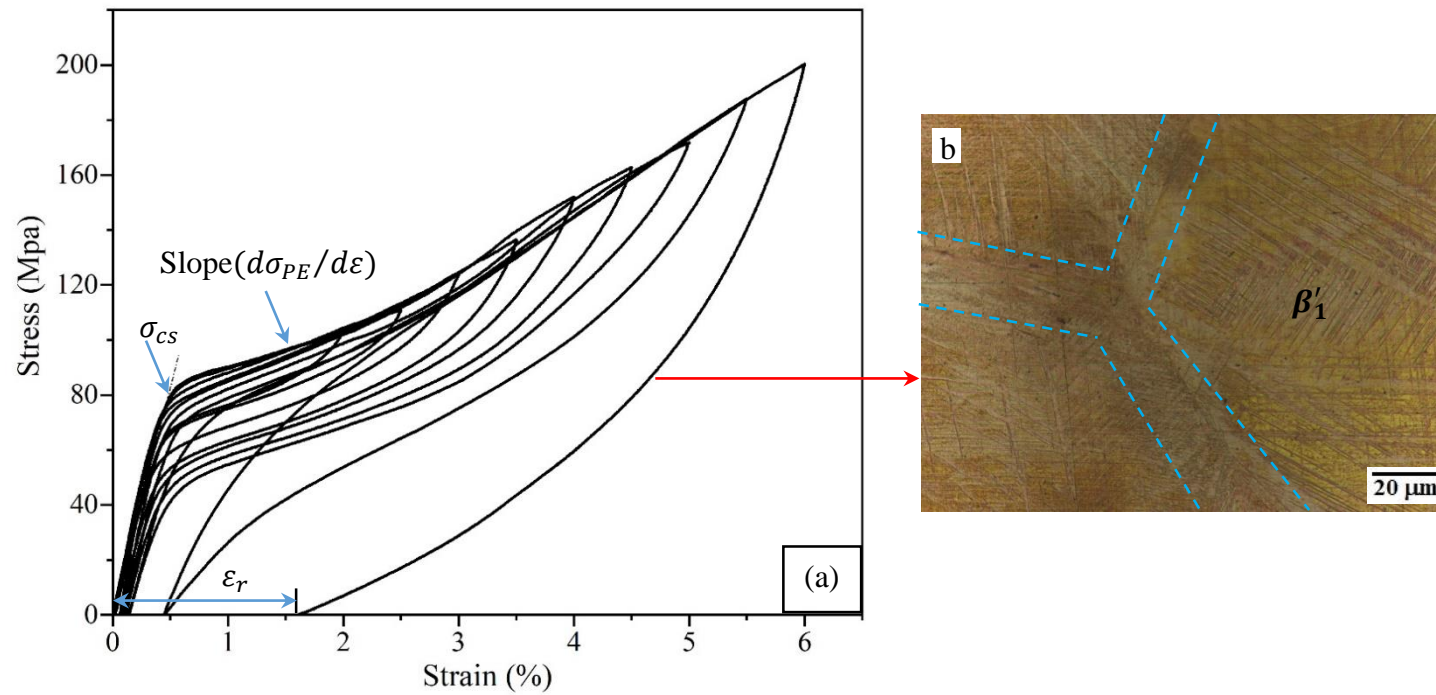


Figure 4.24 (a) Stress-strain hysteresis of the alloy Zr_1 and (b) optical micrograph of the pseudoelastically deformed alloy Zr_1 .

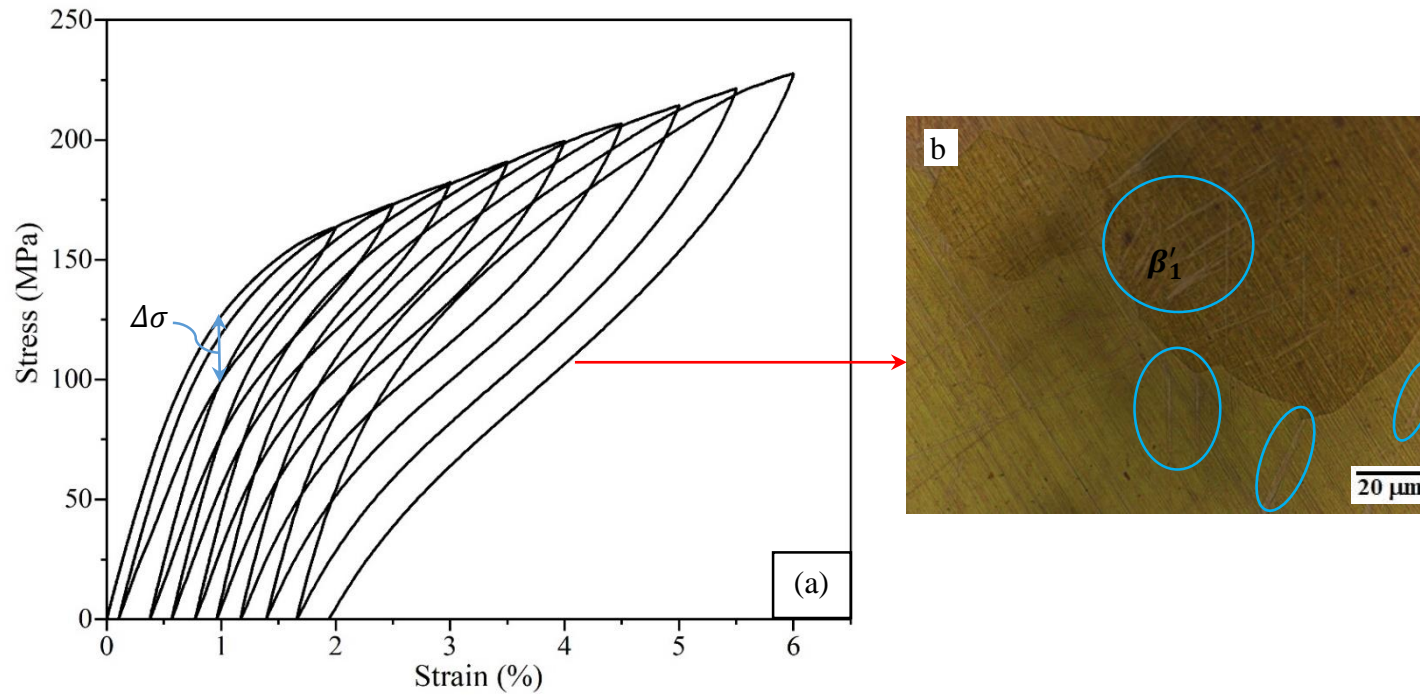


Figure 4.25 (a) Stress-strain hysteresis of the alloy Zr_2 and (b) optical micrograph of the pseudoelastically deformed alloy Zr_2 .

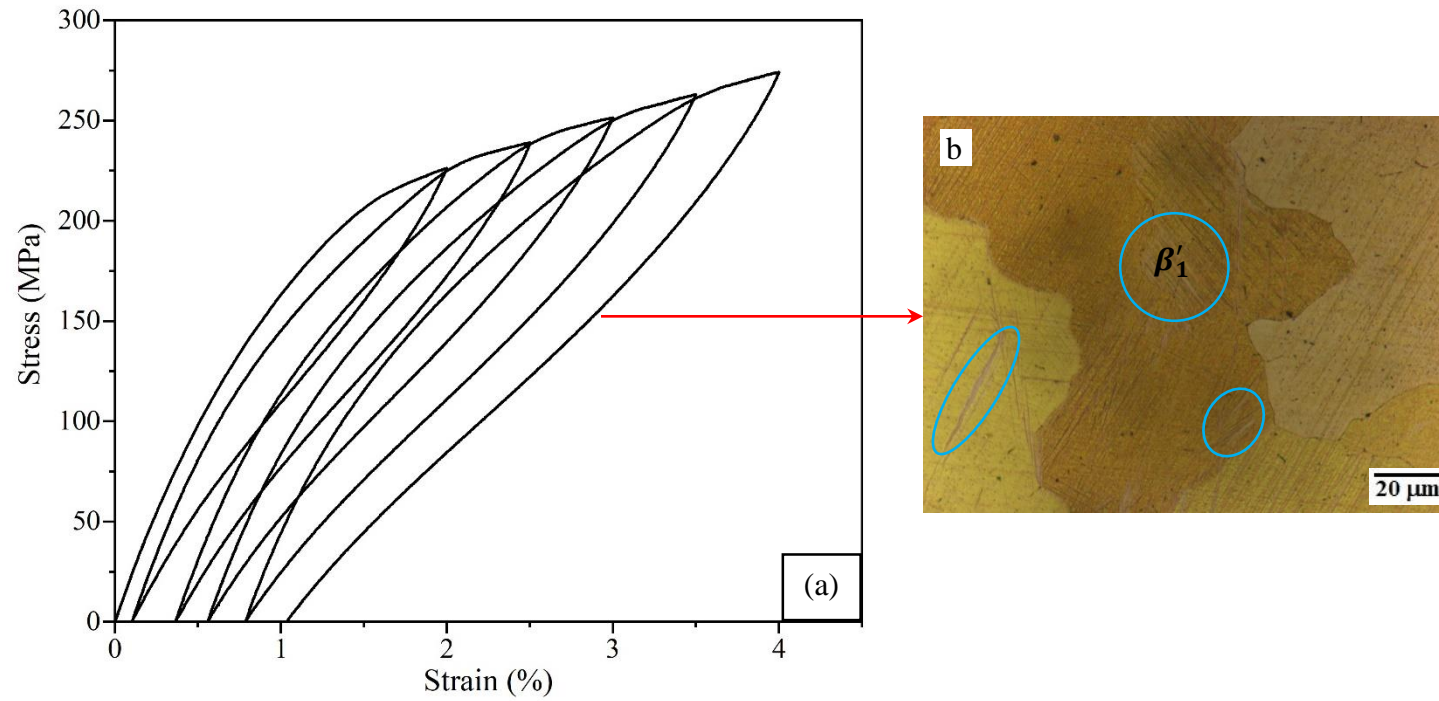


Figure 4.26 (a) Stress-strain hysteresis of the alloy Zr_3 and (b) optical micrograph of the pseudoelastically deformed alloy Zr_3 .

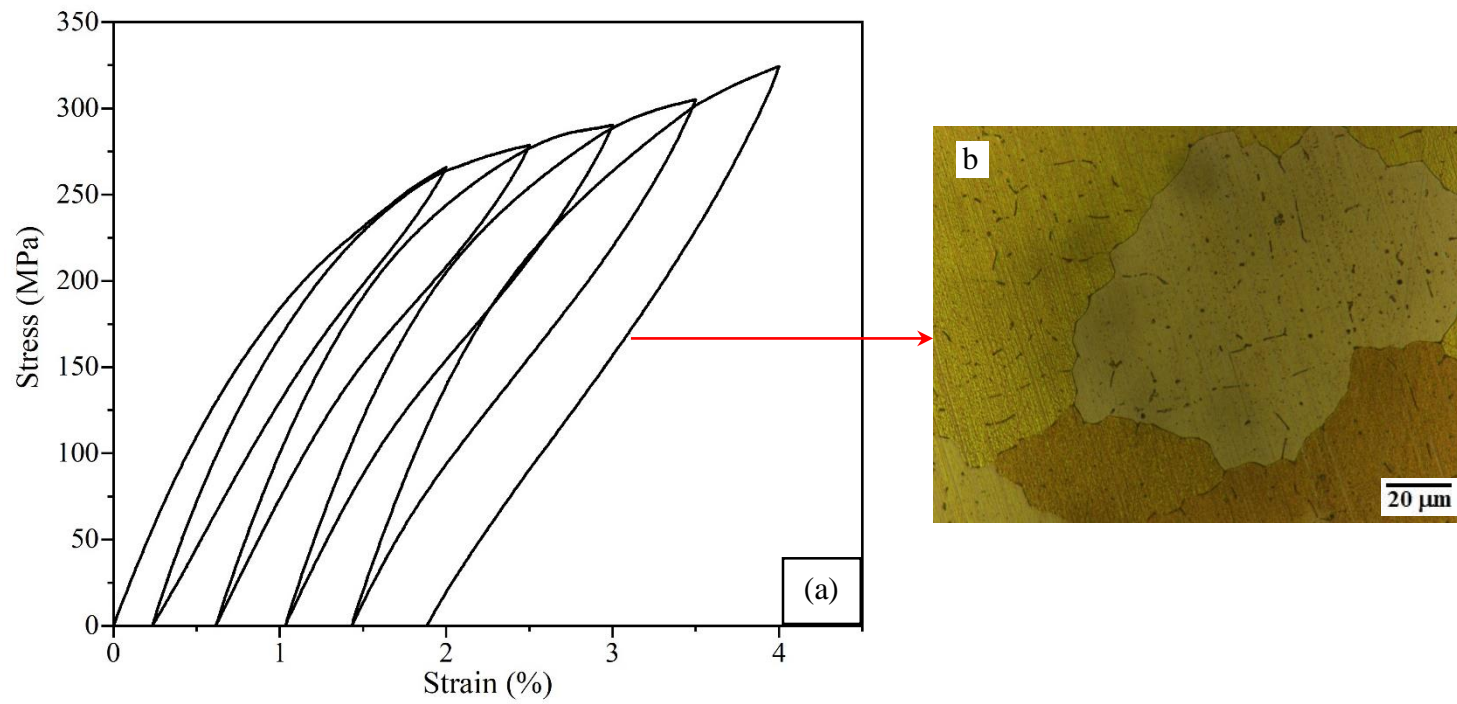


Figure 4.27 (a) Stress-strain hysteresis of the alloy Zr_4 and (b) optical micrograph of the pseudoelastically deformed alloy Zr_4 .

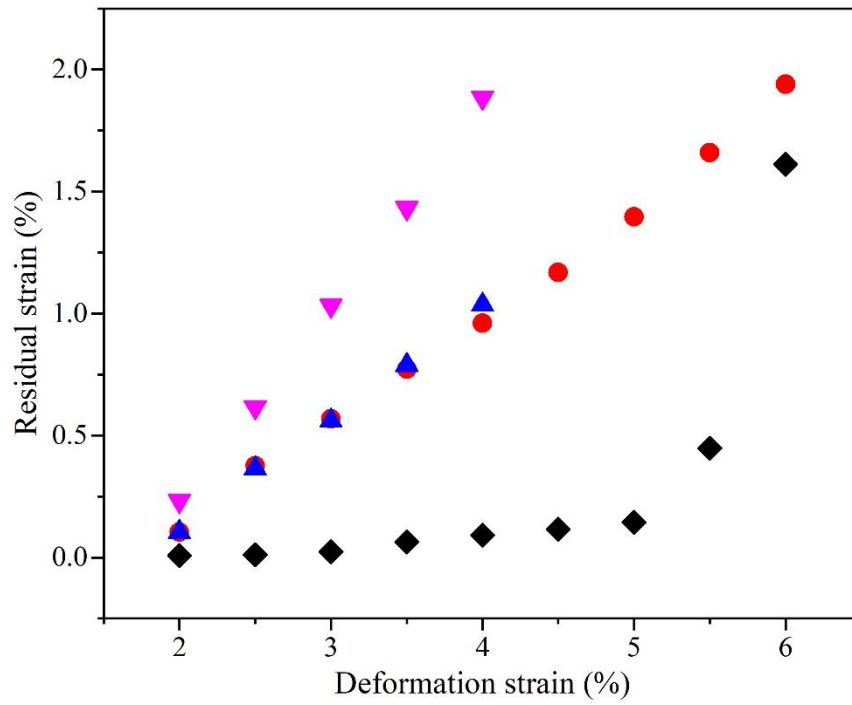


Figure 4.28 Residual strain of Cu-Al-Be-Zr SMAs: Zr_1 (♦), Zr_2 (●), Zr_3 (▲) and Zr_4 (▼) for different deformation strains.

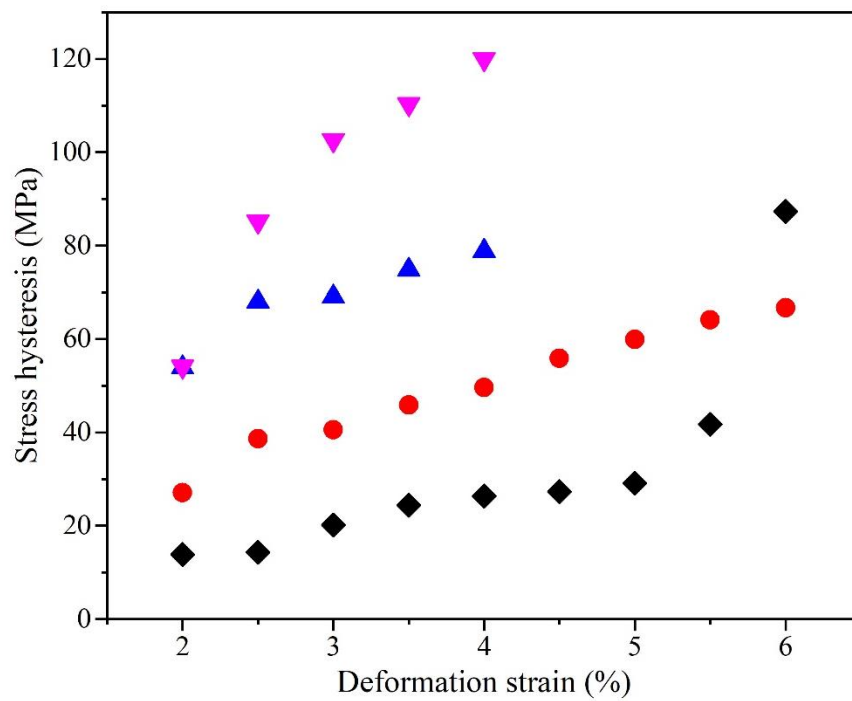
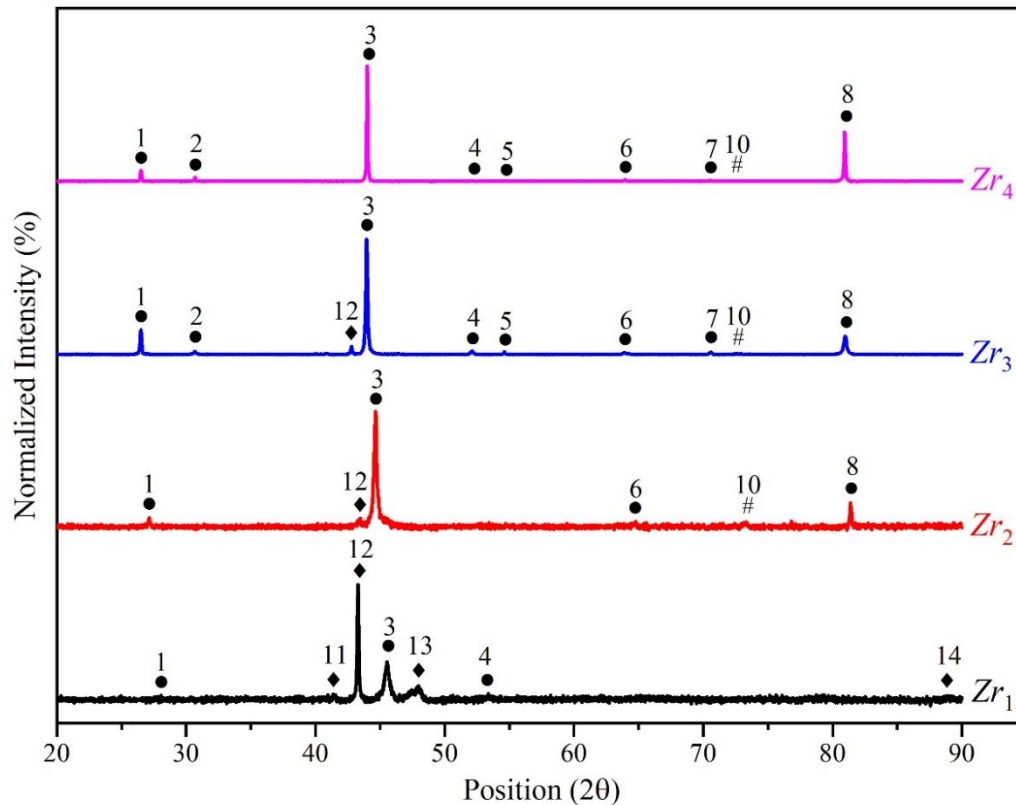


Figure 4.29 Stress hysteresis of Cu-Al-Be-Zr SMAs: Zr_1 (♦), Zr_2 (●), Zr_3 (▲) and Zr_4 (▼) for different deformation strains.



● - β_1 : 1(1 1 1), 2(0 0 2), 3(0 2 2), 4(1 1 3), 5(2 2 2), 6(0 0 4), 7 (1 3 3), 8 (2 2 4);
 # - Al_3Zr : 10(0 1 3); ◆ - β'_1 : 11(2 0 2), 12(0 0 22), 13(2 0 12), 14(2 4 8).

Figure 4.30 Normalized X-ray diffractograms of the pseudoelastically deformed Cu-Al-Be-Zr SMAs.

4.5 CLOSURE

This chapter presented the results and detailed discussion of the influence of ternary- and quaternary-doped elements on phases, grain size, phase transformation temperatures, mechanical, and pseudoelastic properties of the shape memory alloys. Ternary β_1 -phase Cu-Al-Be SMAs exhibit coarse grains, poor ductility, and fails brittle at relatively low tensile stress. Further, it is observed that boron- and zirconium-doped SMAs exhibit good grain refinement with a substantial improvement in the tensile strength and ductility, transforming brittle to ductile dimple fracture, and possess improved pseudoelastic shape recovery. As a whole, the minimal addition of boron-, and zirconium-doping are imperative as a segregate and not as an agglomerate in β_1 -type SMAs for vibration damping applications. The next chapter presents the key conclusions and future scope of the present study.

CHAPTER 5

CONCLUSIONS & FUTURE SCOPE

5.1 CONCLUSIONS

In the present study, investigated the influence of alloying additions containing ternary- and quaternary-doped elements, as well as altering their elemental compositions, on microstructural, mechanical and functional characteristics of shape memory alloys. The main conclusions drawn from the investigation are as follows:

- Addition of aluminium ≥ 11.5 wt.% and beryllium ≥ 0.57 wt.% forms complete austenite (β_1) phase. An increase in both aluminum and beryllium between the range of 11.0-11.8 wt.% and 0.5-0.6 wt.%, respectively, decreases the transformation temperatures. Alloying aluminum and beryllium did not exhibit significant improvement in mechanical properties due to the existence of coarse grains. Ternary base alloy Cu-Al_{11.5}-Be_{0.57} exhibits coarse grains of average size, 1134 ± 29 μm , tensile strength, 216.39 ± 30.17 MPa, ductility, $9.24 \pm 0.66\%$ with intergranular brittle failure, and possesses smaller energy differences, ΔH between austenite and martensite.
- Minimal addition of boron elements effectively refines the grain size and exhibits improved mechanical properties up to 0.15 wt.%. In addition, fracture morphology revealed that the addition of boron to the ternary SMAs transforms intergranular cleavage to transgranular dimple fracture. The maximum grain refinement size of 50 ± 2 μm with serrated grain boundaries exhibited the maximum enhancement in ultimate tensile strength, 744.65 ± 29.34 MPa, ductility, $21.93 \pm 0.56\%$, and a maximum pseudoelasticity of 4% was achieved with alloying Cu-Al_{11.5}-Be_{0.57}-B_{0.15} (wt.%). The presence of B-rich coarse precipitates with 0.2 wt.%B, leads to a negative impact on the grain refinement efficiency, mechanical properties, and pseudoelastic behavior of SMAs.

- Alloying zirconium exhibits an excellent grain refinement up to 0.15 wt.%, and a further increase in $Zr \geq 0.2$ wt.% lowers the grain refinement efficiency due to precipitates agglomeration. The maximum refinement with an average grain size of $65 \pm 7 \mu\text{m}$ is observed in the alloy Zr_3 containing $\text{Cu}_{87.93}\text{-Al}_{11.5}\text{-Be}_{0.57}\text{-Zr}_{0.15}$ (wt.%). A high volume fraction of Al_3Zr precipitates led to higher transformation temperatures.
- Tensile properties are improved by increasing Zr-doping, and the alloy Zr_3 exhibits the maximum enhancement in the tensile strength, 690.12 ± 28.01 MPa and ductility, $21.01 \pm 0.68\%$. A good pseudoelastic strain recovery is achieved in the alloy Zr_1 , i.e., up to 5% deformation strain. SMAs with Zr-doping exhibit improved mechanical properties up to 0.15 wt.%, however, the residual strains are progressively retained with the addition of zirconium ≥ 0.1 wt.% owing to increased precipitates pinning.
- A maximum pseudoelasticity of 5% was achieved in the alloy Zr_1 containing the elemental composition of $\text{Cu}_{87.93}\text{-Al}_{11.5}\text{-Be}_{0.57}\text{-Zr}_{0.05}$, which is suitable for vibration damping applications.

5.2 SCOPE FOR FURTHER RESEARCH

The influence of alloying additions of ternary- and quaternary-doped elements as well as changing their elemental composition on the properties, such as metallurgical, mechanical, and functional responses have been explored in the present study. Based on the practice and comprehension of the investigation results, the following scope of this work is recommended for future research.

- Investigation on the effect of secondary processes for further grain refinement and properties improvisation.
- Investigation on the properties of quaternary base alloy doping with quinary elements for further improvisation.
- Investigation on drawing of the pseudoelastic SMA wires for damper applications in cable-stayed bridges from the optimal combination of SMAs.
- Investigation on vibration damping and isolation characteristics of the SMA embedded hybrid composite structures.

REFERENCES

- Adnyana, D. N. (1986). "Effect of grain size on transformation temperatures in a grain-refined, copper-based, shape-memory alloy." *Metallography*, 19(2), 187–196.
- Agafonov, V., Naudot, P., Dubertret, A., and Dubois, B. (1988). "Influence of the aluminium content on the appearance and stability of martensites in the Cu - Al - Ni system." *Scr. Metall.*, 22(4), 489–494.
- Agapitova, N. V., Nikiforova, L. V., Kopylova, V. M., and Evsyukov, V. A. (1996). "Thermoelastic transformation in Cu - Al - Mn alloys." *Met. Sci. Heat Treat.*, 38(8), 324–326.
- Agrawal, A., and Dube, R. K. (2018). "Methods of fabricating Cu-Al-Ni shape memory alloys." *J. Alloys Compd.*, 750, 235–247.
- Aksu Canbay, C., and Keskin, A. (2014). "Effects of vanadium and cadmium on transformation temperatures of Cu–Al–Mn shape memory alloy." *J. Therm. Anal. Calorim.*, 118(3), 1407–1412.
- Albuquerque, V. H. C. de, Melo, T. A. de A., Gomes, R. M., Lima, S. J. G. de, and Tavares, J. M. R. S. (2010a). "Grain size and temperature influence on the toughness of a CuAlBe shape memory alloy." *Mater. Sci. Eng. A*, 528(1), 459–466.
- Albuquerque, V. H. C. de, Melo, T. A. de A., Oliveira, D. F. de, Gomes, R. M., and Tavares, J. M. R. S. (2010b). "Evaluation of grain refiners influence on the mechanical properties in a CuAlBe shape memory alloy by ultrasonic and mechanical tensile testing." *Mater. Des.*, 31(7), 3275–3281.
- Aldas, K., Eskil, M., Özkul, İ., and Özkul, Oskender. (2014). "Prediction of Af temperature for copper based shape memory alloys." *Indian J. Eng. Mater. Sci.*, 21(August), 429–437.
- Alvandi, S., and Ghassemieh, M. (2014). "Application of Shape Memory Alloys in Seismic Isolation: A Review." *Civ. Eng. Infrastructures J.*, 47(2), 153–171.
- Ammar, O., Haddar, N., and Dieng, L. (2017). "Experimental investigation of the pseudoelastic behaviour of NiTi wires under strain- and stress-controlled cyclic tensile

loadings.” *Intermetallics*, 81, 52–61.

Antonio, J. A. M., and Lfo, L. F. M. (1971). “Grain refinement in aluminum alloyed with titanium and boron.” *Metall. Trans.*, 2(2), 465–471.

Asanovic, V. D., Delijic, K. H., Radusinovic, I. D., and Bosnjak, B. T. (2002). “The Effects of Thermomechanical Treatments on the Microstructure and Properties of Cu-Zn-Al Alloy.” *High Temp. Mater. Process.*, 21(5), 269–280.

Asgarian, B., Salari, N., and Saadati, B. (2016). “Application of Intelligent Passive Devices Based on Shape Memory Alloys in Seismic Control of Structures.” *Structures*, 5, 161–169.

Assis, T. De, Huang, S., Driemeier, C. E., Donohoe, B. S., Kim, C., Kim, S. H., Gonzalez, R., Jameel, H., and Park, S. (2018). “Toward an understanding of the increase in enzymatic hydrolysis by mechanical refining.” *Biotechnol. Biofuels*, 11(1), 1–11.

Auricchio, F., Fugazza, D., and Desroches, R. (2006). “Earthquake performance of steel frames with Nitinol braces.” *J. Earthq. Eng.*, 10(sup001), 45–66.

Aydogdu, Y., Turabi, A. S., Aydogdu, A., Vance, E. D., Kok, M., Kirat, G., and Karaca, H. E. (2016). “The effects of substituting B for Cu on the magnetic and shape memory properties of CuAlMnB alloys.” *Appl. Phys. A*, 122(7), 687.

Bahl, S., Nagar, H., Singh, I., and Sehgal, S. (2020). “Smart materials types, properties and applications: A review.” *Mater. Today Proc.*, 28, 1302–1306.

Balart, M. J., Patel, J. B., and Fan, Z. (2015). “Grain refinement of DHP copper by particle inoculation.” *Int. J. Cast Met. Res.*, 28(4), 242–247.

Balart, M. J., Patel, J. B., Gao, F., and Fan, Z. (2016). “Grain Refinement of Deoxidized Copper.” *Metall. Mater. Trans. A*, 47(10), 4988–5011.

Balo, S. N., and Ceylan, M. (2002). “Effect of Be content on some characteristics of Cu – Al – Be shape memory alloys.” *J. Mater. Process. Technol.*, 124, 200–208.

Basinski, Z. S., and Christian, J. W. (1954). “Experiments on the martensitic transformation in single crystals of indium-thallium alloys.” *Acta Metall.*, 2(1), 148–

166.

Behera, A., and Nayak, D. (2022). “Smart Material Surface Science and application (SMASSA): A most awaited journey in smart technology.” *Appl. Surf. Sci. Adv.*, 9(March), 100242.

Belkahla, S., Flores Zuniga, H., and Guenin, G. (1993). “Elaboration and characterization of new low temperature shape memory Cu-Al-Be alloys.” *Mater. Sci. Eng. A*, 169(1–2), 119–124.

Belkahla, S., and Guenin, G. (1991). “Martensitic transformation and metallurgical study of low temperature Cu-Al-Be ternary alloy.” *Le J. Phys. IV*, 01(C4), C4-145-C4-150.

Bellini, A., Colli, M., and Dragoni, E. (2009). “Mechatronic design of a shape memory alloy actuator for automotive tumble flaps: A case study.” *IEEE Trans. Ind. Electron.*, 56(7), 2644–2656.

Bhattacharya, S., Bhuniya, A., and Banerjee, M. K. (1993). “Influence of minor additions on characteristics of Cu–Al–Ni alloy.” *Mater. Sci. Technol.*, 9(8), 654–658.

Biol, Y. (2012). “Grain refinement of Al–Cu foundry alloys with B additions.” *Int. J. Cast Met. Res.*, 25(2), 117–120.

Blazquez, M. L., Castillo, C. L. D. E. L., Gomez, C., Blazqui, M. L. Z., Castillo, C. L. D. E. L., and Gomez, C. (1989). “Influence of the Composition and Maximum Cycling Temperature on the Microstructure of Cu-Al-Mn Shape Memory Alloys The alloys chosen for this work were produced by induction melting.” *Metallography*, 133, 119–133.

Bolzoni, L., Nowak, M., and Hari Babu, N. (2015). “Grain refining potency of Nb–B inoculation on Al–12Si–0.6Fe–0.5Mn alloy.” *J. Alloys Compd.*, 623, 79–82.

Braghin, F., Cinquemani, S., and Resta, F. (2012). “A low frequency magnetostrictive inertial actuator for vibration control.” *Sensors Actuators A Phys.*, 180, 67–74.

Bublei, I. R., and Titov, P. V. (1990). “Effect of aluminum and manganese on the martensitic transformation characteristics in alloys of the system Cu-Al-Mn.” *Met. Sci.*

Heat Treat., 32(4), 288–290.

Buehler, W. J., Gilfrich, J. V., and Wiley, R. C. (1963). “Effect of Low-Temperature Phase Changes on the Mechanical Properties of Alloys near Composition TiNi.” *J. Appl. Phys.*, 34(5), 1475–1477.

Buehler, W. J., and Wang, F. E. (1968). “A summary of recent research on the nitinol alloys and their potential application in ocean engineering.” *Ocean Eng.*, 1(1), 105–120.

Buehler, W. J., and Wiley, R. C. (1961). “The properties of TiNi and associated phases.” *NOLTR Rep. (AD 266607)*, 61–75.

Bundara, B., Tokuda, M., Kuselj, B., Ule, B., and Tuma, J. V. (2000). “Superelastic tension and bending characteristics of shape memory alloys.” *Met. Mater.*, 6(4), 293–299.

Burkart, M. W., and Read, T. A. (1953). “Diffusionless phase change in the indium-thallium system.” *Trans. AIME*, 197(11), 1516–1524.

Canbay, C. A., and Karagoz, Z. (2013). “Effects of Annealing Temperature on Thermomechanical Properties of Cu–Al–Ni Shape Memory Alloys.” *Int. J. Thermophys.*, 34(7), 1325–1335.

Candido, G. V. da M., Melo, T. A. de A., Albuquerque, V. H. C. De, Gomes, R. M., Lima, S. J. G. de, and Tavares, J. M. R. S. (2012). “Characterization of a CuAlBe Alloy with Different Cr Contents.” *J. Mater. Eng. Perform.*, 21(11), 2398–2406.

Carl, M., Zhang, B., and Young, M. L. (2016). “Texture and Strain Measurements from Bending of NiTi Shape Memory Alloy Wires.” *Shape Mem. Superelasticity*, 2(3), 254–263.

Celada-Casero, C., Sietsma, J., and Santofimia, M. J. (2019). “The role of the austenite grain size in the martensitic transformation in low carbon steels.” *Mater. Des.*, 167, 107625.

Chaisan, K., Wongratanaphisan, D., Choopun, S., Sagawa, T., and Ruankham, P. (2019). “Enhanced crystal formation of methylammonium lead iodide via self-

assembled monolayers and their solvation for perovskite solar cells.” *J. Mater. Sci. Mater. Electron.*, 30(1), 939–949.

Chandrasekaran, L., and Miodownik, A. P. (1979). “The effect of low temperature ageing on the martensite transformation in Cu-Zn-Mn alloys.” *Proc. Int. Conf. Martensitic Transform. ICOMAT 1979*, Cambridge, Massachusetts, 584.

Chang, L.-C., and Read, T. A. (1951). “Plastic deformation and diffusionless changes in metals. The gold-cadmium beta phase.” *Trans. AIME*, 191(January), 47–52.

Chen, C. W. (1957). “Some characteristics of the martensite transformation of Cu-Al-Ni alloys.” *JOM*, 9(10), 1202–1203.

Chen, J., Qiu, Q., Han, Y., and Lau, D. (2019). “Piezoelectric materials for sustainable building structures: Fundamentals and applications.” *Renew. Sustain. Energy Rev.*, 101(September 2018), 14–25.

Chen, Z., Kang, H., Fan, G., Li, J., Lu, Y., Jie, J., Zhang, Y., Li, T., Jian, X., and Wang, T. (2016). “Grain refinement of hypoeutectic Al-Si alloys with B.” *Acta Mater.*, 120, 168–178.

Cheng, T. . (2000). “The mechanism of grain refinement in TiAl alloys by boron addition — an alternative hypothesis.” *Intermetallics*, 8(1), 29–37.

Chentouf, S. M., Bouabdallah, M., Cheniti, H., Eberhardt, A., Patoor, E., and Sari, A. (2010). “Ageing study of Cu–Al–Be hypoeutectoid shape memory alloy.” *Mater. Charact.*, 61(11), 1187–1193.

Chopra, I., and Sirohi, J. (2013). “Historical Developments and Potential Applications: Smart Materials and Structures.” *Smart Struct. Theory*, Cambridge: Cambridge University Press, 1–112.

Chowdhury, P., and Sehitoglu, H. (2017). “Deformation physics of shape memory alloys – Fundamentals at atomistic frontier.” *Prog. Mater. Sci.*, 88, 49–88.

Chung, C. Y., Lam, C. W. H., and Tan, S. S. (1998). “Effect of parent phase ageing on CuZnAl shape memory alloys with Mn and Zr addition.” *Mater. Lett.*, 33(5–6), 291–296.

- Clemente, C. S., Davino, D., Maddaloni, G., Pecce, M. R., and Visone, C. (2016). "A Magnetostrictive Energy Harvesting System for Bridge Structural Health Monitoring." *7th Forum New Mater. - Part E*, 20–25.
- Cornelis, I., and Wayman, C. M. (1974). "Phase transformations in metastable β' CuZn alloys-I. Martensitic transformations." *Acta Metall.*, 22(3), 291–300.
- Cuniberti, A., Montecinos, S., and Lovey, F. C. (2009). "Effect of γ_2 -phase precipitates on the martensitic transformation of a β -CuAlBe shape memory alloy." *Intermetallics*, 17(6), 435–440.
- Dasgupta, R., Jain, A. K., Hussain, S., Pandey, A., and Sampath, V. (2018). "Effect of Alloying Additions on the Properties Affecting Shape Memory Properties of Cu–12.5Al–5Mn Alloy." *Front. Mater. Process. Appl. Res. Technol.*, Singapore: Springer Singapore, 377–390.
- Dasgupta, R., Jain, A. K., Kumar, P., Hussain, S., and Pandey, A. (2015). "Role of alloying additions on the properties of Cu-Al-Mn shape memory alloys." *J. Alloys Compd.*, 620, 60–66.
- Dasgupta, R., Jain, A. K., Kumar, P., Hussein, S., and Pandey, A. (2014). "Effect of alloying constituents on the martensitic phase formation in some Cu-based SMAs." *J. Mater. Res. Technol.*, 3(3), 264–273.
- Davis, J. R., and Committee, A. S. M. I. H. (2001). *Copper and Copper Alloys*. ASM specialty handbook, ASM International.
- Delaey, L., Krishnan, R. V., Tas, H., and Warlimont, H. (1974). "Thermoelasticity, pseudoelasticity and the memory effects associated with martensitic transformations." *J. Mater. Sci.*, 9(9), 1521–1535.
- Delaey, L., and Warlimont, H. (1966). "The diffusionless transformations of the β -phase in copper-zinc-gallium alloys." *Int. J. Mater. Res.*, 57(11), 793–803.
- Deppisch, C., Liu, G., Shang, J. K. K., and Economy, J. (1997). "Processing and mechanical properties of AlB₂ flake reinforced Al-alloy composites." *Mater. Sci. Eng. A*, 225, 153–161.

- DesRoches, R., and Delemont, M. (2002). “Seismic retrofit of simply supported bridges using shape memory alloys.” *Eng. Struct.*, 24(3), 325–332.
- Dieng, L., Helbert, G., Arbab, S., Lecompte, T., and Pilvin, P. (2013). “Use of Shape Memory Alloys damper device to mitigate vibration amplitudes of bridge cables.” *Eng. Struct.*, 56, 1547–1556.
- Ding, Y., Wang, Q., Yin, F., Cui, C., and Hao, G. (2019). “Effect of combined addition of Cu₅₁Zr₁₄ inoculant and Ti element on the microstructure and damping behavior of a Cu-Al-Ni shape memory alloy.” *Mater. Sci. Eng. A*, 743(November 2018), 606–610.
- Dogan, E., Karaman, I., Singh, N., Chivukula, A., Thawabi, H. S., and Arroyave, R. (2012). “The effect of electronic and magnetic valences on the martensitic transformation of CoNiGa shape memory alloys.” *Acta Mater.*, 60(8), 3545–3558.
- Dong, Y. Y., Wang, T. M., Zin, S. J., and Dar, K. Z. (1994). “The shape memory capability and life of Cu-Al-Be-X alloys.” *Mater. Charact.*, 33(2), 163–168.
- Duerig, T., Pelton, A., and Stöckel, D. (1999). “An overview of nitinol medical applications.” *Mater. Sci. Eng. A*, 273–275, 149–160.
- Duerig, T. W., Albrecht, J., and Gessinger, G. H. (1982). “A Shape-Memory Alloy for High-Temperature Applications.” *JOM*, 34(12), 14–20.
- Duerig, T. W., Melton, K. N., Stöckel, D., and Wayman, C. M. (1990). *Engineering Aspects of Shape Memory Alloys*. Butterworth-Heinemann.
- Dutkiewicz, J. (1999). “Superelasticity and Shape Memory Effect in Copper Base Alloys.” *Acta Phys. Pol. A*, 96(2), 197–212.
- Dutkiewicz, J., Cesari, E., Segui, C., and Pons, J. (1991). “RESPONSE OF Cu-AL-Mn ALLOYS TO AGEING IN β PHASE.” *Le J. Phys. IV*, 01(C4), C4-229-C4-234.
- Dutkiewicz, J., Chandrasekaran, M., and Cesari, E. (1993). “Stabilisation of martensite in Cu-Zn-Si.” *Scr. Metall. Mater.*, 29(1), 19–24.
- Dutkiewicz, J., and Morgiel, J. (1989). “Effect of Ageing on Martensitic Transformation in CuZn and CuZnSn Alloys.” *ESOMAT 1989 - Ist Eur. Symp. Martensitic Transform. Sci. Technol.*, Les Ulis, France: EDP Sciences, 141–148.

- Dutkiewicz, J., and Morgiel, J. (1986). “The effect of DO₃ ordering on the parent \rightleftharpoons martensitic transformation in the CuZnAl shape-memory alloy.” *J. Mater. Sci.*, 21(2), 429–434.
- Dvorak, I., and Hawbolt, E. B. (1975). “Transformational elasticity in a polycrystalline Cu-Zn-Sn alloy.” *Metall. Trans. A*, 6(1), 95–99.
- Ergen, S., Uzun, O., Yilmaz, F., and Kiliçaslan, M. F. (2013). “Shape memory properties and microstructural evolution of rapidly solidified CuAlBe alloys.” *Mater. Charact.*, 80, 92–97.
- Eucken, S., Donner, P., and Hornbogen, E. (1988). “On improvement in the mechanical properties of rapidly solidified shape memory alloys.” *Mater. Sci. Eng.*, 98(C), 469–474.
- Fallah, N., and Ebrahimnejad, M. (2013). “Active control of building structures using piezoelectric actuators.” *Appl. Soft Comput.*, 13(1), 449–461.
- Feninat, F. El, Laroche, G., Fiset, M., and Mantovani, D. (2002). “Shape Memory Materials for Biomedical Applications.” *Adv. Eng. Mater.*, 4(3), 91–104.
- Fernandes, D. J., Peres, R. V., Mendes, A. M., and Elias, C. N. (2011). “Understanding the Shape-Memory Alloys Used in Orthodontics.” *ISRN Dent.*, 2011, 1–6.
- Figuroa, C. G., Jacobo, V. H., Cortés-Pérez, J., and Schouwenaars, R. (2020). “Surface Nanostructuring of a CuAlBe Shape Memory Alloy Produces a 10.3 ± 0.6 GPa Nanohardness Martensite Microstructure.” *Materials (Basel)*, 13(24), 5702.
- Flores Zúñiga, H., Belkahla, S., and Guénin, G. (1991). “THE THERMAL AGING AND TWO WAY MEMORY EFFECT (TWME) IN Cu-Al-Be SHAPE MEMORY ALLOY.” *Le J. Phys. IV*, 01(C4), C4-289-C5-294.
- Flores Zúñiga, H., Rios-Jara, D., Belkahla, S., Nika, V., and Guénin, G. (1996). “The training and re-training procedures for the two way memory effect and its degradation in a Cu-Al-Be alloy.” *Scr. Mater.*, 34(12), 1899–1904.
- Flores Zúñiga, H., Rios-Jara, D., Lovey, F. C., and Guénin, G. (1995). “Thermal Stability of Beta Phase in a Cu-Al-Be Shape Memory Alloy.” *Le J. Phys. IV*, 05(C2),

C2-171-C2-174.

Frenzel, J., George, E. P., Dlouhy, A., Somsen, C., Wagner, M. F. X., and Eggeler, G. (2010). "Influence of Ni on martensitic phase transformations in NiTi shape memory alloys." *Acta Mater.*, 58(9), 3444–3458.

Frenzel, J., Wiczorek, A., Opahle, I., Maaß, B., Drautz, R., and Eggeler, G. (2015). "On the effect of alloy composition on martensite start temperatures and latent heats in Ni–Ti-based shape memory alloys." *Acta Mater.*, 90, 213–231.

Friend, C. M. (1989). "The effect of aluminium content on the martensite phase stabilities in metastable CuAlNi alloys." *Scr. Metall.*, 23(10), 1817–1820.

Fu, H., Song, S., Zhuo, L., Zhang, Z., and Xie, J. (2016). "Enhanced mechanical properties of polycrystalline Cu–Al–Ni alloy through grain boundary orientation and composition control." *Mater. Sci. Eng. A*, 650, 218–224.

Fu, X., Guojun, M., Xinqing, Z., and Huibin, X. (2009). "Effects of Nb Content on Yield Strength of NiTiNb Alloys in Martensite State." *Chinese J. Aeronaut.*, 22(6), 658–662.

Fujita, H., and Toshiyoshi, H. (1998). "Micro actuators and their applications." *Microelectronics J.*, 29(9), 637–640.

Furuya, Y., and Shimada, H. (1991). "Shape memory actuators for robotic applications." *Mater. Des.*, 12(1), 21–28.

Garafolo, N. G., and McHugh, G. R. (2018). "Mitigation of flutter vibration using embedded shape memory alloys." *J. Fluids Struct.*, 76, 592–605.

Gil, F. J., and Guilemany, J. M. (1992). "Pseudoelastic hysteresis in Cu-Zn-Al shape-memory single crystals." *J. Mater. Sci. Lett.*, 11(8), 493–495.

Gil, F. J., and Guilemany, J. M. (1993). "Effect of grain size on the pseudoelastic properties of Cu-20.8Zn-6.1Al shape-memory alloy." *J. Mater. Sci. Lett.*, 12(1), 6–7.

Gil, F. J., Peña, J., and Guilemany, J. M. (1999). "Improvement of the grain refinement of Cu-Zn-Al shape memory alloys with manganese, cobalt, and zirconium addition." *J. Mater. Synth. Process.*, 7(2), 127–133.

- Gil, F. J., Solano, E., Peña, J., Engel, E., Mendoza, A., and Planell, J. A. (2004). “Microstructural, mechanical and cytotoxicity evaluation of different NiTi and NiTiCu shape memory alloys.” *J. Mater. Sci. Mater. Med.*, 15(11), 1181–1185.
- Greer, A. L., Bunn, A. M., Tronche, A., Evans, P. V., and Bristow, D. J. (2000). “Modelling of inoculation of metallic melts: application to grain refinement of aluminium by Al-Ti-B.” *Acta Mater.*, 48, 2823–2835.
- Greer, A. L., Cooper, P. S., Meredith, M. W., Schneider, W., Schumacher, P., Spittle, J. A., and Tronche, A. (2003). “Grain Refinement of Aluminium Alloys by Inoculation.” *Adv. Eng. Mater.*, 5(12), 81–91.
- Greninger, A. B. (1939a). “The martensite transformation in beta copper-aluminum alloys.” *Trans. AIME*, 133, 204–227.
- Greninger, A. B. (1939b). “The martensite transformation in beta copper-aluminum alloys.” *AIME Trans*, 133, 204–227.
- Greninger, A. B., and Mooradian, V. G. (1938). “Strain Transformation in Metastable Beta Copper-zinc and Beta Copper-tin Alloys.” *Trans. AIME*, 128, 337–368.
- Gu, X., Li, J., and Li, Y. (2020). “Experimental realisation of the real-time controlled smart magnetorheological elastomer seismic isolation system with shake table.” *Struct. Control Heal. Monit.*, 27(1), e2476.
- Guilemany, J. M., and Gil, F. J. (1990). “The relationship between chemical composition and transformation temperatures, M_s and A_s , in polycrystals and single crystals of Cu-Zn-Al shape-memory alloys.” *Thermochim. Acta*, 167(1), 129–138.
- Guilemany, J. M., and Gil, F. J. (1991). “Kinetic grain growth in Cu-Zn-Al shape memory alloys.” *J. Mater. Sci.*, 26(17), 4626–4630.
- Haidar, M. A., Saud, S. N., and Hamzah, E. (2018). “Microstructure, Mechanical Properties, and Shape Memory Effect of Annealed Cu-Al-Ni-xCo Shape Memory Alloys.” *Metallogr. Microstruct. Anal.*, 7(1), 57–64.
- Han, Y. S., and Kim, Y. G. (1987). “The effects of boron and aging on mechanical properties and martensitic temperatures in CuZnAl shape-memory alloys.” *Scr. Metall.*,

21, 947–952.

Hartl, D. J., and Lagoudas, D. C. (2007). “Aerospace applications of shape memory alloys.” *Proc. Inst. Mech. Eng. Part G J. Aerosp. Eng.*, 221(4), 535–552.

He, Z., Wang, F., Wang, Y., Xia, P., and Yang, B. (2007). “Effects of V and Cr on transformation and deformation characteristics of Ti-Ni superelastic alloy.” *Acta Metall. Sin.*, 43(12), 1293–1296.

Hefzy, M. S., Elahinia, M., Jahadabbar, A., Arn, B., and Nematollahi, M. (2020). “Demonstration of shape memory and superelastic effects of nitinol alloys.” *ASEE Annu. Conf. Expo. Conf. Proc.*, 2020-June(August 2004).

Heller, L., Šittner, P., Pilch, J., and Landa, M. (2009). “Factors Controlling Superelastic Damping Capacity of SMAs.” *J. Mater. Eng. Perform.*, 18(5–6), 603–611.

Higuchi, A., Suzuki, K., Matsumoto, Y., Sugimoto, K., Komatsu, S., and Nakamura, Y. (1982). “SHAPE MEMORY EFFECT IN Cu-Al-Be TERNARY ALLOYS.” *Le J. Phys. Colloq.*, 43(C4), C4-767-C4-772.

Higuchi, A., Suzuki, K., Sugimoto, K., and Nakamura, Y. (1986). “No Title.” *Proc. Int. Conf. Martensitic Transform.*, Nara, Japan, 886–890.

Horiuchi, Y., Inamura, T., Kim, H. Y., Wakashima, K., Miyazaki, S., and Hosoda, H. (2007). “Effect of Boron Concentration on Martensitic Transformation Temperatures, Stress for Inducing Martensite and Slip Stress of Ti-24 mol % Nb-3 mol % Al Superelastic Alloy.” *Mater. Trans.*, 48, 407–413.

Hosseini, S. A., Abbasi, S. M., and Madar, K. Z. (2018). “The effect of boron and zirconium on microstructure and tensile properties of the wrought nickel-based superalloy ATI 718Plus.” *Mater. Sci. Eng. A*, 712, 780–789.

Hsu, C. A., Wang, W. H., Hsu, Y. F., and Rehbach, W. P. (2009). “The refinement treatment of martensite in Cu–11.38wt.%Al–0.43wt.%Be shape memory alloys.” *J. Alloys Compd.*, 474(1–2), 455–462.

Hsu, C., and Wang, W. (1996). “Superplastic forming characteristics of a Cu-Zn-Al-Zr shape memory alloy.” *Mater. Sci. Eng. A*, 205(1–2), 247–253.

- Humbeeck, J. Van, Delaey, L., and Deruyttere, A. (1978). "The Pseudoboelasticity in β Cu-Zn-Al Alloys." *Int. J. Mater. Res.*, 69(9), 575–580.
- Husain, S. W., and Clapp, P. C. (1987a). "The effect of nickel content on the fracture behaviour of Cu-Al-Ni β -phase alloys." *J. Mater. Sci.*, 22(2), 509–516.
- Husain, S. W., and Clapp, P. C. (1987b). "The intergranular embrittlement of Cu-Al-Ni β -phase alloys." *J. Mater. Sci.*, 22(7), 2351–2356.
- Hussain, S., Pandey, A., and Dasgupta, R. (2019). "Designed polycrystalline ultra-high ductile boron doped Cu–Al–Ni based shape memory alloy." *Mater. Lett.*, 240, 157–160.
- Jain, A. K., Hussain, S., Kumar, P., Pandey, A., Rupa, D., and Dasgupta, R. (2016). "Effect of Varying Al/Mn Ratio on Phase Transformation in Cu–Al–Mn Shape Memory Alloys." *Trans. Indian Inst. Met.*, 69(6), 1289–1295.
- James, T., and Gann, T. J. (1982). "The effects of grain size on the martensitic transformation in copper-zinc-aluminum shape memory alloys."
- Jani, J. M., Leary, M., and Subic, A. (2014). "Shape memory alloys in automotive applications." *Appl. Mech. Mater.*, 663, 248–253.
- Janke, L., Czaderski, C., Motavalli, M., and Ruth, J. (2005). "Applications of shape memory alloys in civil engineering structures - Overview, limits and new ideas." *Mater. Struct.*, 38(279), 578–592.
- Janssen, J., Follon, M., and Delaey, L. (1979). "The Fatigue Properties of Superelastic Cu-Zn-Al Alloys." *Strength Met. Alloy.*, P. HAASEN, V. GEROLD, and G. KOSTORZ, eds., Elsevier, 1125–1130.
- Jiao, Y. Q., Wen, Y. H., Li, N., He, J. Q., and Teng, J. (2010). "Effect of solution treatment on damping capacity and shape memory effect of a CuAlMn alloy." *J. Alloys Compd.*, 491(1–2), 627–630.
- Jiao, Z., Wang, Q., Yin, F., and Cui, C. (2018). "Effect of precipitation during parent phase aging on the microstructure and properties of a refined CuAlMn shape memory alloy." *Mater. Sci. Eng. A*, 737, 124–131.

Jones, G. P., and Pearson, J. (1976). “Factors affecting the grain-refinement of aluminum using titanium and boron additives.” *Metall. Trans. B*, 7(2), 223–234.

Jurado, M., Castàn, T., Mañosa, L., Planes, A., Bassas, J., Alcobé, X., and Morin, M. (1997). “Study of the order-disorder phase transitions in Cu-Al-Be shape memory alloys.” *Philos. Mag. A*, 75(5), 1237–1250.

Jurado, M., Mañosa, L., Planes, A., and Stassis, C. (1995). “No Title.” *J. Phys. IV*, 2 C, 165–170.

Kainuma, R., Takahashi, S., and Ishida, K. (1995). “Ductile Shape Memory Alloys of the Cu-Al-Mn System.” *J. Phys. IV*, 05(C8), C8-961-C8-966.

Kainuma, R., Takahashi, S., and Ishida, K. (1996). “Thermoelastic martensite and shape memory effect in ductile Cu-Al-Mn alloys.” *Metall. Mater. Trans. A*, 27(8), 2187–2195.

Kannarpady, G. K., Wolverton, M., Russalian, V. R., Bhattacharyya, A., and Pulnev, S. (2009). “Pseudo-creep in Cu-Al-Ni single crystal shape memory alloys.” *Behav. Mech. Multifunct. Mater. Compos. 2009*, Z. Ounaies and J. Li, eds., SPIE, 118–126.

Kaouache, B., Berveiller, S., Inal, K., Eberhardt, A., and Patoor, E. (2004). “Stress analysis of martensitic transformation in Cu–Al–Be polycrystalline and single-crystalline shape memory alloy.” *Mater. Sci. Eng. A*, 378(1–2), 232–237.

Kaouache, B., Inal, K., Berveiller, S., Eberhardt, A., and Patoor, E. (2006). “Martensitic transformation criteria in Cu–Al–Be shape memory alloy—In situ analysis.” *Mater. Sci. Eng. A*, 438–440, 773–778.

Kato, H., Ozu, T., Hashimoto, S., and Miura, S. (1999). “Cyclic stress–strain response of superelastic Cu–Al–Mn alloy single crystals.” *Mater. Sci. Eng. A*, 264(1–2), 245–253.

Kim, J. W., Roh, D. W., Lee, E. S., and Kim, Y. G. (1990). “Effects on microstructure and tensile properties of a zirconium addition to a Cu-Al-Ni shape memory alloy.” *Metall. Trans. A*, 21(2), 741–744.

Kim, W. C., Kim, Y. J., Kim, Y. S., Hyun, J. I., Hong, S. H., Kim, W. T., and Kim, D.

- H. (2019). "Enhancement of superelastic property in Ti–Zr–Ni–Cu alloy by using glass alloy precursor with high glass forming ability." *Acta Mater.*, 173, 130–141.
- Kök, M., Dağdelen, F., Aydoğdu, A., and Aydoğdu, Y. (2016). "The change of transformation temperature on NiTi shape memory alloy by pressure and thermal ageing." *J. Phys. Conf. Ser.*, 667(1), 012011.
- Köster, W., and Gödecke, T. (1966). "The ternary system copper-manganese-aluminium." *Int. J. Mater. Res.*, 57(12), 889–901.
- Kozlova, L. E., and Titenko, A. N. (2006). "Stress-induced martensitic transformation in polycrystalline aged Cu–Al–Mn alloys." *Mater. Sci. Eng. A*, 438–440(SPEC. ISS.), 738–742.
- Kurdyumov, G., and Khandros, L. (1949). "On the 'thermoelastic' equilibrium on martensitic transformations." *Dokl. Akad. Nauk SSSR*, 66(2), 211–214.
- Kustov, S., Pons, J., Cesari, E., Humbeeck, J. Van, and Morin, M. (2004a). "Stabilization and hyperstabilization of Cu–Al–Be $\beta 1'$ martensite by thermal treatment and plastic deformation." *Mater. Sci. Eng. A*, 378(1–2), 283–288.
- Kustov, S., Pons, J., Cesari, E., Morin, M., and Humbeeck, J. Van. (2004b). "Athermal stabilization of Cu–Al–Be $\beta 1'$ martensite due to plastic deformation and heat treatment." *Mater. Sci. Eng. A*, 373(1–2), 328–338.
- Kuwano, N., Ogata, I., Tomokiyo, Y., and Eguchi, T. (1977). "Formation Process of $\alpha 2$ Phase in Cu–Al Alloys." *Trans. Japan Inst. Met.*, 18(3), 195–203.
- Kwarciaak, J., Bojarski, Z., and Morawiec, H. (1986). "Phase transformation in martensite of Cu-12.4% Al." *J. Mater. Sci.*, 21(3), 788–792.
- Lagoudas, D. C. (Ed.). (2008). *Shape Memory Alloys: Modeling and Engineering Applications*. Springer US.
- Lai, M. O., Lu, L., and Lee, W. H. (1996). "Influence of heat treatment on properties of copper-based shape-memory alloy." 31, 1537–1543.
- Laporte, V., and Mortensen, A. (2009). "Intermediate temperature embrittlement of copper alloys." *Int. Mater. Rev.*, 54(2), 94–116.

- Lara-rodriguez, G. A., Gonzalez, G., Flores-Zúñiga, H., and Cortés-pérez, J. (2006). “The effect of rapid solidification and grain size on the transformation temperatures of Cu-Al-Be melt spun alloys.” *Mater. Charact.*, 57(3), 154–159.
- Lee, J. S. S., and Wayman, C. M. M. (1986a). “Grain refinement of Cu-Zn-Al shape memory alloys.” *Metallography*, 19(4), 401–419.
- Lee, J. S., and Wayman, C. M. (1986b). “Grain Refinement of a Cu-Al-Ni Shape Memory Alloy by Ti and Zr Additions.” *Trans. Japan Inst. Met.*, 27(8), 584–591.
- Leu, S. S., and Hu, C. T. (1991). “The aging effect on Cu–Zn–Al shape memory alloys with low contents of aluminum.” *Metall. Trans. A*, 22(1), 25–33.
- Lexcellent, C. (2013). *Shape-memory Alloys Handbook*. London, UK: ISTE Ltd.
- Li, H., and Huo, L. (2010). “Advances in Structural Control in Civil Engineering in China.” *Math. Probl. Eng.*, 2010, 1–23.
- Li, J., and Ansell, G. S. (1983). “The effect of thermal cycling on the thermoelastic martensitic transformation in a Cu-Zn-Al alloy.” *Metall. Trans. A*, 14(7), 1293–1297.
- Li, M., Xiao, S., Xiao, L., Xu, L., Tian, J., and Chen, Y. (2017). “Effects of carbon and boron addition on microstructure and mechanical properties of TiAl alloys.” *J. Alloys Compd.*, 728, 206–221.
- Li, W., Pan, Q., Xiao, Y., He, Y., and Liu, X. (2011). “Microstructure and mechanical properties of Al-Zn-Cu-Mg-Sc-Zr alloy after retrogression and re-aging treatments.” *J. Cent. South Univ.*, 18, 279–284.
- Li, Y., Li, J., Li, W., and Samali, B. (2013). “Development and characterization of a magnetorheological elastomer based adaptive seismic isolator.” *Smart Mater. Struct.*, 22(3), 035005.
- Liang, G., Tang, Z., Fang, H., Katz, D., and Salama, K. (2006). “Synthesis and X-ray diffraction pattern for MgCu₂.” *J. Alloys Compd.*, 422(1–2), 73–77.
- Liao, G., Gong, X., and Xuan, S. (2014). “Phase based stiffness tuning algorithm for a magnetorheological elastomer dynamic vibration absorber.” *Smart Mater. Struct.*, 23(1).

- Liao, G. J., Gong, X. L., Kang, C. J., and Xuan, S. H. (2011). "The design of an active-adaptive tuned vibration absorber based on magnetorheological elastomer and its vibration attenuation performance." *Smart Mater. Struct.*, 20(7), 075015.
- Limmaneevichitr, C., and Eidhed, W. (2003). "Fading mechanism of grain refinement of aluminum-silicon alloy with Al-Ti-B grain refiners." *Mater. Sci. Eng. A*, 349, 197–206.
- Liu, F., Li, Y., Li, Y., and Xu, H. (2006). "A study on TiNi(Fe,Mo) shape memory alloy." *Mater. Sci. Eng. A*, 438–440(SPEC. ISS.), 896–899.
- Liu, J. L., Huang, H. Y., and Xie, J. X. (2014). "The roles of grain orientation and grain boundary characteristics in the enhanced superelasticity of Cu_{71.8}Al_{17.8}Mn_{10.4} shape memory alloys." *Mater. Des.*, 64, 427–433.
- Lojen, G., Anžel, I., Kneissl, A., Križman, A., Unterweger, E., Kosec, B., and Bizjak, M. (2005). "Microstructure of rapidly solidified Cu–Al–Ni shape memory alloy ribbons." *J. Mater. Process. Technol.*, 162–163(SPEC. ISS.), 220–229.
- López-Ferreño, I., Gómez-Cortés, J. F., Breczewski, T., Ruiz-Larrea, I., Nó, M. L., and San Juan, J. M. (2020). "High-temperature shape memory alloys based on the Cu-Al-Ni system: Design and thermomechanical characterization." *J. Mater. Res. Technol.*, 9(5), 9972–9984.
- Lopez Del Castillo, C., Hernaez, J., and Mellor, B. G. (1986). "The effect of thermal and stress cycling on thermoelastic martensite formation in Cu-Al-Mn alloys." *J. Mater. Sci.*, 21, 4043–4047.
- López Del Castillo, C., Mellor, B. G., Blázquez, M. L., and Gómez, C. (1987). "The influence of composition and grain size on the martensitic transformation temperatures of Cu-Al-Mn shape memory alloys." *Scr. Metall.*, 21(12), 1711–1716.
- Lozovoi, A. Y., and Paxton, A. T. (2008). "Boron in copper: A perfect misfit in the bulk and cohesion enhancer at a grain boundary." *Phys. Rev. B*, 77(16), 1–14.
- Lu, L., Lai, M. O., and Lim, A. S. (1996). "Mechanical fatigue of Cu-based shape memory alloy after different heat treatment." *Scr. Mater.*, 34(1), 157–162.

- Lu, L. Y., Lin, C. C., Lin, G. L., and Lin, C. Y. (2010). “Experiment and analysis of a fuzzy-controlled piezoelectric seismic isolation system.” *J. Sound Vib.*, 329(11), 1992–2014.
- Lu, X., Chen, F., Li, W., and Zheng, Y. (2009). “Effect of Ce addition on the microstructure and damping properties of Cu–Al–Mn shape memory alloys.” *J. Alloys Compd.*, 480(2), 608–611.
- Malimánek, J., and Zárubová, N. (1995). “Calorimetric investigation of the movement of phase interfaces in a Cu–Al–Ni single crystal.” *Scr. Metall. Mater.*, 32(9), 1347–1352.
- Mallik, U. S., and Sampath, V. (2008). “Effect of composition and ageing on damping characteristics of Cu–Al–Mn shape memory alloys.” *Mater. Sci. Eng. A*, 478(1–2), 48–55.
- Mallik, U. S., and Sampath, V. (2009). “Influence of quaternary alloying additions on transformation temperatures and shape memory properties of Cu–Al–Mn shape memory alloy.” *J. Alloys Compd.*, 469(1–2), 156–163.
- Mallik, U. S., and Sampath, V. (2015). “Effect of Grain Refinement on Shape Memory Properties of Cu–Al–Mn SMAs.” *Adv. Mater. Res.*, 1101, 104–107.
- Mañosa, L., Jurado, M., González-Comas, A., Obradó, E., Planes, A., Zarestky, J., Stassis, C., Romero, R., Somoza, A., and Morin, M. (1998). “A comparative study of the post-quench behaviour of Cu–Al–Be and Cu–Zn–Al shape memory alloys.” *Acta Mater.*, 46(3), 1045–1053.
- Marupalli, B. C. G., Behera, A., and Aich, S. (2021). “A Critical Review on Nickel–Titanium Thin-Film Shape Memory Alloy Fabricated by Magnetron Sputtering and Influence of Process Parameters.” *Trans. Indian Inst. Met.*, 74(10), 2521–2540.
- Matsuoka, S., Hasebe, M., Oshima, R., and Fujita, F. E. (1983). “Improvement of Ductility of Melt Spun Cu–Al–Ni Shape Memory Alloy Ribbons by Addition of Ti or Zr.” *Jpn. J. Appl. Phys.*, 22(Part 2, No. 8), L528–L530.
- Matsushita, K., Okamoto, T., and Okamoto, T. (1985). “Effects of manganese and ageing on martensitic transformation of Cu–Al–Mn alloys.” *J. Mater. Sci.*, 20(2), 689–

699.

Mehrpouya, M., and Bidsorkhi, H. C. (2017). “MEMS Applications of NiTi Based Shape Memory Alloys: A Review.” *Micro Nanosyst.*, 8(2), 79–91.

Melo, T. A. A., Oliveira, D. F. De, Lima, S. J. G., Buono, V. T. L., and Gomes, R. M. (2009a). “Nb Modified Cu-Al-Be Shape Memory Alloys.” *Int. Conf. Martensitic Transform.*, John Wiley & Sons, Inc., 591-594.

Melo, T. A. A., Oliveira, D. F. De, Lima, S. J. G., Buono, V. T. L., and Gomes, R. M. (2009b). “Nb Modified Cu-Al-Be Shape Memory Alloys.” *ICOMAT*, Hoboken, NJ, USA: John Wiley & Sons, Inc., 591–594.

Melton, K. N., and Mercier, O. (1979). “The Effect of the Martensitic Phase Transformation on the Low Cycle Fatigue Behaviour of Polycrystalline Ni-Ti and Cu-Zn-Al Alloys.” *Mater. Sci. Eng.*, 40, 81–87.

Miki, M., Maeshiro, N., and Ogino, Y. (1989). “Effects of Additional Elements on the Superplasticity of a Cu-14Al-3Ni Shape Memory Alloy.” *Mater. Trans. JIM*, 30(12), 999–1008.

Miura, S. (2002). “Shape-memory and superelasticity in CuZnSn alloy and its application.” *Mater. Sci. Forum*, 394–395, 399–402.

Miyazaki, S., Kawai, T., and Otsuka, K. (1982). “On the origin of intergranular fracture in β phase shape memory alloys.” *Scr. Metall.*, 16(4), 431–436.

Miyazaki, S., Otsuka, K., and Sakamoto, H. (1981). “The Fracture of Cu-Al-Ni Shape Memory Alloy.” *Trans. Japan Inst. Met.*, 22(4), 244–252.

Mo, J. P. T., Cheung, S. C. P., and Das, R. (2019). “Mechanical Vibration.” *Demystifying Numer. Model.*, Elsevier, 209–233.

Moghaddam, A. O., Ketabchi, M., and Afrasiabi, Y. (2014). “Accumulative Roll Bonding and Post-Deformation Annealing of Cu-Al-Mn Shape Memory Alloy.” *J. Mater. Eng. Perform.*, 23(12), 4429–4435.

Moghaddam, A. O., Mazinani, A., and Ketabchi, M. (2017). “Effect of Accumulative Roll Bonding and Equal Channel Angular Rolling on Microstructural and Mechanical

Properties of Cu–Al–Mn Shape Memory Alloys.” *Trans. Indian Inst. Met.*, 70(7), 1901–1909.

Mohanty, S., Gruzleski, J. E., Mohanty, P. S., and Gruzleski, J. E. (1995). “Mechanism of grain refinement in aluminium.” *Acta Metall. Mater.*, 43(5), 2001–2012.

Montecinos, S. (2015). “Influence of microstructural parameters on damping capacity in CuAlBe shape memory alloys.” *Mater. Des.*, 68, 215–220.

Montecinos, S., and Cuniberti, A. (2008). “Thermomechanical behavior of a CuAlBe shape memory alloy.” *J. Alloys Compd.*, 457(1–2), 332–336.

Montecinos, S., and Cuniberti, A. (2012). “Martensitic transformation and grain size in a Cu–Al–Be alloy.” *Procedia Mater. Sci.*, 149–155.

Montecinos, S., Cuniberti, A., and Castro, M. L. (2010). “Kinetics of isothermal decomposition in polycrystalline β CuAlBe alloys.” *Intermetallics*, 18(1), 36–41.

Montecinos, S., Cuniberti, A., Castro, M. L., and Boeri, R. (2009). “Phase transformations during continuous cooling of polycrystalline β -CuAlBe alloys.” *J. Alloys Compd.*, 467(1–2), 278–283.

Montecinos, S., Cuniberti, A., and Romero, R. (2011). “Effect of grain size on the stress–temperature relationship in a β CuAlBe shape memory alloy.” *Intermetallics*, 19, 35–38.

Montecinos, S., Cuniberti, A., and Sepúlveda, A. (2008). “Grain size and pseudoelastic behaviour of a Cu–Al–Be alloy.” *Mater. Charact.*, 59(2), 117–123.

Montecinos, S., Moroni, M. O., and Sepúlveda, A. (2006). “Superelastic behavior and damping capacity of CuAlBe alloys.” *Mater. Sci. Eng. A*, 419(1–2), 91–97.

Moon, S.-J., Lim, C.-W., Kim, B.-H., and Park, Y. (2007). “Structural vibration control using linear magnetostrictive actuators.” *J. Sound Vib.*, 302(4–5), 875–891.

Morawiec, H., Bojarski, Z., Lelatko, J., and Joszt, K. (1990). “Grain Refinement of Cu–Zn–Al Shape Memory Alloys.” *Int. J. Mater. Res.*, 81(6), 419–423.

Moreau, F., Tidu, A., Barbe, P., Eberhardt, A., and Heizmann, J. J. (1995). “Study of

CuAlBe Shape Memory Alloy by X-Ray Diffraction.” *Le J. Phys. IV*, 05(C2), C2-269-C2-274.

Morris, M. A. (1991). “Influence of boron additions on ductility and microstructure of shape memory Cu-Al-Ni alloys.” *Scr. Metall. Mater.*, 25(11), 2541–2546.

Morris, M. A. (1992). “High temperature properties of ductile Cu-Al-Ni shape memory alloys with boron additions.” *Acta Metall. Mater.*, 40(7), 1573–1586.

Murray, J. L. (1985). “The aluminium-copper system.” *Int. Met. Rev.*, 30(1), 211–234.

Nagasawa, A., and Kawachi, K. (1971). “Memory Effect in Cu-Al Alloy.” *J. Phys. Soc. Japan*, 30(1), 296.

Najah Saud Al-Humairi, S. (2020). “Cu-Based Shape Memory Alloys: Modified Structures and Their Related Properties.” *Recent Adv. Metall. Eng. Electrodepos.*, U. B. Al-Naib, D. Vikraman, and K. Karuppasamy, eds., London, UK: IntechOpen.

Nakahata, T. (2011). “Industrial processing of titanium–nickel (Ti–Ni) shape memory alloys (SMAs) to achieve key properties.” *Shape Mem. Superelastic Alloy.*, Elsevier, 53–62.

Narasimha, G. B. (2020). “An Experimental Investigation on Properties of Cu-Al-Be-X Shape Memory Alloys for Smart Structure Applications.” National Institute of Technology Karnataka, Surathkal.

Nespoli, A., Besseghini, S., Pittaccio, S., Villa, E., and Viscuso, S. (2010). “The high potential of shape memory alloys in developing miniature mechanical devices: A review on shape memory alloy mini-actuators.” *Sensors Actuators A Phys.*, 158(1), 149–160.

Nickel, O. (1957). “No Title.” *Z.metall.*

Niitsu, K., Omori, T., and Kainuma, R. (2011). “Superelasticity at Low Temperatures in Cu-17Al-15Mn (at%) Shape Memory Alloy.” *Mater. Trans.*, 52(8), 1713–1715.

Nishiyama, Z. (1978). *Martensitic Transformation*. (Morris E. Fine, M. Meshii, C. M. Wayman, and Departmen, eds.), New York: Academic Press.

- Nishiyama, Z., and Kajiwara, S. (1963). "Electron Microscope Study of the Crystal Structure of the Martensite in a Copper-Aluminium Alloy." *Jpn. J. Appl. Phys.*, 2(8), 478–486.
- Nnamchi, P., Younes, A., and González, S. (2019). "A review on shape memory metallic alloys and their critical stress for twinning." *Intermetallics*, 105, 61–78.
- Oishi, K., and Brown, L. C. (1971). "Stress-induced martensite formation in Cu–Al–Ni alloys." *Metall. Trans.*, 2(7), 1971–1977.
- Ölander, A. (1932). "Cadmium-Gold Alloys Solid." *J. Am. Chem. Soc.*, 54(10), 3819–3833.
- Oliveira Ramos, A. D. de, Araújo, C. J. de, Oliveira, H. M. R. de, Macêdo, G. A., and Lima, A. G. B. de. (2018). "An experimental investigation of the superelastic fatigue of NiTi SMA wires." *J. Brazilian Soc. Mech. Sci. Eng.*, 40(4), 206.
- Otsuka, K., Nakai, K., and Shimizu, K. (1974). "Structure dependence of superelasticity in Cu-Al-Ni Alloy." *Scr. Metall.*, 8(8), 913–918.
- Otsuka, K., Sakamoto, H., and Shimizu, K. (1979). "Successive stress-induced martensitic transformations and associated transformation pseudoelasticity in Cu-Al-Ni alloys." *Acta Metall.*, 27(4), 585–601.
- Otsuka, K., and Shimizu, K. (1969). "Morphology and Crystallography of Thermoelastic γ' Cu-Al-Ni Martensite." *Jpn. J. Appl. Phys.*, 8(10), 1196–1204.
- Otsuka, K., and Shimizu, K. (1970). "Memory effect and thermoelastic martensite transformation in Cu-Al-Ni alloy." *Scr. Metall.*, 4(6), 469–472.
- Otsuka, K., Wayman, C. ., Nakai, K., Sakamoto, H., and Shimizu, K. (1976). "Superelasticity effects and stress-induced martensitic transformations in Cu-Al-Ni alloys." *Acta Metall.*, 24(3), 207–226.
- Ozbulut, O. E., and Hurlbaeus, S. (2010). "Fuzzy control of piezoelectric friction dampers for seismic protection of smart base isolated buildings." *Bull. Earthq. Eng.*, 8(6), 1435–1455.
- Ozbulut, O. E., Hurlbaeus, S., and Desroches, R. (2011). "Seismic response control

using shape memory alloys: A review.” *J. Intell. Mater. Syst. Struct.*, 22(14), 1531–1549.

Özkul, İ., Kurgun, M. A., Kalay, E., Canbay, C. A., and Aldaş, K. (2019). “Shape memory alloys phenomena: classification of the shape memory alloys production techniques and application fields.” *Eur. Phys. J. Plus*, 134(12).

Parulekar, Y. M., and Reddy, G. R. (2009). “Passive response control systems for seismic response reduction: A state-of-the-art review.” *Int. J. Struct. Stab. Dyn.*, 09(01), 151–177.

Pastia, C., Luca, S.-G., Chira, F., and Roşca, V.-O. (2005). “Structural control systems implemented in civil engineering.” *Bull. Polytech. Inst. Jassy, Constr. Archit. Sect.*, 76–80(1–2), 41–49.

Payandeh, Y., Mirzakhani, B., Bakhtiari, Z., and Hautcoeur, A. (2021). “Precipitation and martensitic transformation in polycrystalline CuAlNi shape memory alloy – Effect of short heat treatment.” *J. Alloys Compd.*, 891, 162046.

Pérez-Landazábal, J. I., Recarte, V., Sánchez-Alarcos, V., Nó, M. L., and Juan, J. S. (2006). “Study of the stability and decomposition process of the β phase in Cu–Al–Ni shape memory alloys.” *Mater. Sci. Eng. A*, 438–440, 734–737.

Perkins, J. (1974). “Substructure of Cu-Zn-Al martensite.” *Metallography*, 7(4), 345–356.

Perkins, J., and Muesing, W. E. (1983). “Martensitic Transformation Cycling Effects in Cu-Zn-Al Shape Memory Alloys.” *Metall. Trans. A*, 14A(M), 33–36.

Perkins, J., and Sponholz, R. O. (1984). “Stress-Induced Martensitic Transformation Cycling and Two-Way Shape Memory Training in Cu-Zn-Al Alloys.” *Metall. Trans. A*, 15(2), 313–321.

Pilz, C. B., Matsumura, E. L., Paganotti, A., Cornejo, D. R., and Silva, R. A. G. (2020). “Microstructure and phase stability of CuAlMnAgZr multicomponent alloys.” *Mater. Chem. Phys.*, 241(October 2019), 122343.

Pops, H., and Ridley, N. (1970). “Influence of aluminum on the martensitic

transformation of beta phase CuZn alloys.” *Metall. Trans.*, 1(9), 2653–2655.

Prashantha, S., Mallikarjun, U. S., and Shashidhara, S. M. (2014). “Effect of Ageing on Shape Memory Effect and Transformation Temperature on Cu-Al-Be Shape Memory Alloy.” *Procedia Mater. Sci.*, 5, 567–574.

Prawdizg, T. J., Zurey, F. T., and Mack, D. J. (1966). “An investigation of the mechanical properties and microstructures of heat treated aluminium bronzes.” *Second Annu. Rep. to Incra*.

Qian, H., Li, H., and Song, G. (2016). “Experimental investigations of building structure with a superelastic shape memory alloy friction damper subject to seismic loads.” *Smart Mater. Struct.*, 25(12), 125026.

Rachinger, W. A. (1958). “A ‘super-elastic’ single crystal calibration bar.” *Br. J. Appl. Phys.*, 9(6), 250–252.

Rapacioli, R., and Ahlers, M. (1977). “Ordering in ternary β phase Cu Zn Al alloys.” *Scr. Metall.*, 11(12), 1147–1150.

Rapacioli, R., and Ahlers, M. (1979). “The influence of short-range disorder on the martensitic transformation in Cu-Zn and Cu-Zn-Al alloys.” *Acta Metall.*, 27(5), 777–784.

Razali, M. F., and Mahmud, A. S. (2015). “Gradient deformation behavior of NiTi alloy by ageing treatment.” *J. Alloys Compd.*, 618, 182–186.

Recarte, V., Pérez-Landazábal, J. ., Rodríguez, P. ., Bocanegra, E. ., Nó, M. ., and San Juan, J. (2004). “Thermodynamics of thermally induced martensitic transformations in Cu–Al–Ni shape memory alloys.” *Acta Mater.*, 52(13), 3941–3948.

Recarte, V., Pérez-Sáez, R. ., Bocanegra, E. ., Nó, M. ., and San Juan, J. (1999). “Dependence of the martensitic transformation characteristics on concentration in Cu–Al–Ni shape memory alloys.” *Mater. Sci. Eng. A*, 273–275, 380–384.

Recarte, V., Pérez-Sáez, R. B., San Juan, J., Bocanegra, E. H., and Nó, M. L. (2002). “Influence of Al and Ni concentration on the Martensitic transformation in Cu-Al-Ni shape-memory alloys.” *Metall. Mater. Trans. A*, 33(8), 2581–2591.

- Reynolds, J. E., and Bever, M. B. (1952). “On the Reversal of the Strain-Induced Martensitic Transformation in the Copper-Zinc System.” *JOM*, 4(10), 1065–1066.
- Rios-Jara, D., Belkahlá, S., Canales, A., Flores, H., and Guénin, G. (1991a). “Elastic constants measurements of β Cu-Al-Be alloys.” *Scr. Metall. Mater.*, 25(6), 1351–1355.
- Rios-Jara, D., Planes, A., Mañosa, L., Ortin, J., Belkahla, S., Morin, M., Guénin, G., and Macqueron, J. L. (1991b). “Martensitic transition entropy change and elastic constants of Cu-Al-Be alloys.” *Le J. Phys. IV*, 01(C4), C4-283-C5-288.
- Roca, P. La, Isola, L., Vermaut, P., and Malarría, J. (2017). “Relationship between grain size and thermal hysteresis of martensitic transformations in Cu-based shape memory alloys.” *Scr. Mater.*, 135, 5–9.
- Rodriguez, P. L., Condo, A. M., and Lovey, F. C. (1996). “Quantitative Analysis of Dislocations in Relation with the Martensitic Transformation in Cu-Zn-Al Alloys.” *Phys. status solidi b*, 197, 279–292.
- Rogueda, C., Vacher, P., Lexcelent, C., Contardo, L., and Guénin, G. (1991). “Pseudoelastic behaviour and two way memory effect in Cu-Zn-Al alloys.” *J. Phys. IV Proceedings, EDP Sci.*, 01(C4), C4-409-C4-414.
- Roh, D. W., Kim, J. W., Cho, T. J., and Kim, Y. G. (1991). “Tensile properties and microstructure of microalloyed Cu-Al-Ni-X shape memory alloys.” *Mater. Sci. Eng. A*, 136(C), 17–23.
- Saadat, S., Salichs, J., Noori, M., Hou, Z., Davoodi, H., Bar-on, I., Suzuki, Y., and Masuda, A. (2002). “An overview of vibration and seismic applications of NiTi shape memory alloy.” *Smart Mater. Struct.*, 11(2), 218–229.
- Sabahi, N., Chen, W., Wang, C.-H., Kruzic, J. J., and Li, X. (2020). “A Review on Additive Manufacturing of Shape-Memory Materials for Biomedical Applications.” *JOM*, 72(3), 1229–1253.
- Saburi, T., and Nenno, S. (1974). “Reversible shape memory in Cu-Zn-Ga.” *Scr. Metall.*, 8(12), 1363–1367.
- Sade, M., Castro Bubani, F. de, Lovey, F. C., and Torra, V. (2014). “Effect of grain

size on stress induced martensitic transformations in a Cu–Al–Be polycrystalline shape-memory alloy. Pseudoelastic cycling effects and microstructural modifications.” *Mater. Sci. Eng. A*, 609, 300–309.

Sade, M., Pelegrina, J. L., Yawny, A., and Lovey, F. C. (2015). “Diffusive phenomena and pseudoelasticity in Cu–Al–Be single crystals.” *J. Alloys Compd.*, 622, 309–317.

Sakamoto, H., Nakai, Y., and Shimizu, K. (1987). “Optimization of Composition for the Appearance of Pseudoelasticity due to Consecutive $\beta_1 \rightleftharpoons \beta_1' \rightleftharpoons \alpha_1'$ Transformations in Cu–Al–Ni Alloy Single Crystals.” *Trans. Japan Inst. Met.*, 28(10), 765–772.

Sampath, V. (2005). “Studies on the effect of grain refinement and thermal processing on shape memory characteristics of Cu–Al–Ni alloys.” *Smart Mater. Struct.*, 14(5), S253–S260.

Sampath, V. (2006). “Improvement of Shape-Memory Characteristics and Mechanical Properties of Copper–Zinc–Aluminum Shape-Memory Alloy with Low Aluminum Content by Grain Refinement.” *Mater. Manuf. Process.*, 21(8), 789–795.

Sampath, V., and Mallik, U. S. (2009). “Influence of minor additions of boron and zirconium on shape memory properties and grain refinement of a Cu–Al–Mn shape memory alloy.” *ESOMAT 2009 - 8th Eur. Symp. Martensitic Transform.*, Les Ulis, France: EDP Sciences, 1–7.

San Juan, J., Nó, M. L., and Schuh, C. A. (2012). “Superelastic cycling of Cu–Al–Ni shape memory alloy micropillars.” *Acta Mater.*, 60(10), 4093–4106.

Santiago, J. J. de M., Alcântara, C. C. de, Costa, E. de S., and Brito, I. C. A. (2019). “Evaluation of Nb–Ni Influence on the Mechanical Behavior in a Cu–Al–Be Shape Memory Alloy.” *Curr. J. Appl. Sci. Technol.*, 32(4), 1–8.

Sarı, U., and Aksoy, İ. (2006). “Electron microscopy study of 2H and 18R martensites in Cu–11.92wt% Al–3.78wt% Ni shape memory alloy.” *J. Alloys Compd.*, 417(1–2), 138–142.

Sarı, U., and Kırındı, T. (2008). “Effects of deformation on microstructure and mechanical properties of a Cu–Al–Ni shape memory alloy.” *Mater. Charact.*, 59(7),

920–929.

Sarma, B., Ray, K. K., and Balasubramanian, V. (1972). “On the shape memory effect in a Cu-Al-Ni alloy.” *Scr. Metall.*, 6(9), 869–874.

Sathish, S., Mallik, U. S., and Raju, T. N. (2014). “Microstructure and Shape Memory Effect of Cu-Zn-Ni Shape Memory Alloys.” *J. Miner. Mater. Charact. Eng.*, 02(02), 71–77.

Saud, S. N., Abu Bakar, T. A., Hamzah, E., Ibrahim, M. K., and Bahador, A. (2015a). “Effect of Quarterly Element Addition of Cobalt on Phase Transformation Characteristics of Cu-Al-Ni Shape Memory Alloys.” *Metall. Mater. Trans. A*, 46(8), 3528–3542.

Saud, S. N., Hamzah, E., Abubakar, T., and Bakhsheshi-Rad, H. R. (2015b). “Thermal aging behavior in Cu–Al–Ni–xCo shape memory alloys.” *J. Therm. Anal. Calorim.*, 119(2), 1273–1284.

Saud, S. N., Hamzah, E., Abubakar, T., Ibrahim, M. K., and Bahador, A. (2015c). “Effect of a fourth alloying element on the microstructure and mechanical properties of Cu–Al–Ni shape memory alloys.” *J. Mater. Res.*, 30(14), 2258–2269.

Saud, S. N., Hamzah, E., Abubakar, T., Zamri, M., and Tanemura, M. (2014). “Influence of Ti additions on the martensitic phase transformation and mechanical properties of Cu–Al–Ni shape memory alloys.” *J. Therm. Anal. Calorim.*, 118(1), 111–122.

Schroeder, T. A., Cornelis, I., and Wayman, C. M. (1976). “The shape memory effect and pseudoelasticity in polycrystalline Cu-Zn alloys.” *Metall. Trans. A*, 7(4), 535–553.

Sedlák, P., Seiner, H., Landa, M., Novák, V., Šittner, P., and Mañosa, L. (2005). “Elastic constants of bcc austenite and 2H orthorhombic martensite in CuAlNi shape memory alloy.” *Acta Mater.*, 53(13), 3643–3661.

Shafeeq, M. M., Gupta, G. K., Malik, M. M., Sampath, V., and Modi, O. P. (2016). “Influence of quenching methods on martensitic transformation and mechanical properties of P/M processed Cu–Al–Ni–Ti shape memory alloys.” *Powder Metall.*,

59(4), 271–280.

Shahmir, H., Nili-Ahmadabadi, M., and Naghdi, F. (2011). “Superelastic behavior of aged and thermomechanical treated NiTi alloy at Af+10°C.” *Mater. Des.*, 32(1), 365–370.

Sharabash, A. M., and Andrawes, B. O. (2009). “Application of shape memory alloy dampers in the seismic control of cable-stayed bridges.” *Eng. Struct.*, 31(2), 607–616.

Shiba, K., Mase, S., Yabe, Y., and Tamura, K. (1998). “Active/passive vibration control systems for tall buildings.” *Smart Mater. Struct.*, 7(5), 588–598.

Shimizu, K., Sakamoto, H., and Otsuka, K. (1978). “Phase diagram associated with stress-induced martensitic transformations in a Cu-Al-Ni alloy.” *Scr. Metall.*, 12(9), 771–776.

Shimoga, G., Kim, T.-H., and Kim, S.-Y. (2021). “An Intermetallic NiTi-Based Shape Memory Coil Spring for Actuator Technologies.” *Metals (Basel)*, 11(8), 1212.

Singh, S. ., Murakami, Y., and Delaey, L. (1978). “Remarks on ordering in ternary β -Cu-Zn-Al alloys.” *Scr. Metall.*, 12(5), 435–438.

Siredey-Schwaller, N., Eberhardt, A., and Bastie, P. (2009). “Parameters influencing the fatigue life of a Cu–Al–Be single-crystal shape memory alloy under repeated bending.” *Smart Mater. Struct.*, 18(2), 025014.

Song, G., Ma, N., and Li, H.-N. (2006). “Applications of shape memory alloys in civil structures.” *Eng. Struct.*, 28(9), 1266–1274.

Spear, K. E. (1976). “Chemical bonding in AlB₂-type borides.” *J. Less Common Met.*, 47, 195–201.

Spencer, B. F., and Nagarajaiah, S. (2003). “State of the Art of Structural Control.” *J. Struct. Eng.*, 129(7), 845–856.

Stipcich, M., and Romero, R. (2017). “ β -Phase thermal degradation in Zr-added Cu–Zn–Al shape memory alloy.” *J. Therm. Anal. Calorim.*, 129(1), 201–207.

Stoeckel, D. (1990). “Shape memory actuators for automotive applications.” *Mater.*

Des., 11(6), 302–307.

Stoeckel, D. (1995). “The Shape Memory Effect - Phenomenon, Alloys, and Applications.” *Shape Mem. Alloy. Power Syst. EPRI*, 1–13.

Sun, K., Yi, X., Sun, B., Gao, W., Wang, H., Meng, X., Cai, W., and Zhao, L. (2019). “The effect of Hf on the microstructure, transformation behaviors and the mechanical properties of Ti-Ni-Cu shape memory alloys.” *J. Alloys Compd.*, 772, 603–611.

Sure, G. N., and Brown, L. C. (1984). “The Mechanical Properties of Grain Refined β -CuAlNi Strain-Memory Alloys.” *Metall. Trans. A*, 15(8), 1613–1621.

Suresh, M., Srinivasan, A., Ravi, K. R., Pillai, U. T. S., and Pai, B. C. (2009). “Influence of boron addition on the grain refinement and mechanical properties of AZ91 Mg alloy.” *Mater. Sci. Eng. A*, 525(1–2), 207–210.

Suresh, N., and Ramamurty, U. (2007). “Effect of aging on mechanical behavior of single crystal Cu–Al–Ni shape memory alloys.” *Mater. Sci. Eng. A*, 454–455, 492–499.

Suresh, N., and Ramamurty, U. (2008). “Aging response and its effect on the functional properties of Cu–Al–Ni shape memory alloys.” *J. Alloys Compd.*, 449(1–2), 113–118.

Sutou, Y., Kainuma, R., and Ishida, K. (1999). “Effect of alloying elements on the shape memory properties of ductile Cu–Al–Mn alloys.” *Mater. Sci. Eng. A*, 273–275, 375–379.

Sutou, Y., Koeda, N., Omori, T., Kainuma, R., and Ishida, K. (2009). “Effects of aging on stress-induced martensitic transformation in ductile Cu-Al-Mn-based shape memory alloys.” *Acta Mater.*, 57(19), 5759–5770.

Sutou, Y., Omori, T., Kainuma, R., and Ishida, K. (2008). “Ductile Cu–Al–Mn Based Shape Memory Alloys: General Properties and Applications.” *Mater. Sci. Technol.*, 24(8), 896–901.

Sutou, Y., Omori, T., Kainuma, R., and Ishida, K. (2013). “Grain size dependence of pseudoelasticity in polycrystalline Cu-Al-Mn-based shape memory sheets.” *Acta Mater.*, 61(10), 3842–3850.

Sutou, Y., Omori, T., Kainuma, R., Ishida, K., and Ono, N. (2002). “Enhancement of

superelasticity in Cu-Al-Mn-Ni shape-memory alloys by texture control.” *Metall. Mater. Trans. A*, 33(9), 2817–2824.

Sutou, Y., Omori, T., Okamoto, T., Kainuma, R., and Ishida, K. (2001). “Effect of grain refinement on the mechanical and shape memory properties of Cu-Al-Mn base alloys.” *Le J. Phys. IV*, 11(PR8), Pr8-185-Pr8-190.

Sutou, Y., Omori, T., Wang, J. J., Kainuma, R., and Ishida, K. (2004). “Characteristics of Cu–Al–Mn-based shape memory alloys and their applications.” *Mater. Sci. Eng. A*, 378(1–2), 278–282.

Sutou, Y., Omori, T., Yamauchi, K., Ono, N., Kainuma, R., and Ishida, K. (2005). “Effect of grain size and texture on pseudoelasticity in Cu – Al – Mn-based shape memory wire.” *Acta Mater.*, 53, 4121–4133.

Suzuki, Y., and Kagawa, Y. (2010). “Active vibration control of a flexible cantilever beam using shape memory alloy actuators.” *Smart Mater. Struct.*, 19(8), 085014.

Suzuki, Y., Xu, Y., Morito, S., Otsuka, K., and Mitose, K. (1998). “Effects of boron addition on microstructure and mechanical properties of Ti–Td–Ni high-temperature shape memory alloys.” *Mater. Lett.*, 36(1–4), 85–94.

Svirid, A. E., Pushin, V. G., Kuranova, N. N., Luk’yanov, A. V., Pushin, A., N.Uksusnikov, A., and M. Ustyugov, Y. (2017). “The structure–phase transformations and mechanical properties of the shape memory effect alloys based on the system Cu–Al–Ni.” *Mater. Today Proc.*, 4(3), 4758–4762.

Swann, P. R., and Warlimont, H. (1963). “The electron-metallography and crystallography of copper-aluminum martensites.” *Acta Metall.*, 11(6), 511–527.

Symans, M. D., and Constantinou, M. C. (1999). “Semi-active control systems for seismic protection of structures: a state-of-the-art review.” *Eng. Struct.*, 21(6), 469–487.

Tadaki, T. (1998). “Cu-based shape memory alloys.” *Shape Mem. Mater.*, K. Otsuka and C. M. Wayman, eds., Cambridge: Cambridge University Press, 97–116.

Tai, N. T., and Ahn, K. K. (2011). “Adaptive proportional–integral–derivative tuning

sliding mode control for a shape memory alloy actuator.” *Smart Mater. Struct.*, 20(5), 055010.

Tamirisakandala, S., Bhat, R. B., Tiley, J. S., and Miracle, D. B. (2005). “Grain refinement of cast titanium alloys via trace boron addition.” *Scr. Mater.*, 53(12), 1421–1426.

Tang, W., Sundman, B., Sandström, R., and Qiu, C. (1999). “New modelling of the B2 phase and its associated martensitic transformation in the Ti-Ni system.” *Acta Mater.*, 47(12), 3457–3468.

Tatar, C., and Kurt, M. (2020). “Phase transformation temperatures and physical characteristics of NiTiCo shape memory alloys produced by arc melting method.” *Eur. Phys. J. Plus*, 135(9), 765.

Teixeira, C. A., Conrado, L. C., and Mendonça, E. S. (2015). “INFLUENCE OF CHROMIUM IN THE PHASE TRANSFORMATION TEMPERATURE OF A CUALNI SHAPE MEMORY ALLOY.”

Torra, V., Isalgue, A., Auguet, C., Carreras, G., Lovey, F. C., and Terriault, P. (2013). “Damping in civil engineering using SMA Part 2 – particular properties of NiTi for damping of stayed cables in bridges.” *Can. Metall. Q.*, 52(1), 81–89.

Torra, V., Isalgue, A., Lovey, F. C., and Sade, M. (2015). “Shape memory alloys as an effective tool to damp oscillations.” *J. Therm. Anal. Calorim.*, 119(3), 1475–1533.

Torra, V., and Tachoire, H. (1992). “Martensitic transformations in shape-memory alloys. Successes and failures of thermal analysis and calorimetry.” *Thermochim. Acta*, 203, 419–444.

Treadway, J., Abolmaali, A., Lu, F., and Aswath, P. (2015). “Tensile and fatigue behavior of superelastic shape memory rods.” *Mater. Des.*, 86, 105–113.

Vishal, P., Kaliperumal, D., and Padhi, R. (2018). “Active Vibration Suppression of Nonlinear Cantilever Beam using Shape Memory Alloy Actuators.” *IFAC-PapersOnLine*, 51(1), 130–135.

Wang, F., Liu, Z.-L., Qiu, D., Taylor, J. A., Easton, M. A., and Zhang, M.-X. (2015).

“The Influence of the Effect of Solute on the Thermodynamic Driving Force on Grain Refinement of Al Alloys.” *Metall. Mater. Trans. A*, 46(1), 505–515.

Wang, J., Moumni, Z., and Zhang, W. (2017). “A thermomechanically coupled finite-strain constitutive model for cyclic pseudoelasticity of polycrystalline shape memory alloys.” *Int. J. Plast.*, 97, 194–221.

Wang, T., Chen, Z., Fu, H., Xu, J., Fu, Y., and Li, T. (2011). “Grain refining potency of Al-B master alloy on pure aluminum.” *Scr. Mater.*, 64, 1121–1124.

Wayman, C. M. (1983). “Thermoelastic Martensitic Transformations and the Nature of the Shape Memory Effect.” *MRS Online Proc. Libr.*, 21(1), 657–667.

Wayman, C. M., and Shimizu, K. (1972). “The Shape Memory (‘Marmem’) Effect in Alloys.” *Met. Sci. J.*, 6(1), 175–183.

Wen, M., Tu, G. F., Zong, Q. Y., and Xie, C. X. (1994). “A study of NiTi shape memory alloy springs and its application in a new robotic actuator.” *Proc. 1994 IEEE Int. Conf. Ind. Technol. - ICIT '94*, IEEE, 215–219.

West, D. R. F., and Thomas, D. L. (1956). “The constitution of copper-rich alloys of the copper-manganese-aluminium system.” *J. Inst. Met.*, 85, 97–104.

Wield, D. V., and Gillam, E. (1972). “Shape memory effect and pseudoelasticity in Cu-Zn-Si.” *Scr. Metall.*, 6(12), 1157–1160.

Wilke, P. S., Johnson, C. D., Grosserode, P. J., and Sciulli, D. (2000). “Whole-spacecraft vibration isolation on small launch vehicles.” *Smart Struct. Mater. 2000 Damping Isol.*, SPIE, 440–451.

Xiao, Y., Zeng, P., and Lei, L. (2016). “Experimental Investigation on the Mechanical Instability of Superelastic NiTi Shape Memory Alloy.” *J. Mater. Eng. Perform.*, 25(9), 3551–3557.

Xie, J.-X., Liu, J.-L., and Huang, H.-Y. (2015). “Structure design of high-performance Cu-based shape memory alloys.” *Rare Met.*, 34(9), 607–624.

Xu, H. P., Song, G. F., and Mao, X. M. (2011). “Influence of Be and Ni to Cu-Al Alloy Shape Memory Performance.” *Adv. Mater. Res.*, 197–198, 1258–1262.

- Xu, J., Li, R., and Li, Q. (2021). “Effect of Agglomeration on Nucleation Potency of Inoculant Particles in the Al-Nb-B Master Alloy : Modeling and Experiments.” *Metall. Mater. Trans. A*, 52, 1077–1094.
- Xu, J. W. (2008). “Effects of Gd addition on microstructure and shape memory effect of Cu–Zn–Al alloy.” *J. Alloys Compd.*, 448(1–2), 331–335.
- Yang, G.-S., Lee, J.-K., and Jang, W.-Y. (2009). “Effect of grain refinement on phase transformation behavior and mechanical properties of Cu-based alloy.” *Trans. Nonferrous Met. Soc. China*, 19(4), 979–983.
- Yang, J., Wang, Q. Z. Z., Yin, F. X. X., Cui, C. X. X., Ji, P. G. G., and Li, B. (2016). “Effects of grain refinement on the structure and properties of a CuAlMn shape memory alloy.” *Mater. Sci. Eng. A*, 664, 215–220.
- Yang, N. Y. C., Laird, C., and Pope, D. P. (1977). “The cyclic stress-strain response of polycrystalline, pseudoelastic Cu-14.5 wt pct Al-3 wt pct Ni alloy.” *Metall. Trans. A*, 8(6), 955–962.
- Yang, Q., Zheng, T., Zhang, D., Liu, X., Fan, J., Qiu, X., Niu, X., and Meng, J. (2013). “Microstructures and tensile properties of Mg–4Al–4La–0.4Mn–xB (x =0, 0.01, 0.02, 0.03) alloy.” *J. Alloys Compd.*, 572, 129–136.
- Yang, S., Zhang, F., Wu, J., Lu, Y., Shi, Z., Wang, C., and Liu, X. (2017a). “Superelasticity and shape memory effect in Cu–Al–Mn–V shape memory alloys.” *Mater. Des.*, 115, 17–25.
- Yang, S., Zhang, F., Wu, J., Zhang, J., Wang, C., and Liu, X. (2017b). “Microstructure characterization, stress–strain behavior, superelasticity and shape memory effect of Cu–Al–Mn–Cr shape memory alloys.” *J. Mater. Sci.*, 52(10), 5917–5927.
- Yang, S., Zhang, J., Chen, X., Chi, M., Wang, C., and Liu, X. (2019). “Excellent superelasticity and fatigue resistance of Cu-Al-Mn-W shape memory single crystal obtained only through annealing polycrystalline cast alloy.” *Mater. Sci. Eng. A*, 749(February), 249–254.
- Yang, W. S., and Mikkola, D. E. (1993). “Ductilization of Ti-Ni-Pd shape memory

alloys with boron additions.” *Scr. Metall. Mater.*, 28, 161–165.

Yawny, A., Lovey, F. C., and Sade, M. (2000). “Pseudoelastic fatigue of Cu-Zn-Al single crystals: The effect of concomitant diffusional processes.” *Mater. Sci. Eng. A*, 290(1–2), 108–121.

Yeung, K. W. K., Cheung, K. M. C., Lu, W. W., and Chung, C. Y. (2004). “Optimization of thermal treatment parameters to alter austenitic phase transition temperature of NiTi alloy for medical implant.” *Mater. Sci. Eng. A*, 383(2), 213–218.

Yi, X., Sun, K., Gao, W., Wang, H., Sun, B., Yao, W., Meng, X., Gao, Z., and Cai, W. (2019). “The precipitation behaviors, martensite transformation and superelasticity in the aged Ni-rich Ti-Ni alloy with the assist of super-high stress.” *Intermetallics*, 104(August 2018), 8–15.

Yoon, S. H., and Yeo, D. J. (2004). “Phase transformations of nitinol shape memory alloy by varying with annealing heat treatment conditions.” *Smart Mater. III, Proc. SPIE 2005*, A. R. Wilson, ed., Bellingham: SPIE, 208.

Yun, C. B., Lee, J. J., and Koo, K. Y. (2011). “Smart structure technologies for civil infrastructures in Korea: Recent research and applications.” *Struct. Infrastruct. Eng.*, 7(9), 673–688.

Zak, G., Kneissl, A. C., and Zatulskij, G. (1996). “Shape memory effect in cryogenic Cu-Al-Mn alloys.” *Scr. Mater.*, 34(3), 363–367.

Zhang, P., Ma, A., Jiang, J., Lu, S., Lin, P., Yang, D., and Liu, G. (2010). “Microstructural evolution and mechanical response of Cu–Al–Be–B shape memory alloy processed by repetitive equal channel angular pressing.” *J. Alloys Compd.*, 497(1–2), 210–214.

Zhang, P., Ma, A., Lu, S., Lin, P., Jiang, J., Ma, H., and Chu, C. (2009a). “Effect of equal channel angular pressing and heat treatment on the microstructure of Cu – Al – Be – B shape memory alloy.” *Mater. Lett.*, 63, 2676–2679.

Zhang, P., Ma, A., Lu, S., Liu, G., Lin, P., Jiang, J., and Chu, C. (2011). “Effect of grain refinement on the mechanical properties of Cu–Al–Be–B shape memory alloy.” *Mater.*

Des., 32(1), 348–352.

Zhang, X., Sui, J., Liu, Q., and Cai, W. (2016). “Effects of Gd addition on the microstructure, mechanical properties and shape memory effect of polycrystalline Cu–Al–Ni shape memory alloy.” *Mater. Lett.*, 180, 223–227.

Zhang, X., Zhang, M., Cui, T., Li, J., Liu, Q., and Wang, H. (2019). “The enhancement of the mechanical properties and the shape memory effect for the Cu–13.0Al–4.0Ni alloy by boron addition.” *J. Alloys Compd.*, 776, 326–333.

Zhang, Y., Camilleri, J. a, and Zhu, S. (2008). “Mechanical properties of superelastic Cu–Al–Be wires at cold temperatures for the seismic protection of bridges.” *Smart Mater. Struct.*, 17(2), 025008.

Zhang, Y., Hu, X., and Zhu, S. (2009b). “Seismic performance of benchmark base-isolated bridges with superelastic Cu–Al–Be restraining damping device.” *Struct. Control Heal. Monit.*, 16(6), 668–685.

Zheng, Y., Li, C., Wan, F., and Long, Y. (2007). “Cu–Al–Mn alloy with shape memory effect at low temperature.” *J. Alloys Compd.*, 441(1–2), 317–322.

Zhu, M., Ye, X., Li, C., Song, G., and Zhai, Q. (2009). “Preparation of single crystal CuAlNiBe SMA and its performances.” *J. Alloys Compd.*, 478(1–2), 404–410.

Zhu, S., and Zhang, Y. (2007). “Seismic behaviour of self-centring braced frame buildings with reusable hysteretic damping brace.” *Earthq. Eng. Struct. Dyn.*, 36(10), 1329–1346.

Ziółkowski, A. (2015). *Pseudoelasticity of Shape Memory Alloys: Theory and Experimental Studies*. Elsevier.

LIST OF PUBLICATIONS BASED ON Ph.D. RESEARCH WORK

Sl. No.	Title of paper	Authors	Journal Name, Year, Volume Number, Issue, Pages)	Month, year of publication	Category*
1	Experimental investigation of the pseudoelastic behavior on Zirconium modified Cu-Al-Be shape memory alloys for seismic applications. https://doi.org/10.1088/1361-665X/ac5ce4	<u>T. Kalinga</u> S. M. Murigendrappa S. Kattimani	Smart Materials and Structures 2022, 31, 055009 (15pp)	March, 2022	1
2	Pseudoelastic behavior of boron-doped β_1 -type Cu-Al-Be shape memory alloys. https://doi.org/10.1007/s11665-021-05825-x	<u>T. Kalinga</u> S. M. Murigendrappa S. Kattimani	Journal of Materials Engineering & Performance, 2021, 30, 6068-6078.	April, 2021	1
3	Role of alloying additions on phase transformations, mechanical and pseudoelastic behavior of Cu-Al-Be shape memory alloys. https://doi.org/10.1016/j.matpr.2021.12.092	<u>T. Kalinga</u> Guniputi Bala Narasimha S. M. Murigendrappa S. Kattimani	Materials Today: Proceedings 2022, 59, 612-616	December, 2021	3

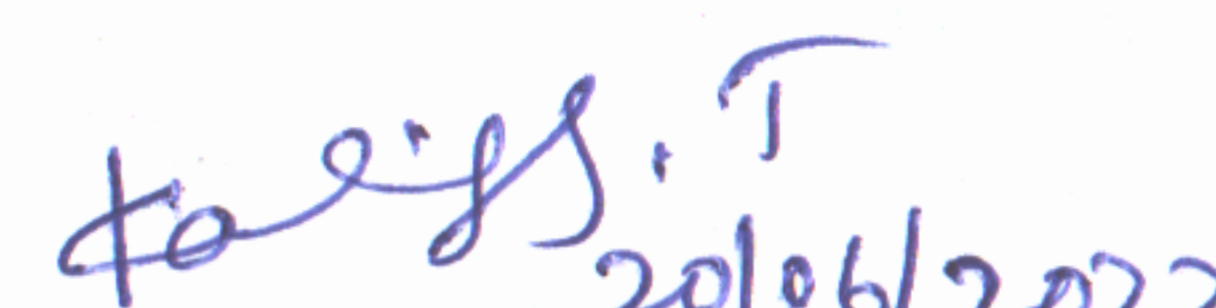
Category* 1: Journal paper, full paper reviewed


3: Conference /Symposium paper, full paper reviewed


5: Others (including paper in workshop, NITK Bulletin, short notes etc.)

2: Journal paper, Abstract reviewed

4: Conference /Symposium paper, Abstract reviewed


Kalinga T
Research Scholar


Prof. S. M. Murigendrappa
Research Guide


Dr. S. Kattimani
Research Co-guide

BIODATA

1. **Name:** Kalinga T
2. **Fathers Name:** Thippeshi Naik
3. **Date of Birth:** 01 -06 -1991
4. **Nationality:** Indian
5. **Marital Status:** Single
6. **Address:**

Permanent Address

#07,
Jodichikkenahalli
Lambanihatti,
Chitradurga – 577524,
Karnataka, India.

Present Address

Department of Mechanical Engineering
National Institute of Technology Karnataka
Surathkal – 575025, Srinavasangar,
Dakshina Kannada, Karnataka, India.

7. **Mobile Number:** 9742550092
8. **E-Mail:** kalingatnaik.jch@gmail.com
9. **Educational qualification:**

Qualification	College/School	University/Board	Year of passing	Performance
Ph.D.	National Institute of Technology Karnataka, Surathkal.	National Institute of Technology Karnataka	Pursuing	8.77 (CGPA)
M.Tech – Machine Design	UBDT College of Engineering, Davangere.	Visvesvaraya Technological University	2015	78.96 %
B.E – Mechanical Engineering	Siddaganga Institute of Technology, Tumkur.	Visvesvaraya Technological University	2013	9.35 (CGPA)

10. Work experience:

Name of the organization	Duration	Position
Prasanna College of Engineering and Technology, Laila, Belthangady, Dakshina Kannada.	2015 - 2016	Assistant Professor

I declare that the above information is true and correct to the best of my knowledge.


(KALINGA T)